Title
Leveraging Hypoxia Towards the Identification and Targeting of Cancer-Specific Cell Surface Antigens

Author
Kirkemo, Lisa Louise

Publication Date
2022

Peer reviewed|Thesis/dissertation

Leveraging Hypoxia Towards the Identification and Targeting of Cancer-Specific Cell Surface Antigens

by
Lisa Louise Kirkemo

DISSERTATION
Submitted in partial satisfaction of the requirements for degree of
DOCTOR OF PHILOSOPHY

in

Chemistry and Chemical Biology

in the

GRADUATE DIVISION
of the
UNIVERSITY OF CALIFORNIA, SAN FRANCISCO

Approved:

DocuSigned by:
James Wells
5F2F4D1A06164C2...

James Wells
Chair

DocuSigned by:
Charles Hart
DocuSigned by:F6...

Charles Hart

DocuSigned by:
Rushika Perera
DocuSigned by:435...

Rushika Perera

DocuSigned by:
Davide Ruggero
14C3B6AD60C5446...

Davide Ruggero

Committee Members

To my family and friends

Acknowledgements

Scientists are not born, they are made. It often starts from a very young age with fantastic teachers and parents, without which there would be neither interest nor opportunity. Later in life, it comes from the peers all around us who strive to change the world for the better. Finally, it comes from the love and support of those in our lives that pick us up when things get rough. Regardless of who in our lives or when, the process is nearly impossible without them. I have been lucky to live a life full of wonderful teachers and mentors, incredible friends, and the most supportive family, without which I would never have chosen this path. My time in graduate school has presented me with many challenges, but the downstream successes have never stemmed from me alone and are instead shared amongst many.

First, I would like to thank my initial scientific mentors, Professor Tom Scanlan and Professor Meredith Hartley. These two incredible scientists were my first research mentors after graduating from college. While I knew my way around the theoretical, I had very little real-world experience at the bench. Instead of favoring experienced researchers, these two spent time and energy training and teaching me how to become a better scientist. They extended a helping hand when necessary, but also gave me an incredible amount of leeway to take risks and learn from doing. They pushed me towards scientific rigor and critical thinking, while giving me the autonomy to feel creative. I certainly would not have chosen this path without you, and my success is in large part because of your initial—and continued—thoughtful mentoring.

Next, without the wonderful scientific community at UCSF, I would not be the scientist I am today. Firstly, I would like to thank my advising professor Jim Wells for his continual guidance, positivity, and scientific freedom that he extended to each and every person in his lab. Jim's lab is such a unique place to develop into a scientist. The team of people that Jim has created is second

to none, and he is continuously bringing his infectious energy and curiosity to the lab atmosphere. The amount of trust and creative liberty that he gives to all of his lab members has helped me become a more creative scientist and patient mentor. I am also grateful for his "work hard, play hard" attitude, especially the yearly ski trips. It was always so refreshing to take a step away from the bench and reconnect with the rest of the lab in a non-science setting. I look forward to many more years working together. To Drs. Charles Hart, Rushika Perera, and Davide Ruggero, my thesis committee members – thank you for your input throughout the last five years. It was always such a treat to be able to ideate and discuss the possibilities with you. You brought so much expertise and curiosity to the process, and I always came away with countless ideas of new things to try.

I am also very grateful to the members of the Wells lab that I have had the great privilege to overlap with over the past five years. I learned so much from everyone and hope to call many of them lifelong friends. I would especially like to thank Dr. Kevin Leung and Dr. Alex Martinko, my initial mentors in lab that taught me everything I needed to know about phage display, mass spectrometry, and antibody discovery; Dr. Sam Pollock, who kept me grounded and kept graduate school life in perspective; Dr. Jamie Byrnes, who taught me to not only become a more critical scientist, but also pushed me to become a better scientific communicator; Dr. Jeff Glasgow, who always had an idea up his sleeve and reminded me to stay curious about the world around me; Drs. Susanna Elledge, Nick Rettko, Irene Lui, and Kata Pance who kept lab fun and were a refreshing step away from the day-to-day; and finally to all members of the Wells lab, who have remained a wonderful group of people and a continuous source of ideas, support, and kindness. I look forward to crossing paths with each and every one of you in the future.

The broader UCSF community also had plenty of gems. In particular, my CCB cohort: Peter Rohweder, Dr. Alison Maxwell, Beatrice Ary, Dr. Dan Schwarz, Doug Wassarman, Dr. Kaitlyn Tsai, Keely Oltion, Kevin Lou, Shizhong Dai, Dr. Susanna Elledge, Dr. Taylor Arhar, Cynthia Chio, Taia Wu, and Dr. Sasha Dickinson. I'm excited to have our paths cross for many years to come!

I would also like to thank the funding institutions that took a chance and funded the science I worked on, specifically the National Institutes of Health and the Ruth L. Kirschstein Predoctoral Individual Fellowship (F31).

Lastly, I would like to thank my family. To my partner, Jason: I love you and am so grateful for the love and support you have shown me throughout my 5 years at UCSF. While I have truly enjoyed our various adventures in the city and around the world, the thing I will remember most is discussing the possibilities for positive change in the world with you. If even a fraction of what we've thought up comes true, I'm excited to be able to live in that world with you and watch it all unfold. To my parents, brother, and family around the world, thank you for being my greatest cheerleaders. You were always a phone call away and could always keep me grounded and optimistic during some of the hardest times. You always believed in me and I am grateful for your continuous love and support. I could not have done this without you all.

Contributions

Chapter 1: Unpublished work that has not yet been submitted for publication. Lisa L. Kirkemo designed and executed the experiments; Irene Lui performed the subtiligase preparation. Lisa L. Kirkemo and James A. Wells conceptualized the project and experiments. James A. Wells oversaw the project.

Chapter 2: Adapted version of published work that has been submitted for publication: Kirkemo, L. L.*, Elledge, S. K.*, Yang, J., Byrnes, J., Glasgow, J., Blelloch, R., & Wells, J. A. (2022). Cell-surface tethered promiscuous biotinylators enable comparative small-scale surface proteomic analysis of human extracellular vesicles and cells.

*Denotes equal contribution to this work.

Chapter 3: Unpublished work that has not yet been submitted for publication. Lisa L. Kirkemo and Nicholas J. Rettko designed and executed the experiments. Lisa L. Kirkemo, Nicholas J. Rettko, and James A. Wells conceptualized the project and experiments. James A. Wells oversaw the project.

Leveraging Hypoxia Towards the Identification and Targeting of Cancer-Specific Cell Surface Antigens

Lisa Louise Kirkemo

Abstract

With the advent of immunotherapy, identification and characterization of cancer-specific antigens is paramount to our ability to leverage this field towards the treatment of cancer. Pursuing the study of these cell surface antigens, especially in the context of cellular stress has become increasingly important. Low oxygen availability, or hypoxia, is a major environmental factor in solid tumors, which influences the metabolic, transcriptomic, and proteomic landscape of these cells. Hypoxia ultimately leads to poorer prognoses for patients with hypoxic solid tumors, and these hypoxia-specific effects suggest that tumor hypoxia can be leveraged for early stage diagnostics, as well as selective targeting of hypoxia-induced antigens in tumors. There are two main modes by which cell surface targets can be leveraged for the selective targeting of diseased cells, namely (1) through direct binding of a tumor cell surface antigen by antibodies and downstream activation of surrounding immune cells or (2) through the interaction of MHC-I peptide complexes with the native T-cell receptor (TCR). This work encompasses novel methods for the identification of both whole protein and MHC-peptide complexes in the context of hypoxic pancreatic cancer. As pancreatic cancer continues to lack tangible treatment options, it has become increasingly important to characterize these tumor types for new and selective therapeutic targets.

In Chapter 1, we perform cell surface proteomics on an array of basal and classical pancreatic adenocarcinoma (PDAC) cells in hypoxia and normal conditions and identify the

membrane protein vasorin (VASN) as a potential marker for hypoxic PDAC. In Chapter 2, we develop a novel method for small-scale cell surface proteomics using membrane tethered forms of the promiscuous biotinylators APEX2 and HRP. In Chapter 3, we design a novel secreted HLA Fc-fusion construct that can be coupled with mass spectrometry to profile the immunopeptidome of disease-phenotypes, including hypoxia and senescence.

Table of Contents

List of Figures

List of Abbreviations

APEX2 – Ascorbate peroxidase 2

BiTE – Bispecific T cell engager

BLI – Biolayer interferometry

CA9 – Carbonic anhydrase 9

DDA – Data dependent acquisition

DNA-APEX2 – Deoxyribonucleic acid conjugated ascorbate peroxidase 2 enzyme

Dox – Doxycycline

DYH11 – Dynein axonemal heavy chain 11

ELISA – Enzyme-linked immunoassay

FBS – Fetal bovine serum

FDR – False discovery rate

GDF15 – Growth differentiation factor 15

GFP – Green fluorescent protein

GlcNAc – N-Acetyl-D-glucosamine

HLA – Human leukocyte antigen

HRP – Horseradish peroxidase

IEDB – Immune epitope database

IF44L – Interferon induced protein 44 like

IgG – Immunoglobulin G

LRRC15 – Leucine rich repeat containing 15

KAD4 – Adenylate kinase 4

K_D – Binding affinity

K_{off} – Dissociation rate

K_{on} – Association rate

MHC – Major histocompatibility complex

PDAC – Pancreatic ductal adenocarcinoma

PGH2 – Prostaglandin H2

pMHC – Peptide MHC or MHC-peptide complex

scFv – Single-chain variable fragment

sEV – Small extracellular vesicle

sHLA – Secreted HLA

SILAC – Stable isotype labeling by amino acids in cell culture

SLC2A1 – Solute carrier family 2 member 1

SPAG4 – Sperm associated antigen 4

STAT1 – Signal transducer and activator of transcription 1

TCR – T cell receptor

TEV – Tobacco etch virus

TME – Tumor microenvironment

TXNIP – Thioredoxin-interacting protein

VASN – Vasorin

WGA-HRP – Wheat-germ agglutinin conjugated horseradish peroxidase

Chapter 1

Characterizing and targeting the cell surface proteome of hypoxic pancreatic cancer

Abstract

Virtually every solid tumor experiences oxygen deprivation, which encourages the survival and proliferation of cancer. Given the ubiquitous nature of low oxygen in the tumor microenvironment (TME), hypoxia can be leveraged to increase specificity of therapeutics towards cancer. Here, we show a cell surface marker called vasorin (VASN) is elevated on an array of oxygen-deprived pancreatic cancer cells. Moreover, work in this study shows that VASN is subsequently cleaved from the surface of cells and its expression and proteolysis plays an important role in the survival of pancreatic cancer under low oxygen. This study provides evidence for the development of both non-invasive, early-detection diagnostics and ultra-selective therapeutic alternatives for a highly metastatic and deadly disease.

Introduction

With the advent of cancer immunotherapies, patients have seen dramatic increases in the availability of treatment options for various malignancies. However, many of these modalities lack efficacy in treating solid tumors, namely because of the unique set of environmental factors that exist within these tumors. As solid tumors make up over 90% of all cancer cases in the United States, additional investigation of basic tumor biology is required. One hallmark of solid tumors is the development of unique tumor microenvironments (TME), which lead to extreme alterations to the surrounding tissues and negatively impact both treatment and diagnostic efficacy (Chouaib et al., 2017). One of the most common microenvironments present in 60% of solid tumor tissue is oxygen deprivation, also known as hypoxia (Molls, 2009). The use of oxygen as a terminal electron acceptor is a critical component of mammalian cell biology. As such, organisms have evolved

highly regulated cellular pathways and gene programs to react to low-oxygen conditions. In response to hypoxic stress, cancer cells activate cellular pathways and gene programs that promote survival, migration, immune privilege, and increased mortality for patients (Vaupel & Mayer, 2007). Hypoxic phenotypes are often present in cancer types with particularly high mortality rates, with pancreatic cancer exhibiting the most severe hypoxic phenotype and accelerated metastatic disease progression (Akakura et al., 2001; Yuen & Díaz, 2014). These factors, compounded by frequent late-stage diagnosis, heavily contributes to the dismal 5% five-year survival rate of pancreatic cancer patients, the lowest among all solid tumor types (Ilic & Ilic, 2016). This late stage diagnosis often precludes the few treatment options available for pancreatic cancer, with the current standard of care including surgical resection, cytotoxic chemotherapy, and radiotherapy (Brunner et al., 2019). The efficacy of the current standard of care could be enhanced through the development of early-stage diagnostic tools. Because hypoxia is a hallmark of early-stage pancreatic tumors, identification and characterization of hypoxia-induced pancreatic cancer antigens could be leveraged for early-stage monitoring and diagnosis of pancreatic cancer patients.

Pancreatic cancer presents as two main subtypes: classical and basal (Adams et al., 2019; Collisson et al., 2011). While both are deadly and prone to metastasis, the basal subtype presents with mesenchymal signatures and undifferentiated histopathology, which leads to worse prognoses for patients with this subtype (Australian Pancreatic Cancer Genome Initiative et al., 2016; Moffitt et al., 2015). Key drivers of the basal subtype have been catalogued, but very little work has been done towards identification of surface markers on either subtype. Work in this area could help in the development of subtype-specific therapeutic development, as well as early-stage diagnostic tools and patient triage.

Here, we utilize cell surface proteomics to identify subtype specific signatures of the cell surface proteome. Moreover, we identify a novel hypoxia-regulated cell surface target in pancreatic cancer called vasorin (VASN), a protein previously implicated in the progression of glioblastoma (Man et al., 2018). Furthermore, using technology developed in our lab, we show that VASN is cleaved at a site proximal to the membrane, with a proteolysis signature matching that of cleavage by the ADAM10/17 protease classes. Finally, we provide mechanistic insights into the functional consequences of such proteolysis in pancreatic cancer by showing an autocrine-like binding paradigm for the cleaved portion of VASN and show that VASN expression is correlated to the downstream expression of a key regulator of epithelial-to-mesenchymal transition (EMT) called nestin. These biological phenomena in cancer provide evidence for the development of non-invasive, early-detection diagnostic alternatives and ultra-selective therapeutic strategies for patients with this deadly disease.

Results

Characterization of the Cell Surface Proteome of Basal and Classical Pancreatic Cancer

The identification of subtype specific cell surface antigens in pancreatic adenocarcinoma (PDAC) remains understudied. We endeavored to better understand the differences present in an array of different classical and basal cell lines **(Figure 1.1A)**. Each cell was interrogated using the biocytin hydrazide cell surface enrichment strategy and subsequent LC-MS/MS analysis to identify cell surface proteome stratification criteria for each class of PDAC **(Figure 1.1B)**. Classical and basal subtypes naturally stratified into two separate groups, with large regions of the surface proteome retaining either classical or basal phenotypes **(Figure 1.1C)**. Moreover, known markers for each subtypes (vimentin for basal; E-Cadherin for classical) showed stereotypical expression profiles,

lending credibility to the performed surface enrichment and label-free quantification strategies **(Figure 1.1D & E)**.

Identification of Vasorin in Hypoxic Pancreatic Cancer

With the goal of identifying hypoxia-specific targets on pancreatic cancer, stable isotope labeling with amino acids in culture (SILAC) and cell surface capture technology were used to profile the effects of hypoxia on the surface proteome of pancreatic cancer. Panc-1 pancreatic cancer cell lines were grown for 5 doublings in SILAC media containing heavy and light isotopes of arginine and lysine. Cells were then subjected to hypoxia (1% O_2) or normoxia (20% O_2), mixed 1:1, and isolated using cell-surface capture for analysis by tryptic LC-MS/MS **(Figure 1.2A)**. These proteomic analyses revealed the presence of a hypoxia-regulated marker called vasorin (VASN), which was almost 8-fold upregulated in hypoxia over normoxia, and has not been previously implicated in pancreatic cancer biology **(Figure 1.2B)**. Although this is the first association of VASN in pancreatic cancer, VASN has previously been shown to be important in numerous cancer-dependent processes. Importantly, VASN has been demonstrated to play an important function in the development of cancer stem cells in glioblastoma through stabilization of NOTCH1 (Man et al., 2018). Indeed, available pancreatic cancer datasets show that high expression of VASN in patients positively correlates with higher tumor grades, indicating that VASN could lead to poorer prognoses for patients **(Figure 1.2C)**.

In order to further characterize VASN and its role in cancer progression, we endeavored to isolate antibodies against the full-length ectodomain of vasorin. Through the use of phage-display, antibody clones against the ectodomain of VASN were isolated. Briefly, the extracellular domain of VASN was cloned onto the N-terminus of an immunoglobulin Fc domain **(Figure 1.2D)**, immobilized on solid phase, and introduced to a library of antibody fragment (Fab)-phage in a

series of iterative selection and amplification steps **(Figure 1.2E)**. Binding Fab-phage were cloned into a Fab expression plasmid and expressed in *E. coli*. Biolayer interferometry (BLI) of expressed Fabs introduced to immobilized VASN antigen revealed strong and selective binding, with K_D measurements ranging from 2.5 nM to 670 pM **(Figure 1.3A & B)**. VASN Fabs were tested for specificity using a Dox-inducible VASN overexpression cell line, and showed specific binding only in the context of the VASN-overexpressing cells **(Figure 1.2F)**. However, when these same Fabs were tested for selective binding towards hypoxic Panc-1 cells, we did not detect preferential binding in the context of hypoxia **(Figure 1.2G)**, indicating that the epitope was either occluded through protein-protein interaction or was being proteolyzed away from the membrane **(Figure 1.2H)**. Previous reports have suggested that the VASN ectodomain undergoes specific proteolytic cleavage, however the precise site had not been discovered (Malapeira et al., 2011, p. 17).

Elucidation of Vasorin Proteolysis in Hypoxic Pancreatic Cancer

To examine VASN cleavage in this system, an N-terminally FLAG-tagged VASN was constructed and VASN overexpressing Panc-1 cells were stably transduced **(Figure 1.4A)**. Using these cells, immunoprecipitation was performed on filtered media from Panc-1 cells grown under hypoxic conditions for 96 hours using the previously isolated Fab clones **(Figure 1.4B)**. Subsequent western blotting with commercially available anti-VASN and anti-FLAG antibodies revealed that the VASN ectodomain was being proteolytically shed and captured by our in-house Fab clones in the media **(Figure 1.4C)**, indicating that VASN undergoes numerous cleavage events under hypoxia *in vitro*. Notably, this cleavage site is distinct from the previously published reports of VASN proteolysis, suggesting that proteolyzed VASN in pancreatic cancer may serve a unique function.

Site Specific Localization of Vasorin Proteolysis in Hypoxic Pancreatic Cancer

In order to more specifically characterize the progression of proteolysis, a C-terminally V5-tagged construct of VASN was expressed in Panc-1 cells **(Figure 1.5A)**. Western blotting of hypoxic Panc-1 cellular lysate revealed a single membrane-proximal proteolytic event **(Figure 1.5B)**. In order to gain residue-specificity for the proteolysis of VASN, we used a lab evolved strain of a peptide ligase called subtiligase to install a biotinylated peptide tag to the neo-N termini of the proteolyzed VASN **(Figure 1.5C)**. These biotinylated fragments were immunoprecipitated and eluted off bead by tryptic digestion before identification by LC-MS/MS. Using this strategy, it was found that VASN was proteolyzed between A-558 and V-559, in agreement with the proteolytic signature of ADAM17 (Mohan et al., 2002)**(Figure 1.5D)**. While it has been previously proposed that VASN is a substrate for ADAM17, the site at which it is cleaved has never been identified. This also provides mechanistic evidence for the association of VASN with NOTCH1, which is also a substrate for ADAM17.

Mechanistic Insights for Vasorin Proteolysis

As ADAM17 proteolysis is generally suggestive of cellular activation, we wanted to test whether the shed fragment exhibited either autocrine or paracrine interactions towards pancreatic cancer cells or cells of the surrounding endothelium. Interestingly, flow cytometry indicated that the cleaved extracellular membrane of VASN re-associates to the membrane of the parent cell **(Figure 1.5E)**, which may suggest an autocrine role of cleaved VASN. Prior experiments utilizing a model of the endothelium—HUVEC cells—showed that VASN did not exhibit appreciable binding, indicating that this cleaved form of VASN acts locally on the tumor cells and not on the surrounding vasculature **(Figure 1.6)**. To better understand the role VASN plays in promoting oncogenesis in an autocrine fashion, we pursued the construction of VASN knockout Panc-1 cells

using two orthogonal CRISPR guide RNAs **(Figure 1.7A & B)** . In the hopes of isolating potential downstream impacts of VASN ablation, we performed whole-cell proteomics of hypoxic control and KO lines and isolated a protein called Nestin, which became severely downregulated upon VASN knockout **(Figure 1.7C)**. Nestin has previously been shown to play an important role in the epithelial-to-mesenchymal (EMT) transition in cancer and in turn regulates the expression of vimentin, N-cadherin, and CD44, all of which are important regulators of EMT.

Discussion

Although long-lasting treatment solutions have been found for many hematological malignancies, treatment options for solid tumors remain limited. A major obstacle to developing diagnostics and therapies for solid tumors is identifying molecular targets found specifically in cancer over healthy tissue. Hypoxic phenotypes have long been linked to poorer prognoses for patients (Dewhirst et al., 2008; Eales et al., 2016; Harris, 2002) and are often present in cancer types with particularly high mortality rates, with pancreatic cancer exhibiting the most severe hypoxic phenotype and accelerated metastatic disease progression. In response to hypoxic stress, pancreatic cancer cells activate highly regulated cellular pathways and gene programs that promote survival, migration, immune privilege, and increased mortality for patients (Akakura et al., 2001; Yuen & Díaz, 2014). Here, we first discover a host of surface markers that differentiate basal from classical subtypes of pancreatic cancer, one of the most deadly solid tumors types (Collisson et al., 2011; Deer et al., 2010; Yuen & Díaz, 2014). Next, we show that one marker, VASN, is upregulated in the context of tumor hypoxia in pancreatic cancer, and seems to correlate negatively with clinical prognosis. While the presence of VASN is increased in the context of cancer through its HIF-1α dependency, we present that the VASN ectodomain is cleaved from the cell surface, and is able to reassociate with hypoxic Panc-1 cells in an autocrine manner. Moreover, through the use of CRISPR

knockouts of VASN, we show that the absence of VASN decreases the expression of a marker called Nestin, which has been implicated in driving EMT in cancer. As hypoxia plays a major role in both the progression and altered proteomic landscape in the majority of solid tumors, we believe that continued work in the areas of TME-specific biomarker discovery will spur the development of safer and more selective therapies.

Methods

Cell culture

Panc-1, KP4, PSN1, MiaPaCa2, PaTu8902, Capan-2, HPAC, and HPAFII were a gift from the Perera lab (UCSF). HEK293-FlpIn cell lines were from frozen stocks maintained by the Wells lab. All PDAC cells were grown in IMDM + 10% FBS + 1% Pen/Strep. Engineered FlpIn cell lines were grown and maintained in DMEM + 10% Tetracycline-negative FBS + 1% Pen/Strep + 100 μg/mL Hygromycin B + 2 μg/mL blasticidin. For induction of hypoxia, cells were allowed 24 hours to adhere to the plate in a normal incubator (20% O_2 + 5 CO_2) before undergoing 96 hours of consecutive growth in 1% O_2 + 5% CO_2.

Cloning

Fc-fusion proteins were cloned into a pFUSE (InvivoGen) vector with a human IgG1 Fc domain as previously described (Martinko et al., 2018a). Fabs were subcloned from the Fab-phagemid into an *E. coli* expression vector pBL347. The heavy chain of the IgG was cloned from the Fab plasmid into a pFUSE (InvivoGen) vector with a human IgG1 Fc domain. The light chain of the IgG was cloned from the Fab plasmid into the same vector, but lacking the Fc domain. FlpIn constructs encoding each extracellular domain fused to the transmembrane anchoring domain of platlet-erived Growth Factor (for Type I membrane proteins) with an HA tag were cloned in the

pcDNA5/FRT/TO Mammalian Expression vector (ThermoFisher). All constructs were sequence verified by Sanger sequencing.

Protein expression and purification

Fabs were expressed in E. coli C43(DE3)Pro+ as previously described (Hornsby et al., 2015). Briefly, cells were grown in autoinduction media for 6 hours at 37ºC, after which the temperature was lowered to 30ºC and the cells were allowed to grow for an additional 16 hours. Proteins were subsequently purified by protein A affinity chromatography and buffer exchanged into PBS (pH 7.4) for storage in 10% glycerol at -80°C. Fab purity was assessed by SDS-PAGE.

IgGs were expressed and purified from Expi293F-BirA cells using transient transfection (Expifectamine, Thermo Fisher Scientific). Enhancers were added 20 hrs after transfection. Cells were incubated for 5 days at 37ºC and 8% CO_2. Media was then harvested by centrifugation at 4,000xg for 20 min. IgGs were purified by Ni-NTA affinity chromatography and buffer exchanged into PBS pH 7.4 and stored in 10% glycerol at -80°C.

Phage display selection

All phage selections were done according to previously established protocols (Martinko et al., 2018a). Briefly, selections with antibody phage library were performed using biotinylated Fc-fusion antigens captured with streptavidin-coated magnetic beads (Promega). Prior to each selection, the phage pool was incubated with 1 μM of biotinylated Fc-domain immobilized on streptavidin beads in order to deplete the library of any binders to the beads or Fc. In total, four rounds of selection were performed with decreasing amounts of Fc-fusion antigens (100 nM, 50 nM, 10 nM and 10 nM). To reduce the deleterious effects of nonspecific binding phage, we employed a ‘catch and release’ strategy, where ECD-Fc-fusion binding Fab-phage were selectively

eluted from the magnetic beads by the addition of 50 μg/mL TEV protease. Individual phage clones from the fourth round of selection were analyzed for binding by ELISA.

Phage titers were performed according to standard protocol. Briefly, TEV or acid eluted phage were used to infect log-phase XL1-Blue *E. coli* cells and were allowed to grow at RT for 20 minutes while shaking. Cells were serially diluted and spotted on an LB agar plate with carbenicillin (50 μg/ml) and incubated overnight at 37ºC. Phage titers were measured for each round of selections against the Fc-only control.

Fab-phage ELISA

For each phage clone, four different conditions were tested – Direct: Fc-fusion of interest, Competition: Fc-fusion with an equal concentration of Fc-fusion in solution, Negative selection: Fc-biotin, and Control: PBSTB. 384-well Nunc Maxisorp flat-bottom clear plates (Thermo Fisher Scientific) were coated with 0.5 μg/mL of NeutrAvidin in PBS overnight at 4°C and subsequently blocked with PBSTB. Plates were washed 3x with PBS containing 0.05% Tween-20 (PBST) and were washed similarly between each of the steps. 20 nM biotinylated Fc-fusion or Fc-biotin was diluted in PBSTB and immobilized on the NeutrAvidin-coated wells for 30 minutes at room temperature, then blocked with PBSTB + 10 μM biotin for 10 minutes. For the competition samples, phage supernatant was diluted 1:5 into PBSTB with 20 nM Fc-fusion 30 minutes prior to addition to the plate. For the direct samples, phage supernatant was diluted 1:5 in PBSTB. Competition and direct samples were added to the plate for 30 minutes at room temperature. Bound phage was detected by incubation with anti-M13-horseradish peroxidase conjugate (Sino Biologics, 1:5000) for 30 minutes, followed by the addition of TMB substrate (VWR International). The reaction was quenched with the addition of 1 M phosphoric acid and the absorbance at 450 nm was measured using a Tecan M200 Pro spectrophotometer. Clones with

high binding to Fc-fusion, low binding to PBSTB/Fc-biotin, and competition signal <0.5*direct binding signal were carried forward.

Binding kinetics analysis

Biolayer interferometry data were measured using an Octet RED384 instrument (ForteBio). Biotinylated VASN Fc-fusion (200 nM) was immobilized on streptavidin (SA) biosensors and a dose curve of each Fab (200, 66.6, 22.2, 7.4 nM in PBS + 0.05% Tween-20 + 0.2% BSA + 10 μM biotin) was used as an analyte. Affinity (K_D) and kinetic parameters (k_{on} and k_{off}) were calculated from a global fit (1:1) of the data using the software suite provided with the Octet RED384 instrument.

FlpIn T-REx cell line generation

FlpIn cells were grown to 70% confluence in the presence of 100 μg/mL zeocin and 10 μg/mL blasticidin in a well of a 6-well plate. Growth media was replaced with Opti-MEM for at least 15 minutes prior to transfection. While cells were incubating in Opti-MEM, plasmids were allowed to mix in Opti-MEM and were incubated for 15 minutes at RT: 1.5 μg pCDNA5/FRT/TO plasmid, 1.5 μg pOG44 plasmid, and 9 μL 1 mg/mL polyethylenimine (PEI) in 200 μL of Opti-MEM. Media in cells was replaced with Opti-MEM/DNA/PEI mixture and incubated for 6 hours at 37°C, 5% CO_2. Transfection media was replaced with 1:1 Opti-MEM/DMEM + 10% Tetracycline-negative FBS + 1% Pen/Strep and incubated at 37°C, 5% CO_2. After 24 hours, media was replaced and drug selection for stable cell lines was initiated by the addition with 100 μg/mL Hygromycin B and 2 μg/mL blasticidin.

Cell surface enriched mass spectrometry sample preparation

Cell surface glycoproteins were captured as previously described (Wollscheid et al., 2009). Briefly, cells were first washed in PBS (pH 6.5) before the cells underwent oxidation with 1.6 mM $NaIO_4$ in PBS (pH 6.5) for 20 minutes at 4°C while rotating. Biocytin hydrazide (1 mM, Biotium) was added to cells in the presence of 10 mM aniline (Sigma Aldrich) to initiate conjugation of the biotin moiety via the oxidized vicinal diols. The reaction was allowed to proceed for 90 minutes at 90 minutes at 4°C while rotating. Cell pellets were washed three times with PBS (pH 6.5) and snap frozen and stored at -80°C.

Frozen cell pellets were lysed with commercial 1X RIPA buffer (Millipore) supplemented with 1X Protease Inhibitor Cocktail (Sigma Aldrich) and 2 mM EDTA for 30 minutes at 4°C while rotating. Cells underwent sonication for 1 min (2 sec on: 2 sec off) on ice at 20% intensity and the cell lysates were spun down at 16,000xg for 10 minutes to remove insoluble particulates. Cell lysates were incubated with NeutrAvidin coated agarose beads (Thermo Scientific) for 1 hour at 4°C while rotating to isolate biotinylated glycoproteins, after which the beads were washed sequentially with pre-warmed RIPA wash buffer (0.5% DOC, 0.1 % SDS, 1% NP40, 1 mM EDTA in PBS, pH 7.4), high salt PBS (PBS pH 7.4, 1 M NaCl), and denaturing urea buffer (50 mM ammonium bicarbonate, 2 M Urea). Proteins were reduced and alkylated through sequential treatment with 5 mM TCEP for 30 minutes at 55°C in the dark, and subsequently treated with 11 mM IAM for 30 minutes at room temperature in the dark. Beads were washed twice with denaturing buffer and resuspended in 1 mL denaturing buffer and digested with 20µg trypsin (Promega). Tryptic peptides were collected and cells were washed twice with denaturing buffer.

To release the remaining trypsin digested N-glycosylated peptides bound to the neutravidin beads, we performed a second on-bead digestion using 2500U PNGase F (New England Biolabs)

at 37°C for 4.5 hours. Similarly, the "PNGase F" fraction was eluted using a spin column. Both tryptic and PNGase F fractions were then desalted using Pierce C18 column (Thermo Fisher) using standard protocol, dried, and dissolved in 0.1% formic acid, 2% acetonitrile prior to LC-MS/MS analysis.

Subtiligase peptide ligation protocol

Panc-1 cells overexpressing C-terminally V5-tagged VASN were grown to confluency in a 225 cm^2 growth plate after 96 hours in hypoxia. Cells were lifted with versene, washed 3x with PBS (pH 6.5), and spun down at 300xg for 5 minutes to collect. Cells were lysed with 1X RIPA buffer (Millipore) supplemented with 1X Protease Inhibitor Cocktail (Sigma Aldrich) and 2 mM EDTA for 30 minutes at 4°C while rotating. Cells underwent sonication for 1 min (2 sec on: 2 sec off) on ice at 20% intensity and the cell lysates were spun down at 16,000xg for 10 minutes to remove insoluble particulates. Cell lysates were incubated with anti-V5-streptavidin antibodies (1:100) for 1 hour at 4°C while rotating. Bound protein was immunoprecipitated by introduction to NeutrAvidin beads (Thermo Scientific) for 30 minutes at 4°C while rotating. Wash beads 2 times with subtiligase reaction buffer (100 mM tricine, 150 mM NaCL in 1X PBS, pH 8.0). Incubate beads in 500 uL of labeling buffer (5 uM M222A stabiligase, 1 mM TE6 Abu-tagged peptide ester, 5% DMSO in subtiligase reaction buffer) for 30 minutes at room temperature, rotating. Wash beads 2x with PBS. Elute off pulldown beads by addition of 200 µl of glycine (pH 2.5) and solution was neutralized with 30 µl of 1 M Tris (pH 8.0). Incubate elution with 100 uL of High Capacity Neutravidin Agarose resin (Thermo Scientific, #29204) for 30 minutes. Incubate at room temperature overnight with trypsin. Save tryptic peptide for further analysis. Elute Abu-tagged peptides by incubating with 5 mg of TEV protease overnight. Solution was desalted using

Pierce C18 column (Thermo Fisher) using standard protocol, dried, and dissolved in 0.1% formic acid, 2% acetonitrile prior to LC-MS/MS analysis.

Whole cell proteomics sample preparation

Cells were lifted using versene and washed 3x with PBS (pH 7.4) and were processed for LC-MS/MS using a PreOmics iST kit (P.O.00027). Briefly, cell pellets were brought up in 50 µl of provided LYSE solution and boiled with agitation for 10 minutes. The provided enzymes mixture (Trypsin and LysC) were resuspended in 210 µl of RESUSPEND buffer, mixed, and added to the lysed cells. Samples were allowed to mix at 500 rpm for 1.5 hours at 37°C, before being quenched with 100 µl of STOP solution. Sample was spun in provided C18 spin cartridge and washed 1X with 200µl of WASH 1 and WASH 2. Peptides were eluted with 2X 100 µl of ELUTE, dried, and resuspended with the provided LC-LOAD solution. Peptides were quantified using Pierce Quantitative Colorimetric Peptide Assay (Thermo Fisher Scientific, 23275).

LC-MS/MS

For samples analyzed on the Q Exactive Plus instrument, approximately 1 µg of peptides was injected to a pre-packed 0.75mm x 150 mm Acclaimed Pepmap C18 reversed phase column (2 µm pore size, Thermo Fisher Scientific) attached to a Q Exactive Plus (Thermo Fisher Scientific) mass spectrometer. For the "tryptic" fraction, peptides were separated using a linear gradient of 3-35% solvent B (Solvent A: 0.1% formic acid, solvent B: 80% acetonitrile, 0.1% formic acid) over 180 minutes at 300 µL/min. Similarly, the "PNGase F" fraction was separated using the same gradient over 120 minutes. Data were collected in data dependent mode using a top 20 method with dynamic exclusion of 35 s and a charge exclusion setting that only samples peptides with a charge of 2, 3, or 4. Full (ms1) scans spectrums were collected as profile data with a resolution of 140,000

(at 200 m/z), AGC target of 3E6, maximum injection time of 120 ms, and scan range of 400-1800 m/z. MS-MS scans were collected as centroid data with a resolution of 17,500 (at 200 m/z), AGC target of 5E4, maximum injection time of 60 ms with normalized collision energy at 27, and an isolation window of 1.5 m/z with an isolation offset of 0.5 m/z.

For samples that were introduced to the timsTOF Pro instrument, approximately 200 ng of peptides were separate using a nanoElute UHPLC system (Bruker) with a pre-packed 25 cm x 75 µm Aurora Series UHPLC column + CaptiveSpray insert (CSI) column (120 A pore size, IonOpticks, AUR2-25075C18A-CSI) and analyzed on a timsTOF Pro (Bruker) mass spectrometer. Peptides were separated using a linear gradient of 2-34% solvent B (Solvent A: 2% acetonitrile, 0.1% formic acid, solvent B: acetonitrile, 0.1% formic acid) over 100 mins at 400 nL/min. Data-dependent acquisition was performed with parallel accumulation-serial fragmentation (PASEF) and trapped ion mobility spectrometry (TIMS) enabled with 10 PASEF scans per topN acquisition cycle. The TIMS analyzer was operated at a fixed duty cycle close to 100% using equal accumulation and ramp times of 100 ms each. Singly charged precursors were excluded by their position in the m/z–ion mobility plane, and precursors that reached a target value of 20,000 arbitrary units were dynamically excluded for 0.4 min. The quadrupole isolation width was set to 2 m/z for m/z < 700 and to 3 m/z for m/z > 700 and a mass scan range of 100-1700 m/z. TIMS elution voltages were calibrated linearly to obtain the reduced ion mobility coefficients (1/K0) using three Agilent ESI-L Tuning Mix ions (m/z 622, 922 and 1,222).

Data analysis/Statistics

For comparative SILAC quantification of samples, datasets were searched using PEAKS Online X version 1.5 against the plasma membrane (PM) annotated human proteome (Swiss-prot GOCC database, August 3, 2017 release). Enzyme specificity was set to trypsin (+ LysC) with up to two

missed cleavages. Cysteine carbamidomethylation was set as the only fixed modification; acetylation (N-term), methionine oxidation, lysine and arginine SILAC labels were set as variable modifications; asparagine deamidation was also set as variable modification for the PNGase F fraction. The precursor mass error tolerance was set to 20 PPM and the fragment mass error tolerance was set to 0.05 Da. Data was filtered at 1% for both protein and peptide FDR and triaged by removing proteins with fewer than 2 unique peptides.

Fab Pulldown of Vasorin Shed Fragment

Removed media from a confluent T225 plate grown in chronic hypoxia (96 hours) and removed cellular debris by centrifugation at 4,000xg for 10 minutes. Media was further cleared through a 0.45 µm filter. A mixture of Fabs (clone E10, G02, G09, and H10) were added at a concentration of 1 µM and allowed to bind for 1 hour at 4°C. Biotinylated Fabs were removed from the media through binding to NeutrAvidin resin for 1 hour at 4°C . Beads were subsequently washed 3x with PBS (pH 7.4) and vasorin was removed by addition of 200 µl of glycine (pH 2.5) and solution was neutralized with 30 µl of 1 M Tris (pH 8.0).

Western Blot

For western blotting of immunoprecipitated vasorin fragments, 135 µl of IP liquid was combined with 45 µl of 4X NuPage buffer (Thermo Fisher). Samples were not denatured or boiled. Samples were run on a Bolt 4-12% Bis-Tris gel (Invitrogen), and transferred to a PVDF membrane (Thermo Scientific) using an iBlot™ (Thermo Scientific). Membranes were blocked for 1 hour in Odyssey® Blocking Buffer (TBS) (LiCOR) prior to staining. Membranes were stained with primary anti-human FLAG antibody or anti-human VASN antibody in blocking buffer for 1 hour at room temperature. Secondary staining was performed using goat anti-rabbit IRDye® 800CW (LiCOR

Biosciences) in blocking buffer for 30 minutes at room temperature. Membranes were washed with three 5 minute washes of TBST between each staining step. Membranes were imaged using an Odyssey® CLx (LiCOR Biosciences).

For cellular-derived samples, cells were lifted with versene and washed twice with PBS prior to lysis. Lysis buffer contained 1x RIPA (EMD Millipore), 1% protease inhibitor cocktail (Sigma-Aldrich), and 1 mM EDTA. Cells were lysed for 20 minutes on ice prior to sonication (1 minute, 20% amp, 2 second on/off pulse). Cells were spun at 16,000 x g at 4°C for 5 minutes, and lysate protein concentration was determined using a Pierce™ BCA Protein Assay (Thermo Scientific). Samples were run on a Bolt 4-12% Bis-Tris gel (Invitrogen), and transferred to a PVDF membrane (Thermo Scientific) using an iBlot™ (Thermo Scientific) on the P0 setting. Membranes were blocked in Odyssey® Blocking Buffer (TBS) (LiCOR) prior to staining. Membranes were stained with primary anti-V5 antibody in blocking buffer for 1 hour at room temperature. Secondary staining was performed using goat anti-rabbit IRDye® 800CW antibody (LiCOR Biosciences) in blocking buffer for 1 hour at room temperature. Membranes were washed with three 5 minute washes of TBST between each staining step. Membranes were imaged using an Odyssey® CLx (LiCOR Biosciences).

Flow Cytometry

All cells were lifted using versene. After lifting, cells were washed once with PBS + 2% BSA to inhibit nonspecific binding. Cells were introduced to a concentration gradient of Vasorin Fc-fusion in PBS + 2% BSA (500, 250, 125, 62.5, 31.25, 15.625, 7.8125 nM) and allowed to bind for 1 hr at 4°C. Samples were washed three times with PBS + 2% BSA. Samples were then incubated with 100 µL Streptavidin-Alexa Fluor 647 (Thermo Fischer, 1:100 in PBS + 2% BSA and incubated for 30-minutes at 4°C while rocking. Samples were washed three times with PBS + 2% BSA,

analyzed in the APC channel, and quantified using a CytoFLEX (Beckman Coulter). All flow cytometry data analysis was performed using FlowJo software.

CRISPR Knockout Protocol

Vasorin knockouts were generated using the RNP-electroporation method as previously described (Liang et al., 2015). One million Panc-1 cells were used per electroporation using the Amaxa 4D Nucleofector kit. Guide RNA and Cas9 complexes were formed using 160 μM crRNA annealed to 160 μM tracrRNA (IDT) and incubated with 40 μM Cas9 protein (IDT). Successful knockout was assessed 40 hours post-electroporation using PCR and sanger sequencing.

Guide RNA sequences:

Alt-R CRISPR-Cas9 crRNA 1: Hs.Cas9.VASN.1.AA

Alt-R CRISPR-Cas9 crRNA 2: Hs.Cas9.VASN.1.AN

PCR primer sequences:

VASN FW: GTGCTCCAGGGTCCCTCTG

VASN REV: GCTGCTGCAGCCCCAG

Figures and Tables

A)

Cell Line	Subtype
Panc-1	Basal
KP4	Basal
PSN1	Basal
MiaPaca2	Basal
Patu8902	Classical
Capan-2	Classical
HPAC	Classical
HPAFII	Classical

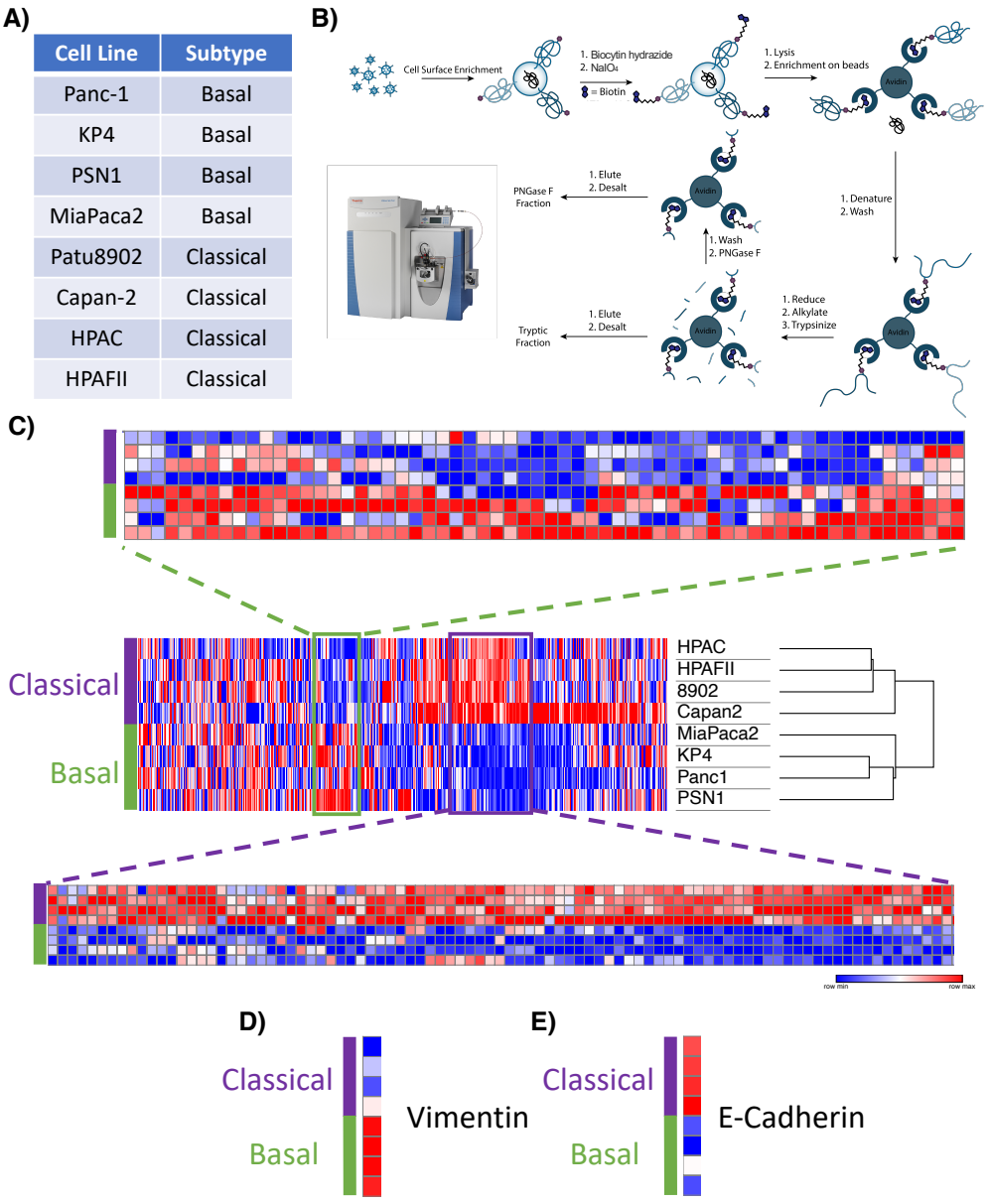

Figure 1.1: Surface proteomics of basal and classical pancreatic cancer cells. A) A total of eight cell lines were studies. Four basal (Panc-1, KP4, PSN1, and MiaPaCa2) and four classical (PaTu8902, Capan-2, HPAC, and HPAFII) were analyzed by LC-MS/MS. B) General workflow for cell surface protein isolation by biocytin hydrazide. C) Heatmap depicting unsupervised clustering of basal and classical subtypes on their respective cell surface protein enrichments. (D) Expression of vimentin across all classical and basal subtypes. (E) Expression of E-Cadherin across all classical and basal subtypes.

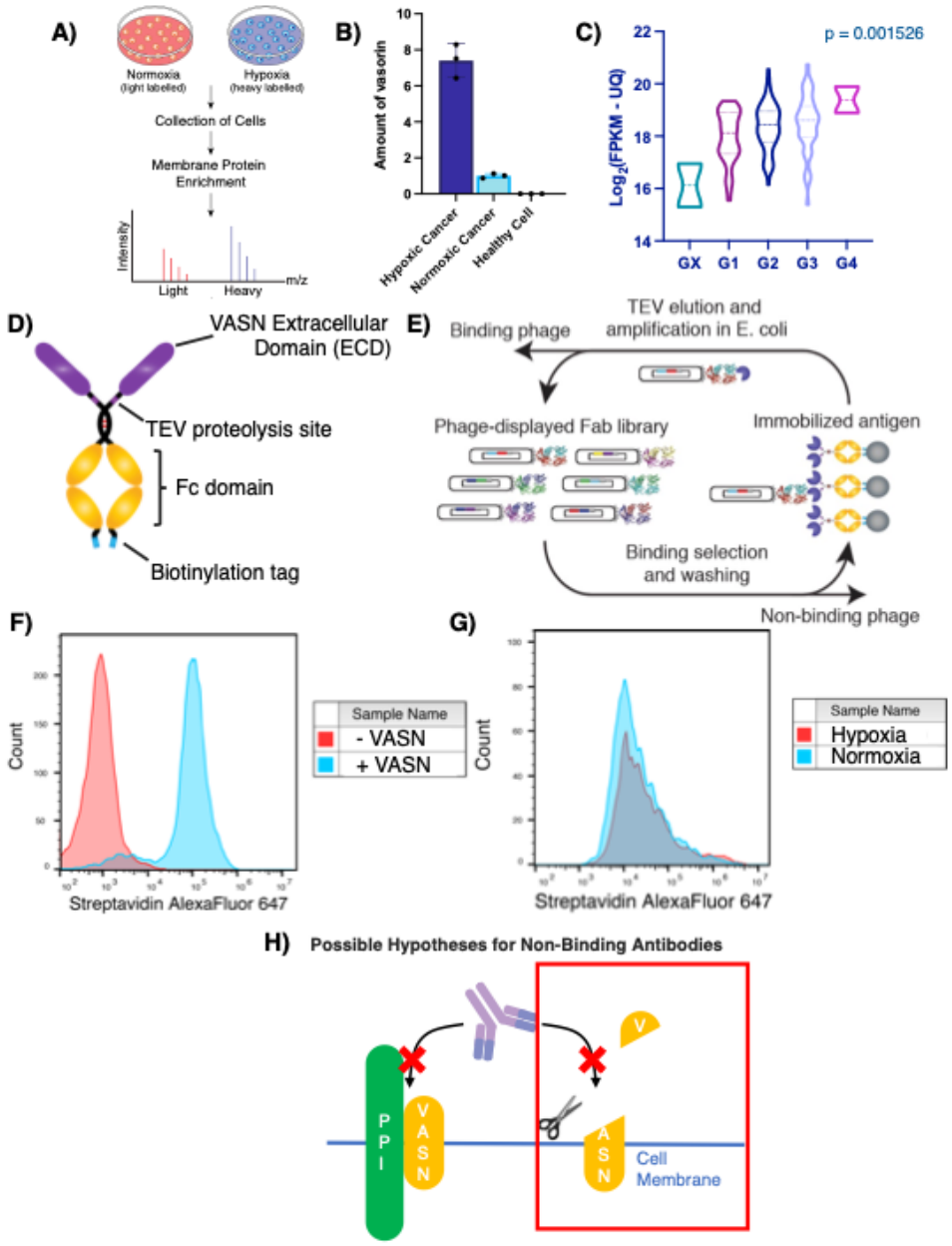

Figure 1.2: Identification and characterization of vasorin (VASN) under hypoxia in Panc-1 cells. (A) Workflow for SILAC based mass spectrometry analysis for hypoxic and normoxic PDAC cells. (B) Fold-increase in VASN expression between hypoxic and normoxic Panc-1 cells after SILAC-based quantitative mass spectrometry. (C) Expression of VASN vs. tumor grade in patients with pancreatic cancer. (D) VASN Fc-fusion antigen used for phage display and downstream antibody isolation. Fc-domain is fused to the extracellular domain of VASN. (E) Four rounds of phage display (100 nM, 50 nM, 10 nM, 10 nM) were performed against VASN-Fc to isolate and purify antibodies. (F) FlpIN cells overexpressing VASN under Dox induction were tested for VASN Fab binding. (G) Anti-VASN Fabs were tested for binding against hypoxic Panc-1 cells over normoxic Panc-1 cells. (H) Possible hypotheses for existence of non-binding Fabs on hypoxic Panc-1 cells.

A)

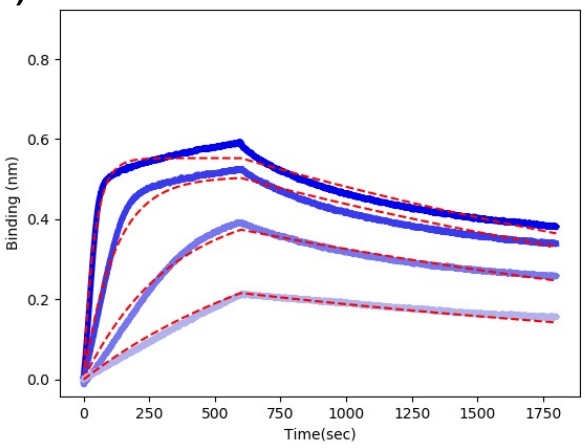

B)

Fab ID	K_D (nM)
C12	1.8 ± 0.001
E02	2.2 ± 0.002
E10	1.2 ± 0.001
G02	1.2 ± 0.0005
G03	2.5 ± 0.002
G09	0.67 ± 0.0008
G12	1.4 ± 0.001
H03	1.5 ± 0.001
H10	0.95 ± 0.0007
H11	1.0 ± 0.0005

Figure 1.3: Biolayer interferometry (BLI) measurements for VASN Fabs. (A) Binding affinity for each Fab was tested at four separate concentrations: 200, 66.6, 22.2, 7.4 nM. (B) Ten unique Fabs were isolated and the K_D measurements were collected using an Octet Red384 (ForteBio) machine.

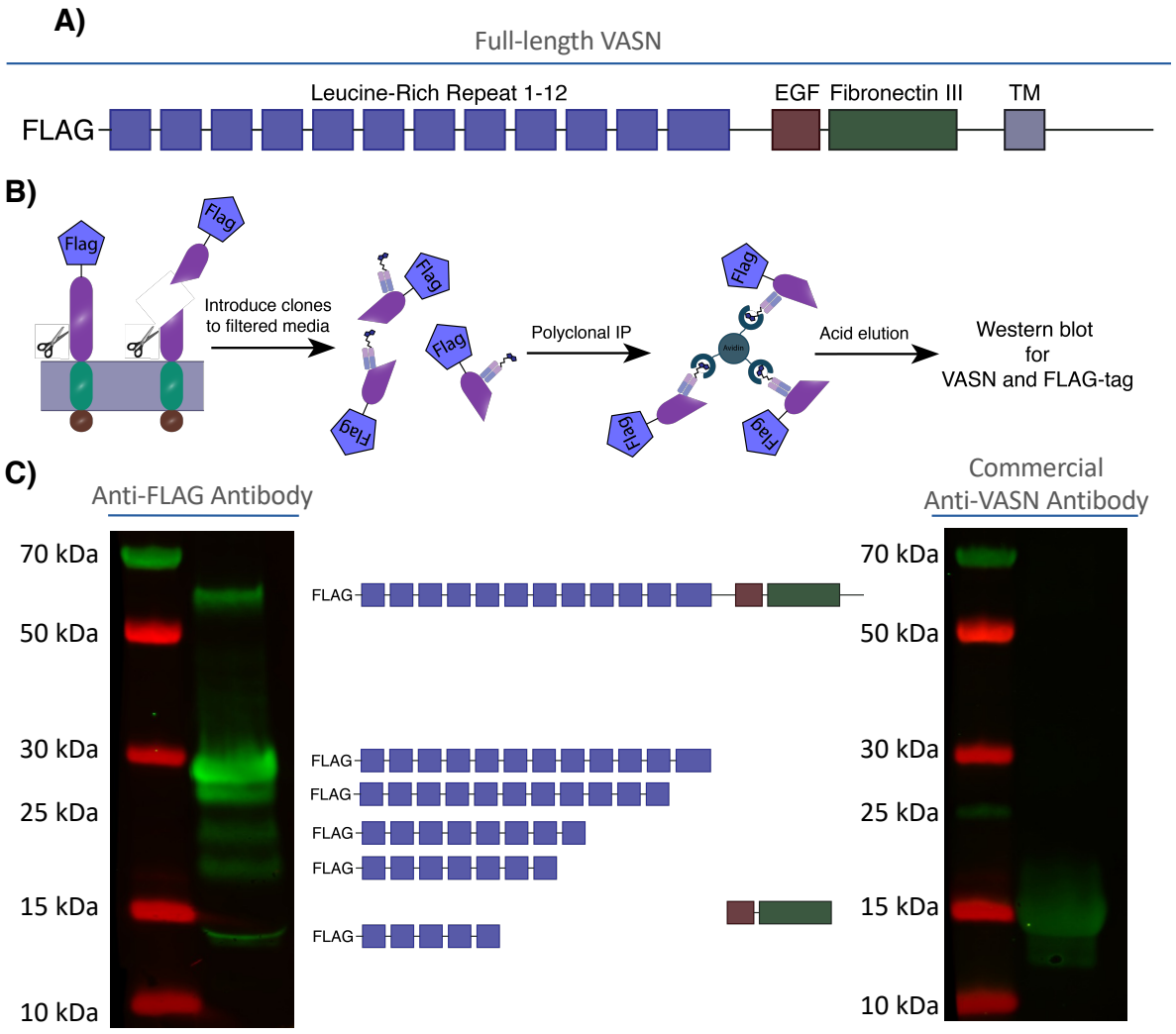

Figure 1.4: Isolation of shed VASN in growth media from Panc-1 cells grown in hypoxia. A) Domain structure of N-terminally FLAG-tagged VASN. B) Workflow for the isolation of shed fragments of VASN from growth media. (C) Western blot images from anti-FLAG and anti-VASN blots after immunoprecipitation of shed fragments from the growth media of hypoxic Panc-1 cells.

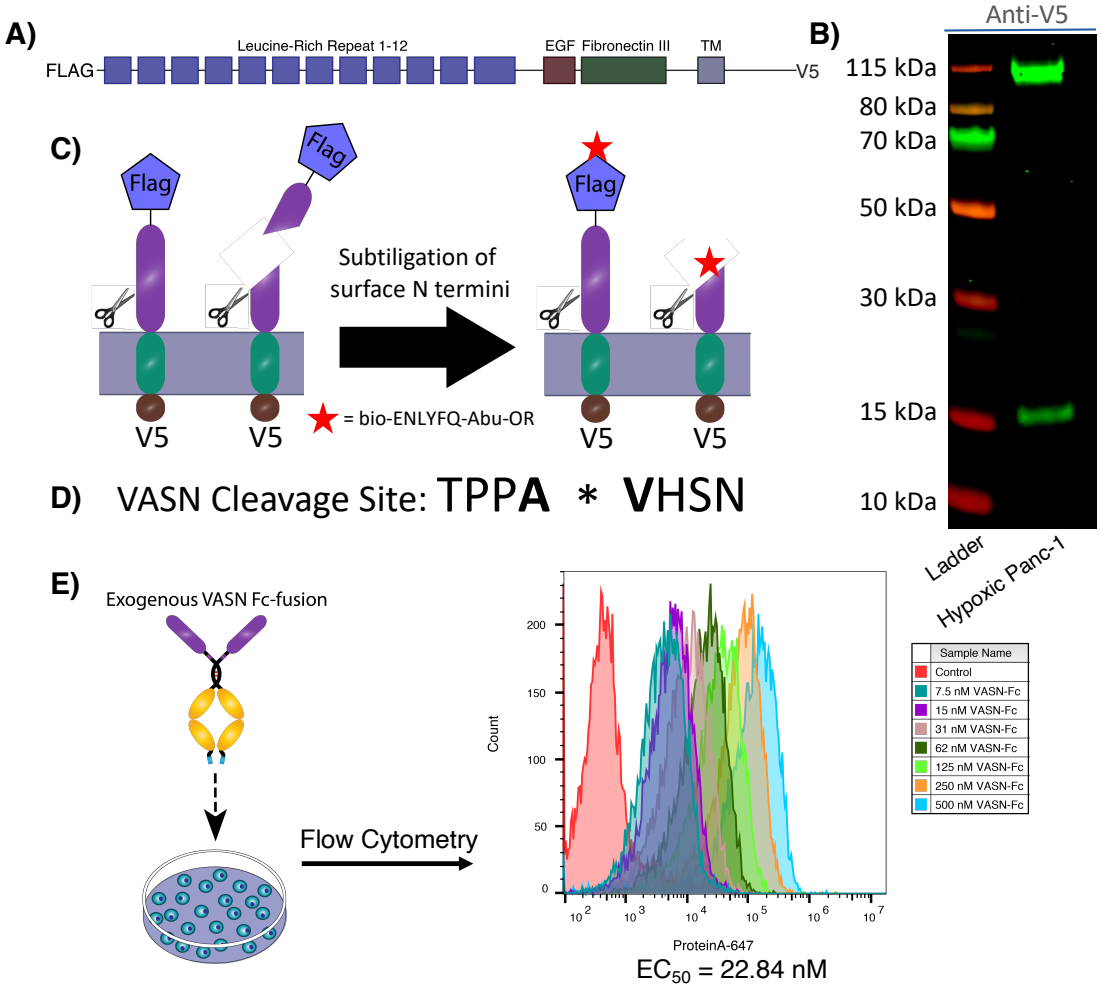

Figure 1.5: Identification and proposed autocrine action of vasorin shed fragment. (A) Domain structure of N-terminally FLAG-tagged, C-terminally V5-tagged VASN. (B) Anti-V5 western blot of hypoxic Panc-1 cells overexpressing V5-tagged VASN shows cleaved form retained at the membrane. (C) Outline of subtiligase peptide ligation towards full-length VASN and cleaved VASN. (D) Identified site of VASN proteolysis. (E) Flow cytometry experiment depicting association of the VASN extracellular domain towards hypoxic Panc-1 cells in a dose-dependent manner.

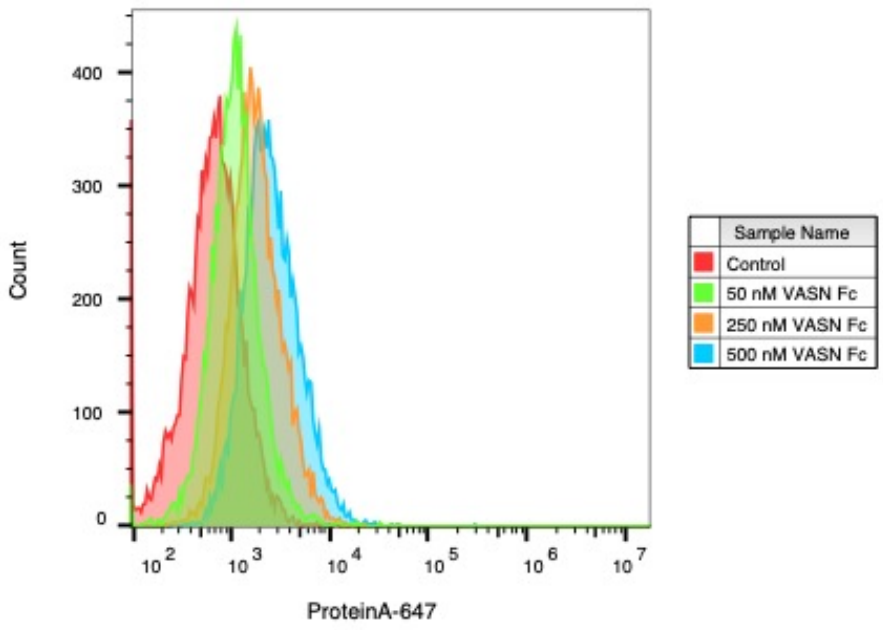

Figure 1.6: VASN ectodomain addition to HUVEC cells. VASN Fc-fusion was added to HUVEC cells at a concentration of 500, 250, and 50 nM and binding was observed through flow cytometry.

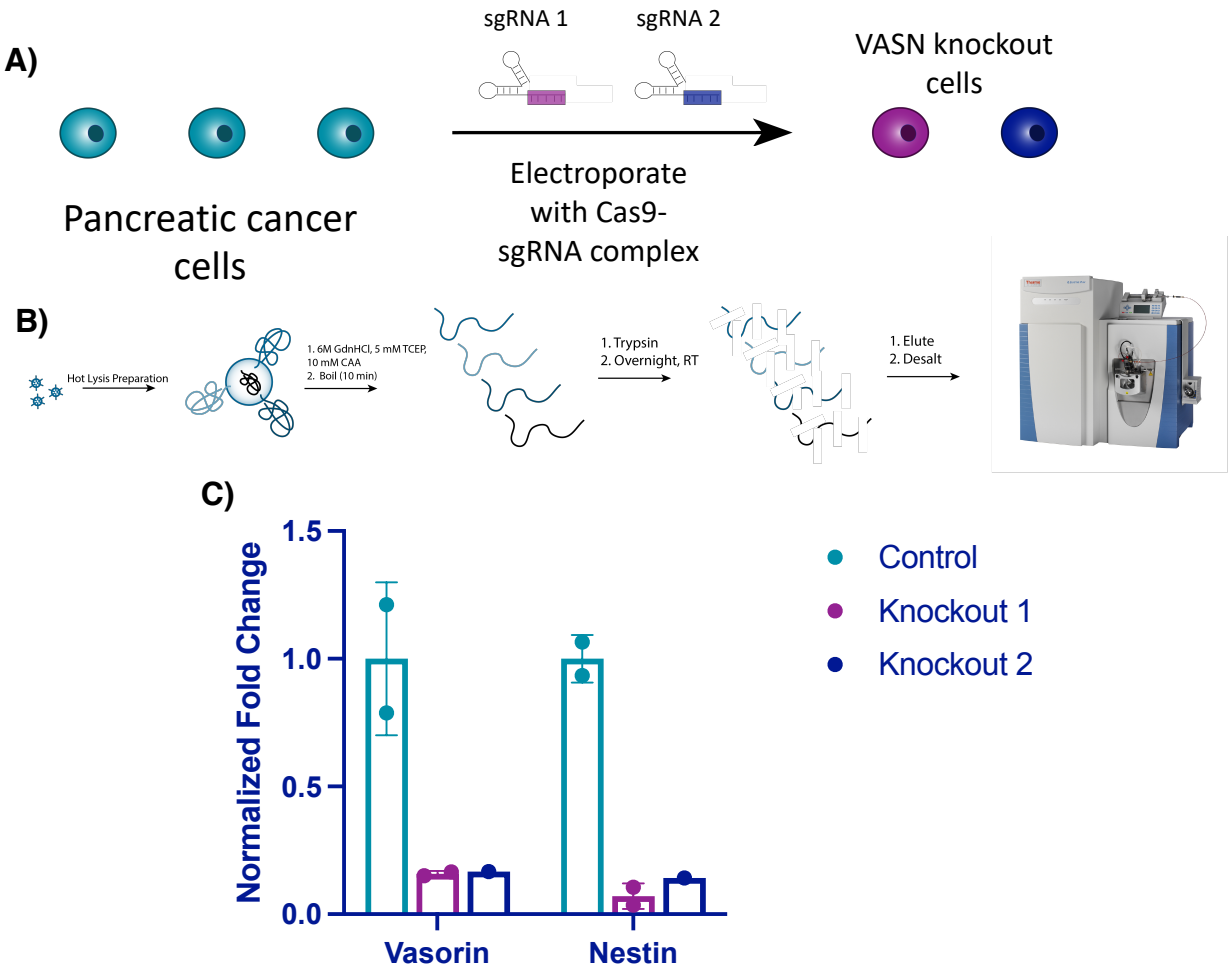

Figure 1.7: Engineering and characterizing Panc-1 cells with and without VASN knockout. A) Panc-1 cells underwent electroporation with CRISPR Cas9 and two different guides against VASN to form two VASN knockout lines. B) Whole cell lysates from control and VASN KO samples were prepared and analyzed by LC-MS/MS. (C) Label free quantification of control and VASN KO cells showed successful KO of VASN and subsequent decrease in Nestin expression.

Chapter 2

Cell-surface tethered promiscuous biotinylators enable comparative small-scale surface proteomic analysis of human extracellular vesicles and cells

Abstract

Characterization of cell surface proteome differences between cancer and healthy cells is a valuable approach for the identification of novel diagnostic and therapeutic targets. However, selective sampling of surface proteins for proteomics requires large samples (>10e6 cells) and long labeling times. These limitations preclude analysis of material-limited biological samples or the capture of rapid surface proteomic changes. Here, we present two labeling approaches to tether exogenous peroxidases (APEX2 and HRP) directly to cells, enabling rapid, small-scale cell surface biotinylation without the need to engineer cells. We used a novel lipidated DNA-tethered APEX2 (DNA-APEX2), which upon addition to cells promoted cell agnostic membrane-proximal labeling. Alternatively, we employed horseradish peroxidase (HRP) fused to the glycan binding domain of wheat germ agglutinin (WGA-HRP). This approach yielded a rapid and commercially inexpensive means to directly label cells containing common N-Acetylglucosamine (GlcNAc) and sialic acid glycans on their surface. The facile WGA-HRP method permitted high surface coverage of cellular samples and enabled the first comparative surface proteome characterization of cells and cell-derived small extracellular vesicles (EV), leading to the robust quantification of 953 cell and EV surface annotated proteins. We identified a newly-recognized subset of EV-enriched markers, as well as proteins that are uniquely upregulated on Myc oncogene-transformed prostate cancer EVs. These two cell-tethered enzyme surface biotinylation approaches are highly advantageous for rapidly and directly labeling surface proteins across a range of material-limited sample types.

Introduction

The cell surface proteome, termed the surfaceome, serves as the main communication hub between a cell and the extracellular environment (Wollscheid et al., 2009). As such, this cellular compartment often reveals the first signs of cellular distress and disease, and is of substantial

interest to the medical community for diagnostic and therapeutic development (Leth-Larsen et al., 2010). The precise and comprehensive profiling of the surfaceome, termed surfaceomics, provides critical insights for our overall understanding of human health and can inform drug development efforts. Several strategies have emerged for either selective or comprehensive surfaceomics, including biocytin hydrazide labeling of surface glycoproteins (Wollscheid et al., 2009), chemical biotinylation of lysines via NHS-ester labeling (Huang, 2012), and promiscuous biotinylator fusion proteins (APEX2, BioID, SPPLAT) (Rees et al., 2015; Sears et al., 2019; Wollscheid et al., 2009). Membrane protein enrichment is a necessary step in surfaceomics, due to the inherent low abundance of membrane proteins compared to cytosolic proteins, and their identification can be overwhelmed by cytosolic contaminants. While each of these strategies robustly label surface proteins, they: (1) require large sample inputs (biocytin hydrazide), (2) require production of genetically engineered cells (APEX2, BioID), (3) label only partner proteins by binding targeting antibodies fused to APEX2 or HRP (SPPLAT), (4) require extensive sample manipulation (biocytin hydrazide), or (4) exhibit increased nonspecific labeling (NHS-ester) (Bausch-Fluck et al., 2012; Elschenbroich et al., 2010; Griffin & Schnitzer, 2011; Kuhlmann et al., 2018). Moreover, many of these methods are not able to capture short and transient changes that occur at the cell surface, such as binding, adhesion, assembly, and signaling (Kalxdorf et al., 2017). These current methods complicate the direct characterization of small clinical samples such as extracellular vesicles in patient serum. As biological research increasingly depends on animal models and patient-derived samples, the requirement for simple and robust methods amenable to direct labelling of material-limited samples for proteomic analysis will become paramount.

Exosomes and other small extracellular vesicles (EVs) are produced by both healthy and diseased cells (Colombo et al., 2014). In cancer, these small EVs contribute to tumor growth and

metastasis, modulate the immune response, and mediate treatment resistance (Al-Nedawi et al., 2008; Edgar, 2016; Kalluri & LeBleu, 2020; Shurtleff et al., 2018). Consequently, these extracellular vesicles are a focus of intense clinical investigation. Recent studies suggest that small EVs incorporate proteins and RNA from the parent tumor from which they originate (Hoshino et al., 2015; Soung et al., 2017), and certain proteins may be preferentially shuttled into EVs (Poggio et al., 2019). There is also strong evidence that cancer-derived EVs are unique from the EVs derived from healthy surrounding tissues, and therefore represent a promising target for non-invasive, early-detection diagnostics or EV-focused therapies (Kalluri & LeBleu, 2020; Skog et al., 2008; Zhou et al., 2020). However, strategies for the unbiased profiling of small EV membrane proteomes remain limited. Isolation of high-quality, enriched small EV populations is challenging, requiring numerous centrifugation steps and a final sucrose gradient isolation, precluding the use of current labeling methods for membrane proteome characterization (Poggio et al., 2019; Shurtleff et al., 2018). Strategies to characterize the surface proteome of small EVs would propel biomarker discovery and enable the differential characterization of small EVs from that of the parent cell. These important studies could help illuminate mechanisms underlying preferential protein shuttling to different extracellular vesicle populations.

Here, we functionalize the promiscuous biotinylators, APEX2 and HRP, as non-cellularly encoded exogenous membrane tethering reagents for small-scale surfaceomics, requiring <5e5 cells. This method is 10-100 fold more rapid than other existing protocols and requires fewer wash steps with less sample loss. Likewise, due to its selectivity towards tyrosines, it is not hindered by variability in individual protein glycosylation status (Leth-Larsen et al., 2010) or by impeding complete tryptic peptide cleavage through modification of lysines (Hacker et al., 2017), like biocytin hydrazide or NHS-biotin methods, respectively. Using this robust new strategy, we

performed surfaceomics on cells and corresponding small EVs from a cellular model of prostate cancer using the prostate epithelial cell line, RWPE-1 with or without oncogenic Myc induction. While certain proteins show increased expression in both parental cell and EV surfaces, a subset of proteins were found to be either pan-EV markers (ITIH4, MFGE8, TF, DSG1, TSPAN14, AZGP1, and IGSF8) or selectively enriched with Myc overexpression in cancer-derived EVs (ANPEP, SLC38A5, FN1, SFRP1, CDH13, THBS1, and CD44). These differentially-regulated proteins pose interesting questions related to preferential protein shuttling, and the proteins upregulated in both cellular and EV contexts reveal candidates for early-stage urine or serum-based detection without invasive surgical intervention. We believe these simple, rapid, and direct surfaceomic labeling tools may be broadly applied to small-scale surfaceomics on primary tissues.

Results

Generation of promiscuous cell-surface tethered peroxidases for exogenous addition to cells

Both APEX2 and HRP are broadly used promiscuous proximity biotinylators that label nearby tyrosine residues in proteins through a radical intermediate mechanism using a biotin-tyramide reagent **(Figure 2.1A)** (Hung et al., 2016; Martell et al., 2016). HRP has been targeted to specific cell-surface proteins through antibody conjugation to label target proteins and their binding partners (Rees et al., 2015). More recently, HRP was used as a soluble cell surface labeler to identify rapid cell surface proteome changes in response to insulin (Y. Li et al., 2021). Genetically encoded, membrane-targeted APEX2 and HRP have also permitted promiscuous labeling of proteins in specific cellular compartments, but these efforts required cellular engineering (Hung et al., 2016; J. Li et al., 2020). We sought to expand the use of these tools to biotinylate surface proteins of cells without the need for cellular engineering, enabling the specific enrichment of surface-resident proteins for mass spectrometry analysis.

The first approach we tested was to tether a DNA-APEX2 conjugate to the cell membrane through a lipidated DNA anchor. Gartner and co-workers have shown lipidated DNA anchors can tether together molecules or even cells (McGinnis et al., 2019; Weber et al., 2014). Here the lipidated DNA is first added to cells, then hybridized with a complimentary strand of DNA conjugated to APEX2 **(Figure 2.1B, left panel)**. To conjugate DNA to APEX2, we leveraged the single unpaired cysteine in the protein for site-specific bioconjugation of the complementary DNA. We first reacted APEX2 with DBCO-maleimide, after which the DBCO moiety was readily conjugated with azido-DNA. The kinetics of coupling was monitored using LC-MS and the conjugate was purified by nickel column chromatography, yielding a single conjugated product **(Figure 2.3A)** that retained full enzymatic function relative to unlabeled APEX2 **(Figure 2.3B)**. Microscopy was used to observe the colocalization of DNA-conjugated APEX2 to the membrane **(Figure 2.1C)**. This result was recapitulated using flow cytometry, indicating that this approach results in surface tethering of APEX2, an important step towards the specific labeling of the cell surfaceome **(Figure 2.3C).**

To avoid the need for bioconjugation, we also tested a commercially available reagent where the promiscuous biotinylator HRP is conjugated to the lectin wheat germ-agglutinin (WGA) **(Figure 2.1, right panel)**. WGA-HRP is used regularly in the glycobiology and neuroscience fields to label cell membranes for immuno-histochemistry and live cell imaging (Mathiasen et al., 2017; T. Wang & Miller, 2016). This is an inexpensive and widely available tool that only requires the presence of surface protein N-acetylglucosamine (GlcNAc) and sialic acid glycans to localize HRP to the membrane. The successful and rapid colocalization of WGA-HRP to the plasma membrane compared to HRP alone was verified using immunocytochemistry, indicating this approach is a potential alternative for cell surface labeling **(Figure 2.1D)**. Further testing showed

that adding WGA-HRP to cells in the presence hydrogen peroxide and biotin-tyramide led to robust surface labeling even with no pre-incubation time **(Figure 2.4)**.

Cell-tethered biotinylators more effectively label the surfaceome than non-tethered biotinylators and are comparable to biocytin hydrazide

Next, we set out to optimize labeling conditions for small-scale sample characterization. As APEX2 is kinetically slower than HRP (Lam et al., 2015), we used APEX2 to establish a suitable concentration range of enzyme for cell surface labeling. We found that 0.5 μM APEX2 produced maximal labeling of cells **(Figure 2.6A)** and maintained equivalent labeling across a range of cell numbers (2.5e5 – 1e6 cells; **Figure 2.6B**). Next, we compared the efficiency of DNA-APEX2, WGA-HRP, and their non-tethered counterparts to biotinylate a small sample of 5e5 Expi293 cells. We found a 5- to 10-fold increase in biotin labeling for both tethered DNA-APEX2 and WGA-HRP relative to non-tethered controls as assessed by flow cytometry **(Figure 2.5A)** and western blotting **(Figure 2.5B)**. Moreover, tethered DNA-APEX2 and WGA-HRP systems exhibited similar biotinylation efficiency, suggesting either system is suitable for small-scale surfaceomics. Having both systems is useful, as some cells may not widely express glycoproteins recognized by commercially available lectin-HRP conjugates—such as some prokaryotic species—and therefore could require the glycan-agnostic DNA-tethered APEX2 construct (Schäffer & Messner, 2017).

To compare the degree of surface protein enrichment these two systems offer, we enriched biotinylated proteins generated with either approach and compared the resulting enrichments using LC-MS/MS. As an initial efficacy comparison, cell surface labeling with DNA-labeled APEX2 or WGA-HRP was compared using 5e5 cells. In order to eliminate the possibility of suspension cell-specific results, we used a popular cell line model of pancreatic cancer, KP-4. We observed that the WGA-HRP identified slightly more plasma membrane annotated proteins in the Uniprot Gene

Ontology Cellular Component Plasma Membrane (GOCC-PM) database (>2 unique peptides, found in all replicates) relative to DNA-APEX2, totaling 501 and 467, respectively. Notably, the number of IDs for both cell-tethered enzymes was higher than their untethered counterparts, with HRP identifying 389 cell surface proteins and APEX2 identifying 247 **(Figure 2.5C)**. Importantly, in the upset plot shown, the group with the highest intersection includes all four enzyme contexts, showcasing the reproducibility of labeling through a similar free-radical based mechanism. The cell-tethered biotinylators also showed heightened surface enrichment compared to their untethered counterparts, as illustrated by the higher overall intensities for proteins annotated to the plasma membrane **(Figure 2.7A-B)**. As equal amounts of total protein is injected on the LC-MS/MS instrument, the higher intensities for plama membrane proteins suggest that localizing the enzyme to the membrane increases labeling of the membrane compartment, which we have previously observed with other enzymatic reactions (Weeks et al., 2021).

As the mode of tethering WGA-HRP involves GlcNAc and sialic acid glycans, we wanted to determine whether there was a bias towards Uniprot annotated 'Glycoprotein' vs 'Non-Glycoprotein' surface proteins identified across the WGA-HRP, APEX2-DNA, APEX2, and HRP labeling methods. We looked specifically at surface annotated proteins found in the SURFY database, which is the most stringent surface protein database and requires that proteins have a predicted transmembrane domain (Bausch-Fluck et al., 2018). We performed this analysis by measuring the average MS1 intensity across the top three peptides (LFQ area) for SURFY glycoproteins and non-glycoproteins for each sample and dividing that by the total LFQ area found across all GOCC-PM annotated proteins detected in each sample. We found similar normalized areas of non-glycosylated surface proteins across all samples **(Figure 2.8)**. If a bias existed towards glycosylated proteins in the WGA-HRP compared to the glycan agnostic APEX2-DNA sample,

then we would have seen a larger percentage of non-glycosylated surface proteins identified in APEX2-DNA over WGA-HRP. Due to the large labeling radius of the HRP enzyme, we find it unsurprising that the WGA-HRP method is able to capture non-glycosylated proteins on the surface to the same degree (Rees et al., 2015). There is a slight increase in the area percentage of glycoproteins detected in the WGA-HRP compared to the APEX2-DNA sample, but this is likely due to the fact that a greater number of surface proteins in general are detected with WGA-HRP. As HRP is known to have faster kinetics compared to APEX2, it was anticipated that WGA-HRP would outperform DNA-APEX2 in cell surface protein identifications. The heightened labeling of WGA-HRP was consistent with every cell line tested, including another pancreatic cancer model, PaTu8902, which resulted in more proteins identified in the WGA-HRP sample over DNA-APEX2 for both 1 and 2 minute time points **(Figure 2.9)**.

To confirm that the improved labeling by WGA-HRP was due to the binding of sugar units on the cell surface, we performed a sugar-blocking experiment with WGA-HRP using N-acetyl-D-glucosamine (GlcNAc) that would block the conjugate from binding to the cell. By pre-incubating WGA-HRP with excess GlcNAc, the ability of WGA-HRP to label the cell surface was markedly lower than WGA-HRP without GlcNAc as observed by microscopy **(Figure 2.5D)**. A similar effect was also seen by flow cytometry **(Figure 2.10)**. In addition, we also tested an on-plate protocol for simpler cell surface labeling of adherent KP-4 cells. We showed that cell surface labeling in this manner was comparable to labeling when the cells were in suspension **(Figure 2.11)**.

As WGA-HRP consistently outperformed DNA-APEX2 by proteomics and represents a more facile method amenable to broad application in the field, we chose to compare the proteomic labeling results of WGA-HRP to other standard cell surface labeling methods (sulfo-NHS-LC-LC-

biotin and biocytin hydrazide) on a prostate epithelial cell line, RWPE-1 with and without oncogenic c-Myc overexpression. Sulfo-NHS-LC-LC-biotin reacts with primary amines to form amide conjugates, but has notoriously high background contamination with intracellular proteins (Weekes et al., 2010). Biocytin hydrazide labeling is a two-step process that first involves oxidizing vicinal diols on glycoproteins at the cell surface, then reacting the aldehyde byproducts with biocytin hydrazide (Elschenbroich et al., 2010). Both WGA-HRP and biocytin hydrazide had similar levels of cell surface enrichment on the peptide and protein level when cross-referenced with the SURFY curated database for extracellular surface proteins with a predicted transmembrane domain **(Figure 2.13A)**. Sulfo-NHS-LC-LC-biotin and whole cell lysis returned the lowest percentage of cell surface enrichment, suggesting a larger portion of the total sulfo-NHS-LC-LC-biotin protein identifications were of intracellular origin, despite the use of the cell-impermeable format. These same enrichment levels were seen when the datasets were searched with the curated GOCC-PM database, as well as Uniprot's entire human proteome database **(Figure 2.13B)**. Of the proteins quantified across all four conditions, biocytin hydrazide and WGA-HRP returned higher overall intensity values for SURFY-specified proteins than either sulfo-NHS-LC-LC-biotin or whole cell lysis. Importantly, although biocytin hydrazide shows slightly higher cell surface enrichment compared to WGA-HRP, we were unable to perform the comparative analysis at 500,000 cells--instead requiring 1.5 million--as the protocol yielded too few cells for analysis. All three methods were highly reproducible across replicates **(Figure 2.14A-C)**. Compared to existing methods, WGA-HRP not only labels cells efficiently with much lower input material requirements, it is also able to enrich for cell surface proteins to a similar extent in a fraction of the time.

WGA-HRP identifies surface markers of Myc-driven prostate cancer in both cells and small EVs

Prostate cancer remains one of the most common epithelial cancers in the elderly male population, especially in Western nations (Litwin & Tan, 2017; Rawla, 2019). While metastatic progression of prostate cancer has been linked to many somatic mutations and epigenetic alterations (PTEN, p53, Myc etc.), more recent work determined that alterations in Myc occurs in some of the earliest phases of disease, i.e. in tumor-initiating cells (Koh et al., 2010). This finding promotes the idea that the development of early-stage diagnostic tools that measure these Myc-driven disease manifestations could improve detection and overall patient disease outcomes (Koh et al., 2010; Rebello et al., 2017). One mode of early detection that has gained prominence is the use of prostate cancer-derived exosomes in patient serum and urine (Duijvesz et al., 2013; McKiernan et al., 2016). Small EVs are known to play important roles in the progression of prostate cancer, including increasing tumor progression, angiogenesis, metastasis, and immune evasion, making this subcellular particle an extremely informative prognostic tool for disease progression (Akoto & Saini, 2021; Lorenc et al., 2020; Saber et al., 2020).

To elucidate promising targets in Myc induced prostate cancer, we utilized our WGA-HRP method to biotinylate cells from both normal epithelial prostate cells (RWPE-1 Control) and oncogenic Myc-induced prostate cancer cells (RWPE-1 Myc, **Figure 2.12A**). Importantly, by using an isogenic system, we are able to delineate specific Myc-driven protein expression changes, which could be helpful in the identification of non-invasive, early-detection diagnostics for cancer driven by early Myc induction. In addition to having marked overexpression of c-Myc in the RWPE-1 Myc cells compared to Control, they also grow with a more mesenchymal and elongated morphology compared to their Control cell counterparts **(Figure 2.12B)**, which would suggest

large cell surface changes upon oncogenic Myc induction. We initially used WGA-HRP to quantitatively compare the cell surface profiles of Myc-induced prostate cancer to Control cells and found large and bidirectional variations in their surfaceomes **(Figure 2.12C, 2.12D)**. We have highlighted the 15 most upregulated proteins in each cell type that are annotated as extracellular surface proteins in the GOCC-PM database. Proteins that are also found in the most restrictive SURFY database that requires a predicted transmembrane domain are bolded in the figure. Proteins annotated to be secreted (Uniprot) from the cell are italicized (Bausch-Fluck et al., 2018). Vimentin, a marker known to be associated with epithelial-to-mesenchymal transition (EMT) showed heightened expression, in the context of oncogenic Myc, as well as CDH2 (N-Cadherin), another marker of EMT **(Figure 2.12D)** (Liu et al., 2015; Nakajima et al., 2004). While vimentin has traditionally been described as an intracellular protein, an extracellular membrane-bound form has been found to be important in the context of cancer (Mitra et al., 2015; Noh et al., 2016). ANPEP and fibronectin-1 were also highly upregulated. Notably, a number of HLA molecules were downregulated in the Myc induced RWPE cells, consistent with prior findings of loss of MHC class I presentation in prostate cancer (Blades et al., 1995; Cornel et al., 2020; Dhatchinamoorthy et al., 2021). A subset of these findings were verified by both western blot **(Figure 2.12E)** and microscopy **(Figure 2.12F)**, which highlights the robustness of the protein quantification afforded by using this method.

Next, we wanted to use our WGA-HRP method to quantify cell surface proteins on a sucrose-gradient purified population of small EVs derived from both normal epithelial prostate cells (RWPE-1 Control) and oncogenic Myc-induced prostate cancer cells (RWPE-1 Myc, **Figure 2.15A**). While sucrose gradient centrifugation generally yields a mixture of vesicle populations, we wanted to confirm that our preparation enriched for vesicles originating from multiple vesicular

bodies (MVBs), consistent with an exosome-enriched sample (Mathieu et al., 2021). To do so, we prepared EVs from both Control and Myc cells and carried out label-free quantification (LFQ) mass spectrometry on the whole EV lysates. After normalizing for cell number, we found the Myc cells produced nearly 40% more EVs than the corresponding control cells, which is consistent with previous work that has shown Myc overexpression yields higher quantities of EVs (Kilinc et al., 2021). After averaging the intensities between Control and Myc derived EVs, many of the highest intensity proteins (CD9, SDCB1, CD81, LAMP1, LAMP2, ALIX, and CD63) are consistent with MVB-derived vesicle biogenesis, supporting that the sample was likely enriched in EVs rather than other sedimentable particles that can co-isolate during centrifugation **(Figure 2.15B)**. Due to the complex process and extensive washing involved in small EV isolation, many standard labeling methods are not amenable for EV surface labeling. Using WGA-HRP, we are able to biotinylate the small EVs before the sucrose gradient purification and isolation steps **(Figure 2.15C)**. This delineated an important subset of proteins that are differentially expressed under Myc induction, which could serve as interesting targets for early-detection in patient urine or serum **(Figure 2.15D)**. This subset included fibronectin-1 (FN1) and ANPEP **(Figure 2.15E)**, which were further validated by quantitative western blotting **(Figure 2.15F)**. A subset of these targets display similar phenotypic changes to the parent cell, suggesting that they could be biomarker candidates for non-invasive indicators of disease progression. While certain proteins are shuttled to vesicle compartments largely based off of the extent of expression in the parent cell (Control: IFITM3, BST2, HLA-B, Myc: ANPEP, SLC38A5, FN1), remarkably some proteins are singled out for small EV packaging, indicating a pronounced differential shuttling mechanism of the proteome between cells and EVs. This pattern was recapitulated in both the RWPE-1 Control cells and corresponding EVs, as well as the Myc cells and EVs, where the majority of markers were unique

to either cellular or EV origin **(Figure 2.16A-2.16B)**. These protein targets are of extreme interest for not only biomarker discovery, but also understanding the role of small EVs in secondary disease roles, such as interfering with immune function or priming the metastatic niche (Costa-Silva et al., 2015).

Due to the difficulty of proteomic characterization of vesicular populations, our current understanding of EV protein shuttling remains limited. Prior proteomic EV analysis has involved whole EV preparations, which lacks a surface protein enrichment step (Bandu et al., 2019; Bilen et al., 2017; Hosseini-Beheshti et al., 2012). Not only is whole EV lysate analysis less advantageous for the specific identification of cell surface proteins on EVs, but it makes it impossible to compare cellular and EV samples due to the inherent surface area-to-volume differences between cells and the vesicles they produce (Doyle & Wang, 2019; Santucci et al., 2019). Our WGA-HRP method allows us to compare surface proteins between small EV populations, as well as between small EV and cell samples **(Figure 2.17A)**. By principle component analysis (PCA), each sample separates by oncogenic status and origin **(Figure 2.17B)**. Indeed, when performing functional annotation for each gene cluster defined by the PCA, 'extracellular exosome' and 'extracellular vesicle' are the highest ranking annotation features differentiating the EVs from their parent cells **(Figure 2.17C)**. Through this comparison, we were able to delineate a host of proteins that were upregulated in EVs over their parent cells and vice versa **(Figure 2.17D)**. Notably, secreted proteins were more highly represented in the EV surface proteome compared to cells. A subset of proteins were highly upregulated in the small EVs compared to parent cell, including ITIH4, MFGE8, TF, DSG1, TSPAN14, AZGP1, and IGSF8, **(Figure 2.17E)** and a subset of the findings were validated by western blot **(Figure 2.17F)**. The samples showed good overlap between replicates across all four datasets, with cellular and EV

samples clustering by origin and oncogenic status **(Figure 2.18)**. To our knowledge, this is the first experiment to wholistically characterize the surface proteome of both small EVs and parental cells. These data strongly suggest that protein triage into EVs is a controlled process, enabling only a subset of the cell surface proteome to be shuttled to this important compartment. Our data shows that there are a variety of pan-prostate-EV markers, notably lactadherin (MFGE8), serotransferrin (TF), inter-alpha-trypsin inhibitor (ITIH4), immunoglobulin superfamily 8 (IGSF8), desmoglein-1 (DSG1), tetraspanin-14 (TSPAN14), and zinc-alpha-2-glycoprotein (AZGP1) **(Figure 2.17D)**, which do not seem to be Myc-specific. Some of the pan-prostate EV targets in our data have previously been linked to cancer-specific contexts, and we show here that they are also found on Control EVs (Philley et al., 2017; Shimagaki et al., 2019; Tutanov et al., 2020). Our work suggests that these markers are more broadly associated with small EVs, regardless of disease status, outlining an expanded set of targets to probe these vital compartments.

Discussion

The importance of understanding and characterizing cellular and EV membrane compartments is vital for improving our understanding of vesicle biogenesis. New, improved methodologies amenable to small-scale and rapid surface proteome characterization are essential for continued development in the areas of therapeutics, diagnostics, and basic research. We sought to develop a simple, rapid surface protein labeling approach that was compatible with small sample sizes, while remaining specific to the cell surface. We took advantage of fast peroxidase enzymes and either complementary lipidated DNA technology (DNA-APEX2) or the glycan binding moiety wheat germ agglutinin (WGA-HRP) and demonstrated that tethering was much more effective than soluble addition, with increases in protein identification of between 30-90%. Additionally, we

compared WGA-HRP to the existing methods, sulfo-NHS-LC-LC-biotin and biocytin hydrazide. While these alternative methods are robust, they are unable to capture time-sensitive changes, and are either plagued by low selectivity/specificity (NHS-Biotin) (Weekes et al., 2010) or the requirement for large sample inputs (biocytin hydrazide).

There are many advantages of our new methods over the current cell surface labeling technologies. Compared to both sulfo-NHS-LC-LC-biotin and biocytin hydrazide, WGA-HRP experiments require 2 minutes instead of 30 or 120 minutes, respectively. It is also able to enrich cell surface proteins much more efficiently than sulfo-NHS-LC-LC-biotin labeling. Furthermore, NHS peptide isolation and preparation is complicated due to the reactivity of NHS chemistry towards free-amines, which blocks tryptic and LysC cleavages typically used in proteomics (Chandler & Costello, 2016; Hacker et al., 2017).

The hydrazide method is highly effective for enriching cell surface proteins, but it is challenging for small sample sizes, due to the two-step labeling process and cell loss from the oxidation step and extensive washing. Additionally, neither NHS-biotin nor biocytin hydrazide are able to capture short time points to encompass dynamic changes at the cell surface. Due to the fast kinetics of peroxidase enzymes (1-2 min), our approaches could enable kinetic experiments to capture rapid post-translational trafficking of surfaces proteins, such as response to insulin, certain drug treatments, T-cell activation and synapse formation, and GPCR activation (Gupte et al., 2019; Y. Li et al., 2021; Valitutti et al., 2010). Another disadvantage of the hydrazide method is that it can only enrich for proteins that are glycosylated at the cell surface and it is estimated that 10-15% of cell surface proteins are not glycosylated (Apweiler, 1999). Glycosylation patterns also readily change during tumorigenesis, which can alter the quantification of glycan-based labeling methods, such as biocytin hydrazide (Reily et al., 2019). While the WGA-HRP method requires glycosylated

proteins to be present to bind, it is still able to label non-glycosylated proteins nearby due to its large labeling radius. It is a possibility that certain cells may have low or uneven levels of glycosylation on their surfaces. In these cases, the DNA-APEX2 method can be utilized to obtain effective labeling. However, both these peroxidase-based methods require the presence of tyrosine residues (natural abundance 3.3%) to react with the biotin-tyramide radical, which is not equally abundant in all proteins (Dyer, 1971).

With the WGA-HRP method, we were able to compare the surfaceome of small EVs to parental cells for Myc-induced prostate cancer cells and identified proteins that were upregulated in Myc-induced cells and EVs, as well as proteins that were differentially shuttled between EVs and parental cells. We found a number of Myc specific markers in our study, which were enriched in both Myc EV and Myc Cell samples. These include ANPEP, SLC38A5, FN1, CDH13, VIM, and CA12. ANPEP is a membrane-bound ectopeptidase that degrades N-termini with neutral amino acids and was found 140-fold upregulated in the Myc-induced cell compared to the Control cell and 49-fold upregulated in the Myc-induced EV compared to Control EV. This peptidase has been associated with angiogenesis and cancer growth (Guzman-Rojas et al., 2012; Sørensen et al., 2013; Wickström et al., 2011). Recent studies have shown ANPEP is systematically upregulated on isogenic cell lines expressing proliferative oncogenes (Leung et al., 2020; Martinko et al., 2018b) or in tubular sclerosis bladder cancers (Wei et al., 2020), suggesting it is commonly upregulated in cancers. The second most differentially expressed protein between the Myc and Control samples was SLC38A5 (23 and 73-fold upregulated in cells and EVs, respectively). SLC38A5 is a glutamine co-transporter and has previously been shown to be a downstream target of c-Myc in glutamine-addicted cancers. Moreover, given that SLC38A5-based glutamine transport leads to proton flux and intracellular alkanization, overexpression of SLC38A5 has also

been hypothesized to be a strategy for pH regulation in cancer cells that regularly experience intracellular acidification due to high glycolytic flux (Bhutia & Ganapathy, 2016; Wise et al., 2008). Additionally, Fibronectin-1 (FN1) was also found to be upregulated in Myc samples over Control samples (5 and 63-fold upregulated in cells and EVs, respectively), and has been shown to drive all stages of tumorigenesis (J. P. Wang & Hielscher, 2017). Importantly, FN1 provides an extracellular scaffold by which other matrix proteins can be deposited. Through these interactions with matrix proteins and cell-associated integrins, FN1 regulates cellular fate decisions, proliferation, and metastasis (Efthymiou et al., 2020).

While some proteins were present in both the EV and cellular samples, others were only found enriched in Myc EVs. THBS1, also known as thrombospondin-1 was over 10-fold upregulated in Myc EVs over Control EVs. Interestingly, this relationship was not found in the parent cells, which suggests that THBS1 is differentially shuttled into oncogenic EVs. The role of this protein has newly been associated with the growth and metastasis of glioblastoma and a potential serum prognostic factor in myeloid leukemia (Daubon et al., 2019; Zhu et al., 2020). Moreover, using a model of THBS1 overexpressing breast cancer, recent work has shown that exosomes laden with THBS1 promote cancer cell migration via disruption of the endothelial barrier (Cen et al., 2019).

Another such target is CD44, which was over 8-fold upregulated in the Myc EVs over Control EVs. CD44 has long been known to drive cancer progression and aberrant cell signaling (Chen et al., 2018). Recently, CD44 has also been found to be preferentially loaded into cancer-derived exosomes and has been implicated in driving chemoresistance in a model of doxorubicin-treated breast cancer (Zhu et al., 2020). Similarly, it has been shown that exosome-mediated transfer of CD44 from cells with high metastatic potential promoted migratory behavior in

neighboring cells with low metastatic potential (Shen et al., 2021). These targets delineate an important subset of proteins that are triaged into EVs and could play long-range roles in promoting tumorigenesis and downstream metastasis (Costa-Silva et al., 2015; Demory Beckler et al., 2013; Hoshino et al., 2015; Peinado et al., 2012).

As research shifts into analyzing native biological samples from extracellular vesicles to xenograft models or patient biopsies, it will become increasingly important to develop sensitive, effective methods to label these small samples sizes. It is our hope that these tools will provide much needed avenues by which to pursue pressing biological questions in the areas of diagnostic and therapeutic development, as well as basic research.

Materials and Methods

Large-Scale APEX2 Expression, Purification, and Heme Reconstitution

APEX2 was expressed using previous methods in BL21(DE3)pLysS cells (Howarth & Ting, 2008). Briefly, APEX2 expression plasmid was transfected into competent BL21(DE3)pLysS cells and heat shocked for 45 seconds before being placed on ice. Cells were plated on LB/Carb plates and grown overnight at 37°C. A single colony was isolated and grown in a mixture of 30 ml of 2XYT + Carb overnight at 37°C while shaking. The overnight culture was combined with 3 L of 2XYT with Carb and placed in a 37°C shaking incubator. At an OD600 of 0.6, 100 µg/ml of IPTG was added and the temperature of the incubator was lowered to 30°C. Cells were allowed to incubate for 3.5 hours and were spun down at 6,000xg for 20 minutes. Cell pellet was resuspended in protease inhibitor containing resuspension buffer (5 mM Imidazole, 300 mM NaCl, 20 mM Tris pH=8) and mixed thoroughly. The mixture was sonicated at 50% (5 seconds on:15 seconds off) for 5 minutes on ice to avoid bubble formation. Lysate was mixed by inversion at 4°C for 15 minutes and spun down at 19,000xg for 20 minutes. The slurry was introduced to 5 ml of washed

Nickel resin slurry and allowed to bind by gravity filtration. The beads were washed 3x with wash buffer (30 mM Imidazole, 300 mM NaCl, 20 mM Tris pH=8) and eluted in 5 ml of elution buffer (250 mM Imidazole, 300 mM NaCl, 20 mM Tris pH=8) before undergoing buffer exchange into PBS.

Enzyme underwent heme reconstitution as per previous methods (Cheek et al., 1999). Briefly, 50 mg of hemin-Cl (Sigma) was diluted in 2.0 mL of 10 mM NaOH. The mixture was thoroughly resuspended, then diluted further using 8.0 mL of 20 mM KPO_4, pH 7.0, and vortexed extensively. Mixture was spun down at 4,000xg 2x to eliminate insoluble hemin. APEX2 was diluted 1:2 in 20 mM KPO_4. 6 ml of heme stock was added to 2 ml of APEX over 20 minutes and allowed to rotate at 4°C wrapped in tin foil for 3 hours. The mixture was introduced to a column with 20 ml of DEAE Sepharose pre-equilibrated in 20 mM KPO_4, pH 7.0 buffer. Enzyme was eluted using 100 mM KPO_4 and spin concentrated. To verify complete reconstitution, absorbance was measured at 403 and 280 nm. A403/280 > 2.0 is considered sufficient for reconstitution. The isolated protein was flash frozen and stored at -80°C for long-term storage. Each batch of enzyme was run out on a 4-12% Bis-Tris gel to confirm purity **(Figure 2.2)**.

APEX2 DNA labeling protocol

APEX2 was incubated at 50 μM with 40 molar equivalents of maleimide-DBCO for 5 hours at room temperature in PBS. The reaction was desalted with Zeba columns (7 kDa cutoff). 2.5 molar equivalents of Azido-DNA was added to the reaction and incubated at 4°C overnight. Successful conjugation was monitored by LC-MS before the mixture was purified by nickel column.

Cell culture

Prior to all experiments, cells were tested for the presence of mycoplasma (MycoAlert PLUS, Lonza, LT07-703). Expi293 suspension cells were maintained in Expi293 media (Thermo, A1435101) while rotating at 125 rpm in a 37°C incubator with 8% CO_2. Cells were split every 3 days by diluting into new media. Adherent PaTu8902 and KP-4 cells were grown in pre-warmed Iscove's Modified Dulbecco's Media (IMDM) supplemented with 10% FBS (Gemini Bio-Products, 100-106) and 5% Penicillin/Streptomycin (Thermo Fisher Scientific, 15-140-122) at 37°C in a 5% CO_2-humidified incubator. Adherent RWPE-1 prostate cells were grown in complete keratinocyte-SFM (Thermo; 17005-042) supplemented with bovine pituitary extract (BPE), recombinant EGF, and 5% penicillin/streptomycin at 37°C in a 5% CO_2-humidified incubator. The media was exchanged every two days. For splitting, cells were lifted with 0.05% Trypsin (Life Technologies) and quenched with 5% FBS before spinning down cells to remove residual trypsin and FBS. Cells were then plated in pre-warmed complete keratinocyte-SFM media.

Microscopy

Cells were plated at a density of 15,000 cells per well in a 96-well clear bottom plate (Greiner Bio-One, 655090) pre-treated with poly-D-lysine (Thermo Scientific, A3890401). Cells were allowed 48 hours to reattach and grow undisturbed. Cells were washed 3x in cold PBS. For DNA-APEX2, 100 µl of 0.5 µM enzyme solution was combined with anchor and co-anchor at a final concentration of 1 µm. For all other enzymes, enzyme was combined with PBS at a final concentration of 0.5 µM. For sugar blocking studies, 100 µl of diluted enzyme solution (0.5 µM) was combined with 100 mg/ml N-acetyl-D-glucosamine (Sigma Aldrich, A3286-5G). Cells were allowed to sit on ice for 5 minutes to allow WGA to bind fully, as labeling was not altered by increased incubation time (**Figure 2.4)**. Biotin tyramide (Sigma Aldrich, SML2135-50MG) was

added to cells with a final concentration of 500 μM before adding 1 mM of H_2O_2. Reaction was allowed to continue for 2 minutes before rinsing cells 3x with 1X quench buffer (10 mM sodium ascorbate + 5 mM Trolox + 1 mM sodium pyruvate). The cells were rinsed 2x with PBS and crosslinked with 4% PFA for 10 minutes at RT. Cells were washed 3x with PBS before introduction to 1:100 primary antibody. Primary antibodies used were: HisTag-650 (Invitrogen, MA1-21315-D650), Streptavidin-488 (Thermo Fisher Scientific, S-11223), biotin-conjugated anti-HRP (Rockland, 200-4638-0100), ANPEP (R&D Systems, AF3815), vimentin (Cell Signaling Technology, 5741S), and HLA-B (ProteinTech, 17260-1-AP). Cells were washed 3x in PBS and imaged on an IN Cell Analyzer 6500. Images were processed in Fiji using the Bio Formats plugin (Linkert et al., 2010; Schindelin et al., 2012).

Cell-tethered APEX2, soluble APEX2, cell-tethered WGA-HRP and soluble HRP cell surface labeling

Cultured cells were grown for 3 days in tissue culture plates and dissociated by addition of versene (PBS + 0.05% EDTA). Cells were washed 3x in PBS (pH 6.5), resuspended in PBS (pH 6.5) and aliquoted to 500,000 cells per sample. Samples were resuspended in 100 μL of PBS (pH 6.5). For anchored APEX2 samples, lipidated anchor DNA was allowed to bind for 5 minutes at 1 μM on ice, followed by 1 μM of lipidated co-anchor DNA on ice for 5 minutes. 0.5 μM DNA-labeled APEX2 was allowed to bind on cells for 5 minutes before final wash with PBS (pH 6.5). For soluble APEX2, WGA-HRP, and soluble HRP samples, cells were resuspended in 0.5 μM of the corresponding enzyme. WGA-HRP was allowed to bind to cells for 5 minutes on ice. Biotin tyramide was added at a final concentration of 500 μM and mixed thoroughly, before the addition of 1 mM H_2O_2. Cells underwent labeling in a heated shaker (500 rpm) at 37°C for 2 minutes before

being quenched with 5 mM Trolox/10 mM Sodium Ascorbate/1 mM Sodium Pyruvate. Cells were washed 2x in quench buffer and spun down. The pellet was either further processed for flow cytometry, western blot, or flash frozen in liquid nitrogen for mass spectrometry.

On plate WGA-HRP cell surface labeling

KP-4 cells were grown on a 6 cm tissue culture treated plate and washed 3x with PBS (pH 6.5). 2 mL of 0.5 μM WGA-HRP in PBS (pH 6.5) was added to the plate, followed by biotin tyramide (0.5mM final concentration) and H_2O_2 (1mM final concentration). After a 2 minute incubation at 37°C, the cells were washed 2x with 5 mM Trolox/10 mM Sodium Ascorbate/1 mM Sodium Pyruvate quenching solution. The cells were washed 1x with PBS before being lifted with versene (PBS + 0.05% EDTA). Once lifted, the cells were washed once with PBS and subsequentially processed for flow cytometry analysis.

Biocytin hydrazide cell surface labeling

Cultured cells were grown for 3 days in tissue culture plates and dissociated by addition of versene (PBS + 0.05% EDTA). Cells were washed 3x in PBS (pH 6.5), resuspended in PBS (pH 6.5) and aliquoted to 1.5 million cells per sample. Samples were resuspended in 100 μL of PBS (pH 6.5) and fresh sodium periodate (Sigma Aldrich, 311448, 1 μL of a 160 mM solution) was added to each sample. The samples were mixed, covered in foil, and incubated while rotating at 4°C for 20 minutes. Following three washes with PBS (pH 6.5), the samples were resuspended in 100 μL of PBS (pH 6.5) with the addition of 1 μL of aniline (Sigma Aldrich, 242284, diluted 1:10 in water) and 1 μL of 100 mM biocytin hydrazide (Biotium, 90060). The reaction proceeded while rotating at 4°C for 90 minutes. The samples were then washed 2x with PBS (pH 6.5) and spun down. The

pellet was either further processed for flow cytometry, western blot, or flash frozen in liquid nitrogen for mass spectrometry.

Sulfo-NHS-LC-LC-biotin cell surface labeling

Cultured cells were grown for 3 days in tissue culture plates and dissociated by addition of versene (PBS + 0.05% EDTA). Cells were washed 3x in PBS (pH 7.4), resuspended in PBS (pH 8) and aliquoted to 1.5 million cells per sample. Samples were resuspended in 50 µL of PBS (pH 8). An aliquot of EZ-Link Sulfo-NHS-LC-LC-Biotin (ThermoFisher, 21338) was resuspended in 150 µL of PBS (pH 8). 7.5 µL was added to each cell sample and the reaction proceeded while rotating at 4°C for 30 minutes. The reaction was quenched by the addition of 2.5 µL of 1M Tris (pH 8.0). The samples were washed 2x in PBS (pH 8.0) and spun down. The pellet was either further processed for flow cytometry, western blot, or flash frozen in liquid nitrogen for mass spectrometry.

Flow cytometry for cell surface biotinylation

After labeling and quench washes, cells were washed once with PBS + 2% BSA to inhibit nonspecific binding. Samples were then incubated with 100 µL Streptavidin-Alexa Fluor 647 (Thermo Fischer, 1:100 in PBS + 2% BSA). Following a 30-minute incubation at 4°C while rocking, samples were washed three times with PBS + 2% BSA. Samples were analyzed in the APC channel and quantified using a CytoFLEX (Beckman Coulter). All flow cytometry data analysis was performed using FlowJo software.

RWPE-1 small EV isolation and labeling protocol

RWPE-1 Control and Myc cells were plated at 7 million and 4 million cells per plate, respectively, across 16 x 15 cm^2 plates and allowed to grow in normal keratinocyte-SFM media with provided supplements. Small EVs were isolated as previously described (Poggio et al., 2019). Briefly, two

days prior to EV isolation, media was replaced with 15 milliliters BPE-free keratinocyte-SFM media. For vesicle enrichment, media was isolated after two days in BPE-free media and centrifuged at 300 x g for 10 minutes at RT, followed by 2,000 x g for 20 minutes at 4°C. Large debris was cleared by a 12,000 x g spin for 40 minutes at 4°C. The pre-cleared supernatant was spun a final time at 100,000 x g at 4°C for 1 hr to pellet extracellular vesicles. Isolated extracellular vesicles were brought up in 50 µl of PBS with 0.5 µM of WGA-HRP and the mixture was allowed to bind on ice for 5 minutes. WGA-HRP bound vesicles were placed on a shaker (500 rpm) at 37°C before the addition of biotin tyramide (0.5 mM final concentration) and H_2O_2 (1 mM final concentration). Vesicles underwent labeling for 2 minutes before being quenched with 5 mM Trolox/10 mM Sodium Ascorbate/1 mM Sodium Pyruvate. Biotinylated small EVs were purified from other sedimentable particles by further centrifugation on a sucrose gradient (20-60%) for 16 hours at 4°C at 100,000xg. Precisely, the gradient was loaded using 0%, 20%, 40%, and 60% sucrose fractions from top to bottom. The sample was loaded at the bottom in 60% sucrose and the purified small EVs were isolated in the 20-40% sucrose fractions. Differential sucrose centrifugation yielded between 3-5 µg of small EVs.

Western blot protocol

Cultured cells were grown in 15 cm^2 tissue culture plates and dissociated by addition of versene (PBS + 0.05% EDTA). Cells were washed in PBS (pH 6.5) and resuspended in 100 µl PBS (pH 6.5) at a concentration of 10 million cells/ml in PBS (pH 6.5). Cells were labeled, reaction was quenched with 1X NuPage Loading Buffer, and immediately boiled for 5 minutes. To enable proper addition of lysate to gel wells, the mixture was thinned with addition of nuclease, and the disulfides were reduced with BME. The samples were subjected to electrophoresis in a 4-12% NuPage Gel until the dye front reached the bottom of the gel cast. For cell and EV blots, equal

amounts of protein content quantified by BCA assay were prepared in 1X NuPage Loading Buffer with BME and boiled for 5 minutes. Samples were loaded and subjected to electrophoresis in a 4-12% NuPage Gel until the dye front reached the bottom of the gel cast. Prepared gels were placed in iBlot2 transfer stacks and transferred using the P0 setting on the iBlot 2 Gel Transfer Device. The PVDF membrane was blocked in TBS Odyssey Blocking buffer for 1 hour at RT. Membranes were washed in TBST and incubated with Strepavidin-800 (1:10,000 dilution, Licor, 926-32230) for 30 minutes in TBS Odyssey Blocking buffer + 0.1% Tween 20. Membranes were washed in TBST 3x with a final wash in water. Membranes were visualized using an Odyssey DLx imager. Western blot samples were run and quantified 2-3 times and a representative image was displayed in figures.

For cell and EV blots, equal amounts of protein content quantified by BCA assay was prepared in 1X NuPage Loading Buffer with BME and boiled for 5 minutes. Samples were loaded and subjected to electrophoresis in a 4-12% NuPage Gel until the dye front reached the bottom of the gel cast. Prepared gels were placed in iBlot2 transfer stacks and transferred using the P0 setting on the iBlot 2 Gel Transfer Device. The PVDF membrane was blocked in TBS Odyssey Blocking buffer for 1 hour at RT. Membranes were washed in TBST and incubated overnight in primary antibody at 4°C in TBS Odyssey Blocking buffer + 0.1% Tween 20 while shaking. Primary antibodies used were ANPEP (R&D Systems, AF3815), FN1 (Abcam, ab2413), vimentin (Cell Signaling Technology, 5741S), ITIH4 (Atlas Antibodies, HPA003948), MFGE8 (Thermo Scientific, PA5-82036), IGSF8 (R&D Systems, AF3117-SP). Membranes were washed in 3x TBST before introduction to a 1:10,000 dilution of secondary antibody in TBS Odyssey Blocking buffer + 0.1% Tween 20 for 1 hour at room temperature while shaking. Secondary antibodies used were Goat Anti-Rabbit HRP (Thermo Scientific, 31460) and Rabbit Anti-Sheep HRP (Thermo

Scientific, 31480). Blots were imaged after 5 minutes in the presence of SuperSignal West Pico PLUS Chemiluminescent Substrate (Thermo Fisher Scientific, 34577) and imaged using a ChemiDoc XRS+. Western blot samples were run and quantified 2-3 times and a representative image was displayed in figures. EV blot was run once due to limited sample availability. EVs derived for western blotting were cultured and harvested independently of either biological replicate used for mass spectrometry analysis.

Proteomic preparation for whole EVs

Whole EV pellets were previously flash frozen after collection. EVs were processed for LC-MS/MS using a PreOmics iST kit (P.O.00027). Briefly, EV pellets were brought up in 50 µl of provided LYSE solution and boiled with agitation for 10 minutes. The provided enzymes mixture (Trypsin and LysC) were resuspended in 210 µl of RESUSPEND buffer, mixed, and added to the lysed EVs. Samples were allowed to mix at 500 rpm for 1.5 hours at 37°C, before being quenched with 100 µl of STOP solution. Sample was spun in provided C18 spin cartridge and washed 1X with 200µl of WASH 1 and WASH 2. Peptides were eluted with 2X 100 µl of ELUTE, dried, and resuspended with the provided LC-LOAD solution. Peptides were quantified using Pierce Quantitative Colorimetric Peptide Assay (Thermo Fisher Scientific, 23275).

Proteomic preparation for surface enriched samples

Frozen cell and EV pellets were lysed using 2X RIPA buffer (VWR) with protease inhibitor cocktail (Sigma-Aldrich; St. Louis, MO) at 4°C for 30 mins. Cell lysate was then sonicated, clarified, and incubated with 100 µl of neutravidin agarose slurry (Thermo Fisher Scientific, 29204) at 4°C for 1 hr. The bound neutravidin beads were washed in 2 ml Bio-spin column (Bio-Rad, 732-6008) with 5 ml RIPA buffer, 5 ml high salt buffer (1M NaCl, PBS pH 7.5), and 5 ml

urea buffer (2M urea, 50mM ammonium bicarbonate) to remove non-specific proteins. Beads were allowed to fully drain before transferring to a Low-bind Eppendorf Tube (022431081) with 2M Urea. Sample was spun down at 1,000xg and aspirated to remove excess liquid. Samples were brought up in 100 µl of 4M Urea digestion buffer (50 mM Tris pH 8.5, 10 mM TCEP, 20 mM IAA, 4 M Urea) and allowed to reduce and alkylate for 10 mins at 55°C while shaking. After the addition of 2 µg of total reconstituted Trypsin/LysC, the sample was incubated for 2 hours at RT. To activate the trypsin, mixture was diluted with 200 µl of 50 mM Tris pH 8.5 to a final Urea concentration of below 1.5 M. The mixture was covered and allowed to incubate overnight at RT. The mixture was isolated from the beads by centrifugation in a collection column (Pierce; 69725) before being acidified with 10% TFA until pH of 2.0 was reached. During this time, a Pierce C18 spin column (Pierce, 89873) was prepared as per manufacturing instructions. Briefly, C18 resin was washed twice with 200 µl of 50% LC-MS/MS grade ACN. The column was equilibrated with two 200µl washes of 5% ACN/0.5% TFA. The pre-acidified sample was loaded into the C18 column and allowed to fully elute before washing twice with 200 µl washes of 5% ACN/0.5% TFA. One final wash of 200 µl 5% ACN/1% FA was done to remove any residual TFA from the elution. Samples were eluted in 70% ACN, dried, and dissolved in 0.1% formic acid, 2% acetonitrile prior to LC-MS/MS analysis. Peptides were quantified using Pierce Quantitative Colorimetric Peptide Assay (Thermo Fisher Scientific, 23275).

LC-MS/MS

Liquid chromatography and mass spectrometry was performed as previously described (Meier et al., 2020). Briefly, approximately 200 ng of peptides were separate using a nanoElute UHPLC system (Bruker) with a pre-packed 25 cm x 75 µm Aurora Series UHPLC column + CaptiveSpray insert (CSI) column (120 A pore size, IonOpticks, AUR2-25075C18A-CSI) and analyzed on a

timsTOF Pro (Bruker) mass spectrometer. Peptides were separated using a linear gradient of 2-34% solvent B (Solvent A: 2% acetonitrile, 0.1% formic acid, solvent B: acetonitrile, 0.1% formic acid) over 100 mins at 400 nL/min. Data-dependent acquisition was performed with parallel accumulation-serial fragmentation (PASEF) and trapped ion mobility spectrometry (TIMS) enabled with 10 PASEF scans per topN acquisition cycle. The TIMS analyzer was operated at a fixed duty cycle close to 100% using equal accumulation and ramp times of 100 ms each. Singly charged precursors were excluded by their position in the m/z–ion mobility plane, and precursors that reached a target value of 20,000 arbitrary units were dynamically excluded for 0.4 min. The quadrupole isolation width was set to 2 m/z for m/z < 700 and to 3 m/z for m/z > 700 and a mass scan range of 100-1700 m/z. TIMS elution voltages were calibrated linearly to obtain the reduced ion mobility coefficients (1/K0) using three Agilent ESI-L Tuning Mix ions (m/z 622, 922 and 1,222).

Data Processing and Analysis

Briefly, for general database searching, peptides for each individual dataset were searched using PEAKS Online X version 1.5 against both the plasma membrane (PM) annotated human proteome (Swiss-prot GOCC database, August 3, 2017 release) and the entire Swiss-prot Human Proteome (Swiss-prot). We acknowledge the identification of a number of proteins not traditionally annotated to the plasma membrane, which were published in the final Swiss-prot GOCC-PM database used. Additionally, to not miss any key surface markers such as secreted proteins or anchored proteins without a transmembrane domain, we chose to initially avoid searching with a more stringent protein list, such as the curated SURFY database. However, following the analysis we bolded proteins found in the SURFY database and italicized proteins known to be secreted (Uniprot). Enzyme specificity was set to trypsin + LysC with up to two missed cleavages. Cysteine

carbamidomethylation was set as the only fixed modification; acetylation (N-term) and methionine oxidation were set as variable modifications. The precursor mass error tolerance was set to 20 PPM and the fragment mass error tolerance was set to 0.05 Da. Data was filtered at 1% for both protein and peptide FDR and triaged by removing proteins with fewer than 2 unique peptides. All mass spectrometry database searching was based off of two biological replicates. Biological replicates underwent washing, labeling, and downstream LC-MS/MS preparation separately.

For comparative label-free quantification of cellular and EV samples, datasets were searched using PEAKS Online X version 1.5 against the plasma membrane (PM) annotated human proteome (Swiss-prot GOCC database, August 3, 2017 release). Enzyme specificity was set to trypsin + LysC with up to two missed cleavages. Cysteine carbamidomethylation was set as the only fixed modification; acetylation (N-term) and methionine oxidation were set as variable modifications. The precursor mass error tolerance was set to 20 PPM and the fragment mass error tolerance was set to 0.05 Da. Data was filtered at 1% for both protein and peptide FDR and triaged by removing proteins with fewer than 2 unique peptides. Label free quantification of protein was completed by taking the average intensity of the top three most intense peptides for each protein. Data was normalized by total area sum intensity for each sample. Using Perseus, all peak areas were log2(x) transformed and missing values were imputed separately for each sample using the standard settings (width of 0.3, downshift of 1.8). Significance was based off of a standard unpaired Student t test with unequal variances across all four replicates. Reported peak area values represent the averages of all four replicates--two biological and two technical replicates. For representation of the data in figures, a Z-score was computed and is defined as (LFQ Area - Mean LFQ Area)/Standard Deviation. Protein IDs that were not annotated to be secreted or expressed extracellularly were removed. Further, in the Cell versus EV graph, any proteins that showed a

standard deviation (SD) greater than 1.5 between Control and Myc of each sample type (EV or Cell) were removed to avoid representation of oncogene-specific changes. EVs and cells from different biological replicates were cultured on different days. Desalting, quantification, and LC-MS/MS runs were performed together. The mass spectrometry proteomics data have been deposited to the ProteomeXchange Consortium via the PRIDE (Mathieu et al., 2021) partner repository with the dataset identifier PXD028523.

To compare replicates of data in **(Figure 2.13)**, a simple linear regression was performed on total area sum intensity normalized data. Replicate 1 was graphed against Replicate 2 for biocytin hydrazide, NHS-biotin, and WGA-HRP, and the resulting data was shown with calculated R and p-values as determined using the simple linear regression software suite in Prism. For the supplementary heatmap output, total area normalized LFQ data found in **(Figure 2.17)** was loaded into Morpheus (software.broadinstitute.org/Morpheus) and data points were clustered by the Pearson correlation between all replicates on both columns and rows. This same data was used in Perseus to produce the principle component analysis (PCA). Distinct gene clusters were further analyzed by functional annotation using the DAVID Bioinformatics Resource 6.8.

Acknowledgments

We acknowledge the members of the Wells lab for their support. Special thanks to Alice Ting, PhD and Tess Branon, PhD for their helpful advice regarding enzyme purification. We would also like to acknowledge and thank the lab of Zev Gartner, PhD for providing materials and methods for DNA-lipid tethering. Additionally, we would like to thank Rushika Perera, PhD for donating the pancreatic cancer cell lines PaTu8902 and KP-4, which were used in this manuscript. J.A.W. was supported by generous funding from the Chan Zuckerberg Biohub Investigator Program, the

Harry and Dianna Hind Professorship, NIH (R35GM122451), and NCI (R01CA248323). The NIH F31 Ruth L Kirschstein National Research Service Award (1F31CA247527) supported L.L.K. The National Science Foundation Graduate Research Fellowship Program (1650113) supported S.K.E. R.B. and J.Y. were supported by funding from the NIH (U01CA244452).

Figures and Tables

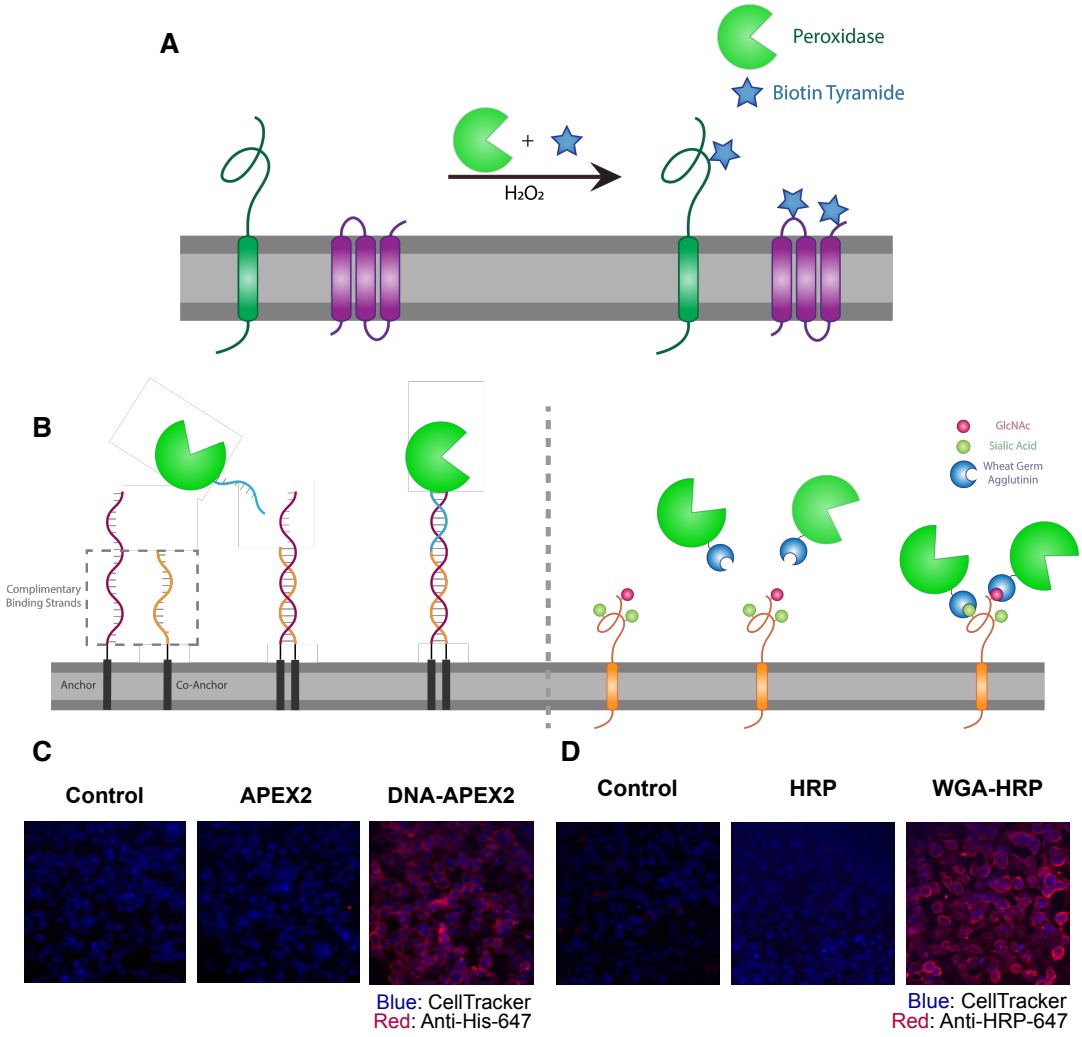

Figure 2.1: Direct labeling of promiscuous biotinylators to the cell membrane for rapid cell surface proteome characterization of small-scale biological samples. (A) Outline of enzymatic reaction mechanism. APEX2 and HRP both require biotin tyramide and hydrogen peroxide to produce the biotin-radical intermediate. (B) Tethering either enzyme is completed through differing mechanisms: (i) APEX2 is tethered through bio-conjugation of a single-strand of DNA, which is complementary to an exogenously added sequence of lipidated-DNA attached to the membrane, (ii) Commercially available wheat germ agglutinin (WGA)-HRP associates with native GlcNAc and sialic acid glycan moieties on cell surface proteins. (C) Microscopy images depicting the localization of DNA-APEX2 to the cell surface of KP-4 cells after introduction of the lipidated-DNA complementary strands. (D) Microscopy images depicting the localization of WGA-HRP to the membrane of KP-4 cells. All microscopy images are representative of two biological replicates.

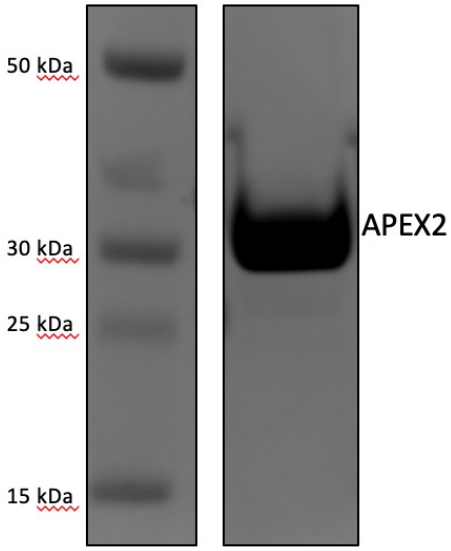

Figure 2.2: Expression, purification, and validation of APEX2 enzyme. His-tagged APEX2 was expressed in BL21(DE3)pLysS cells and purified by a nickel column. 10 µg of purified enzyme was run out on a 4-12% Bis-Tris gel to confirm purity.

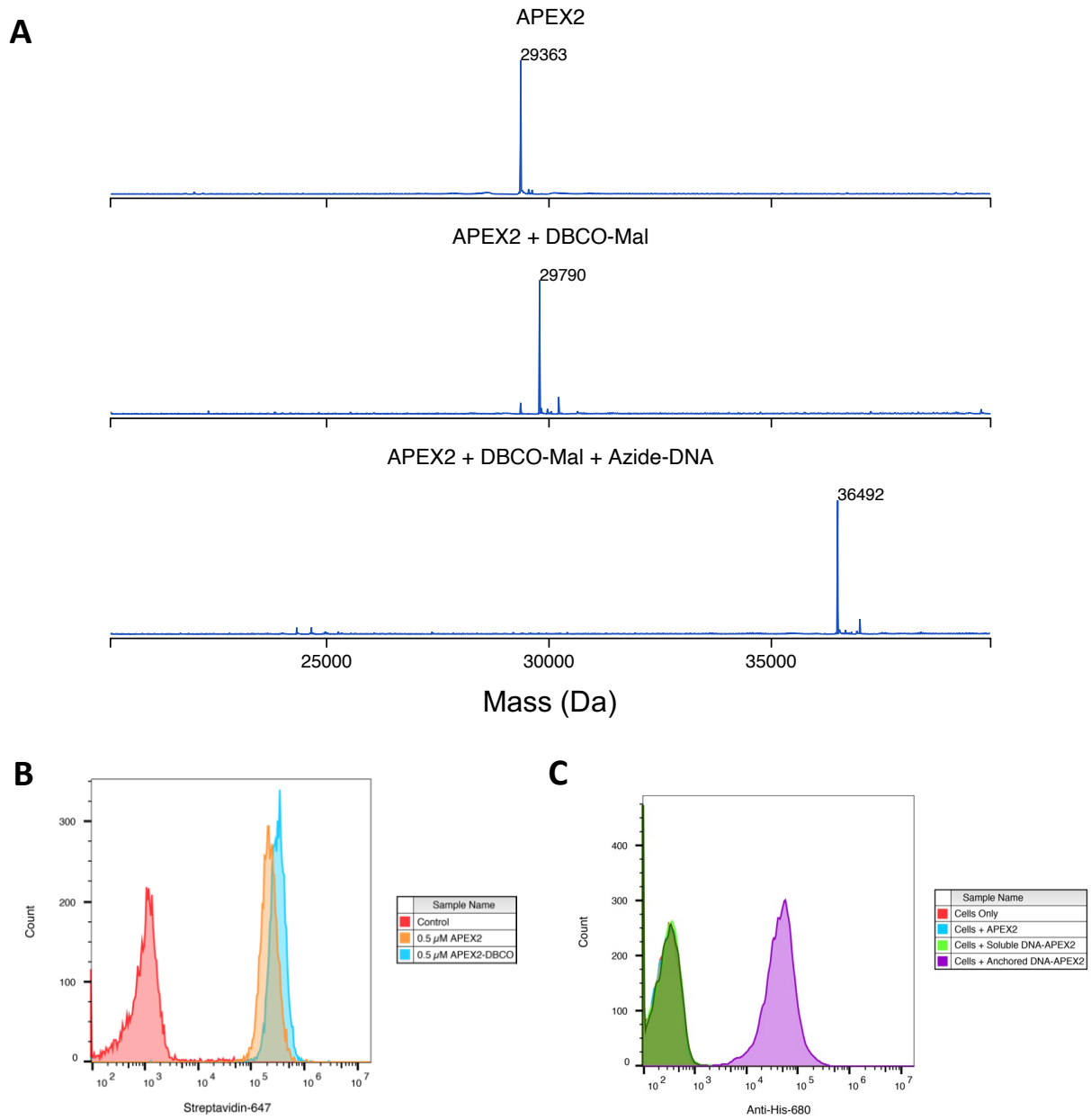

Figure 2.3: Labeling and efficacy of APEX2 with DNA. (A) APEX2 was first conjugated with DBCO-Maleimide (DBCO-Mal) reagent at 40 equivalents for 5 hours (80% conversion to the singly labeled product). Following desalting, 3 equivalences of Azide-DNA was added to the conjugate and purified by a Nickel column. Both reactions were monitored by LC-MS as shown. (B) 500,000 Expi293 cells were labeled with 0.5 μM purified APEX2 and DBCO-labeled APEX2 for 2 min. Extent of biotinylation of target cells was quantified by flow cytometry staining with streptavidin-647. (C) The DNA-APEX2 conjugate was shown to be tethered in the presence of the lipidated DNA (purple) and not in the absence (green), as detected by an Anti-His 680 antibody. Unlabeled APEX2 (blue) additionally did not result in a signal shift. Flow cytometry images are representative of one biological replicate.

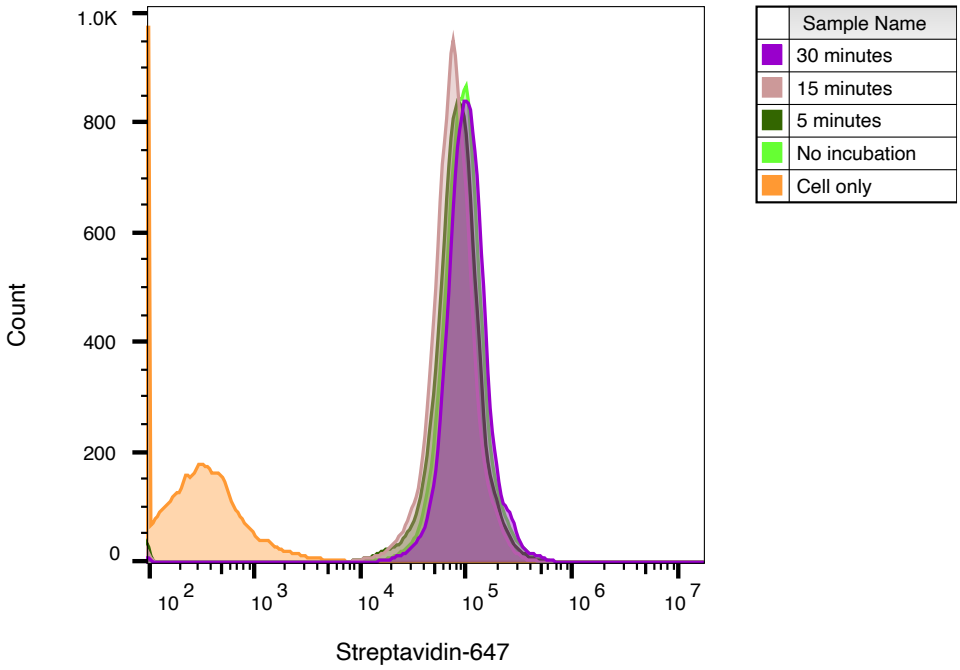

Figure 2.4: WGA-HRP pre-incubation time on cells has no effect on labeling efficiency. WGA-HRP was incubated on Expi293 cells for 0-30 min to determine optimal incubation time on ice before labeling. All tested times resulted in similar cell surface biotinylation efficiencies and signified that no incubation time was needed. Flow cytometry images are representative of one biological replicate.

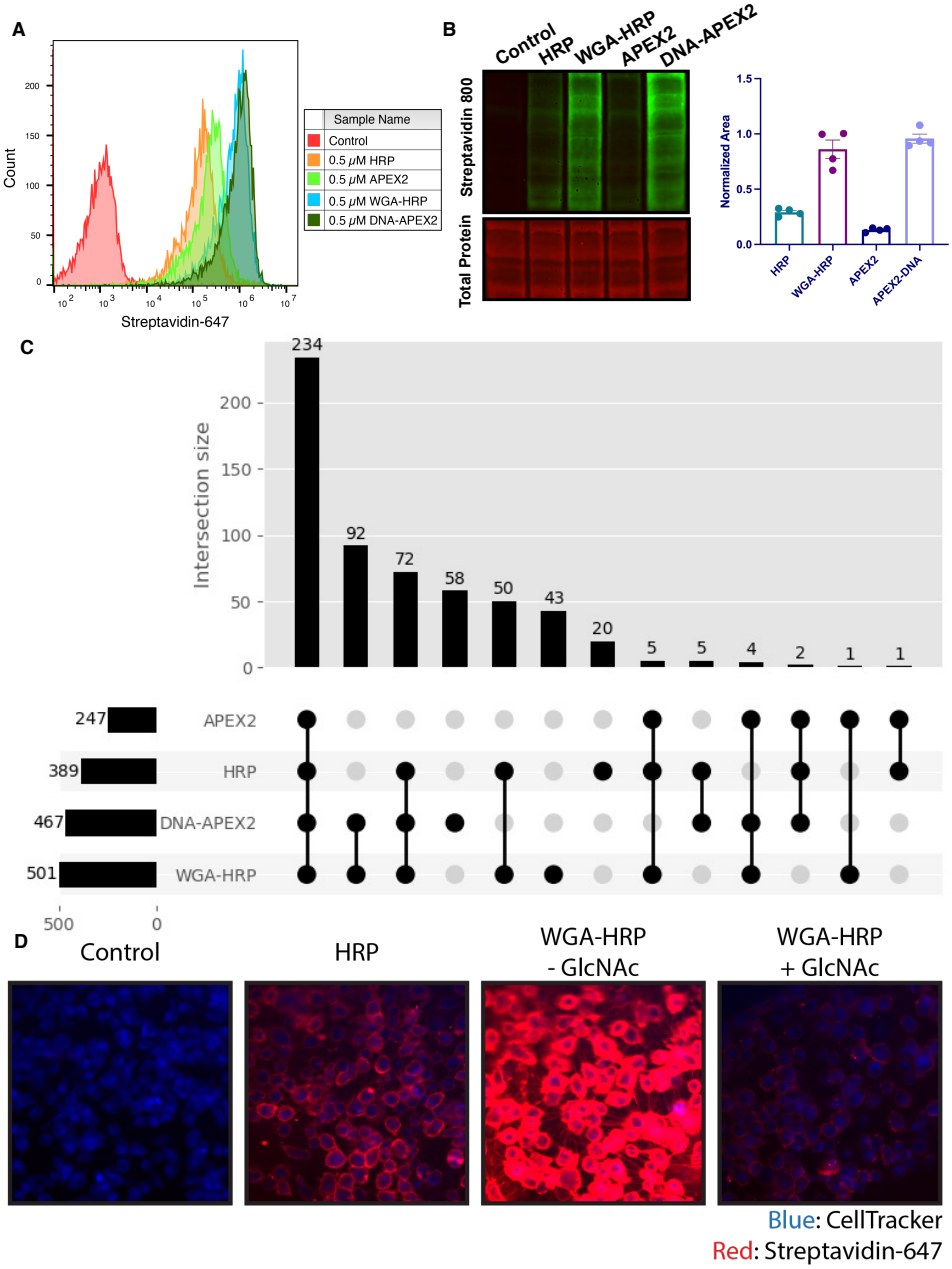

Figure 2.5: Membrane-localized peroxidases increases membrane proteome biotinylation compared to non-tethered counterparts. (A) Biotinylation of Expi293 cells treated with free enzyme (APEX2 or HRP) or cell-tethered enzyme (DNA-APEX2 or WGA-HRP) shown by flow cytometry. Signal is read out using Streptavidin-AlexaFluor-647. (B) Comparison of cell labeling with either free enzyme (APEX2 or HRP) or cell-tethered enzyme (DNA-APEX2 or WGA-HRP) shown by Streptavidin-800 western blot and total protein stain. Normalized area is plotted to the right. (C) Number of cell membrane proteins identified by mass spectrometry (>2 unique peptides, <1% FDR, found in both biological replicates) after treating 500,000 KP-4 pancreatic cancer cells with either free enzyme (APEX2 or HRP) or cell-tethered enzyme (DNA-APEX2 or WGA-HRP). (D) Microscopy images depicting extent of labeling with free HRP compared to WGA-HRP with and without the blocking sugar GlcNAc. All western blot images, microscopy images, mass spectrometry data, and flow cytometry data are representative of two biological replicates.

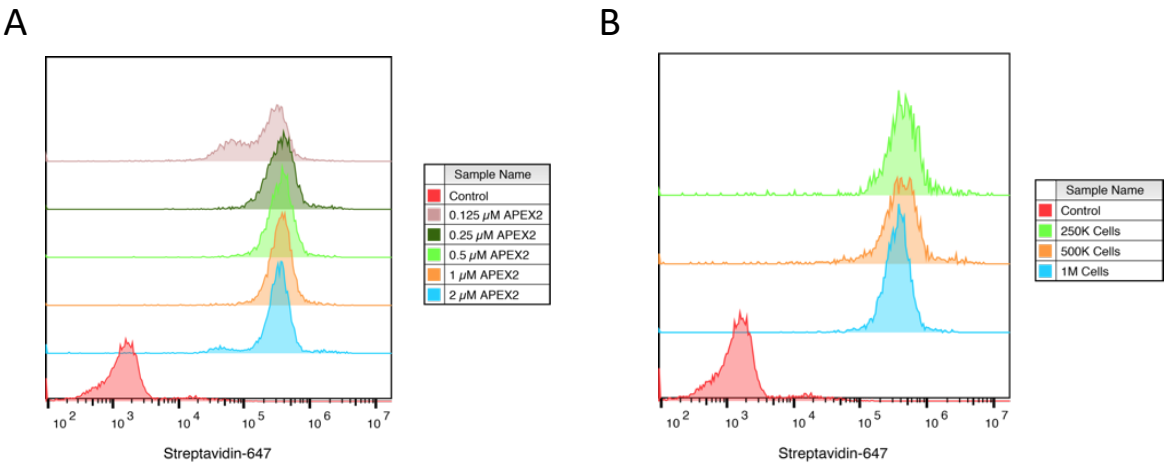

Figure 2.6: Optimization of APEX2 concentrations on cell by flow cytometry. (A) 500,000 Expi293 cells were labeled for 2 min with increasing amounts of purified APEX2 enzyme and extent of labeling was quantified by flow cytometry staining with streptavidin-647. (B) Varying numbers of Expi293 cells were labeled for 2 min with 0.5 μM APEX2 to test range of cell numbers for labeling. Flow cytometry images are representative of one biological replicate.

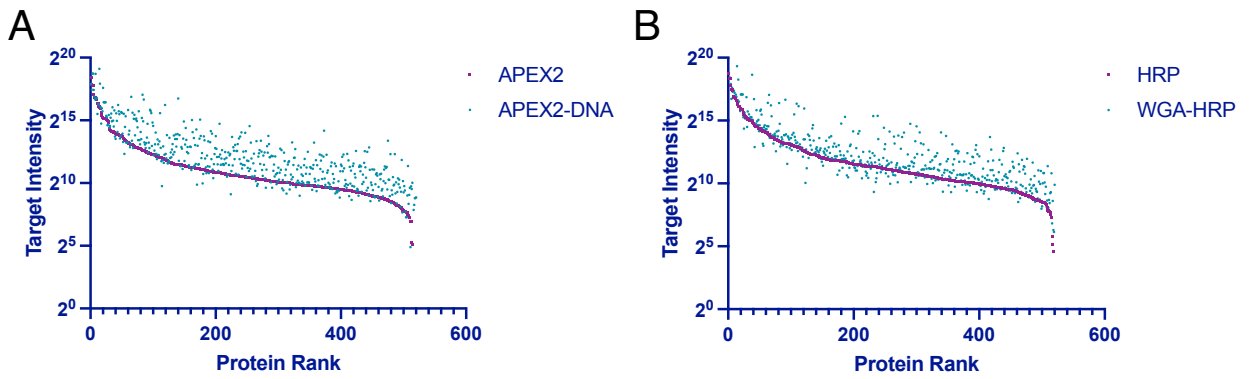

Figure 2.7: Rank ordered intensities for surface annotated proteins detected in tethered and untethered enzyme samples. (A) A rank ordered list of MS1 intensities (area) for surface annotated proteins found in APEX2 and DNA-APEX2 samples. (B) A rank ordered list of MS1 intensities (area) for surface annotated proteins found in HRP and WGA-HRP samples. The average of two biological replicates are plotted.

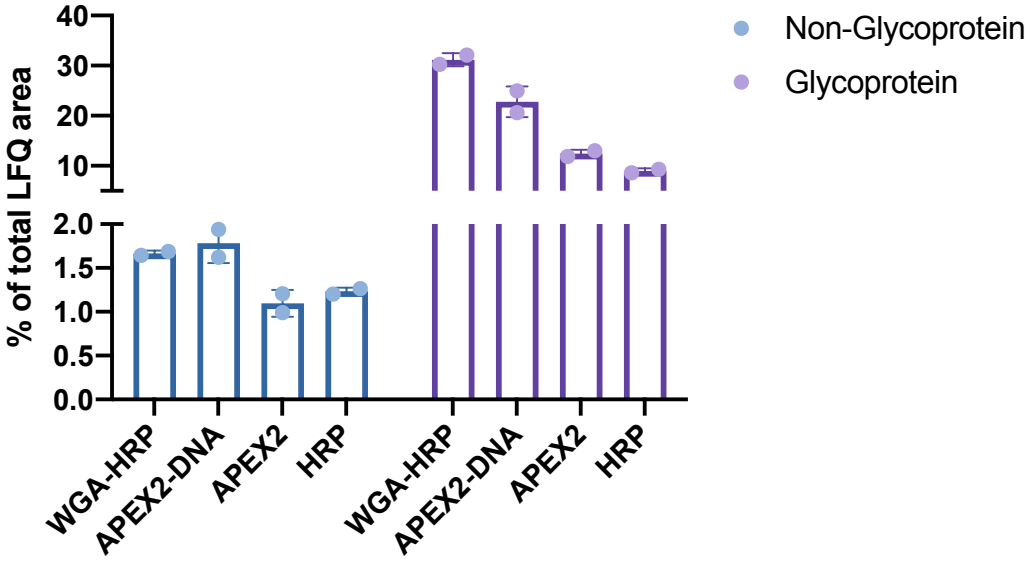

Figure 2.8: Comparison of enrichment for glycosylated and non-glycosylated proteins. Total MS1 intensities (LFQ area) of Uniprot annotated glycoproteins compared to non-glycoproteins in the SURFY database for each labeling method compared to the total area sum intensity.

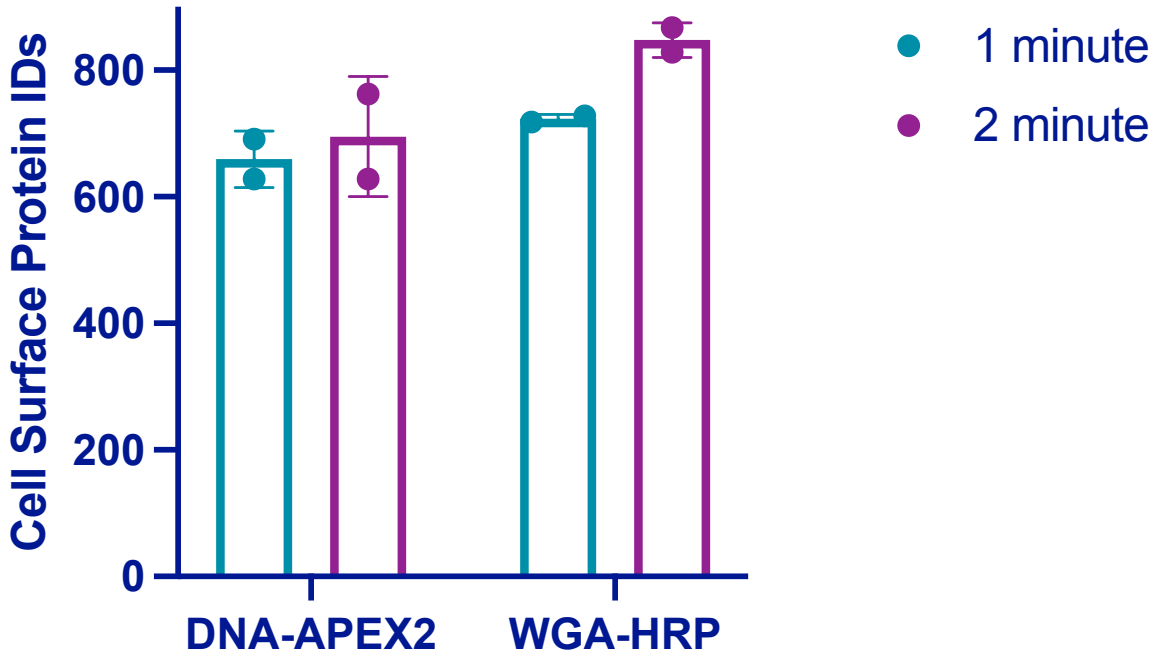

Figure 2.9: Target intensities and total plasma membrane protein identifications for DNA-APEX2 and WGA-HRP labeling experiments as a function of time. 500,000 PaTu8902 pancreatic cancer cells were labeled with either 0.5 μM DNA-APEX2 or 0.5 μM WGA-HRP for 1 or 2 minutes at 37°C. After cell surface enrichment and mass spectrometry analysis, the plasma membrane derived protein identifications were totaled. Two biological replicates are plotted.

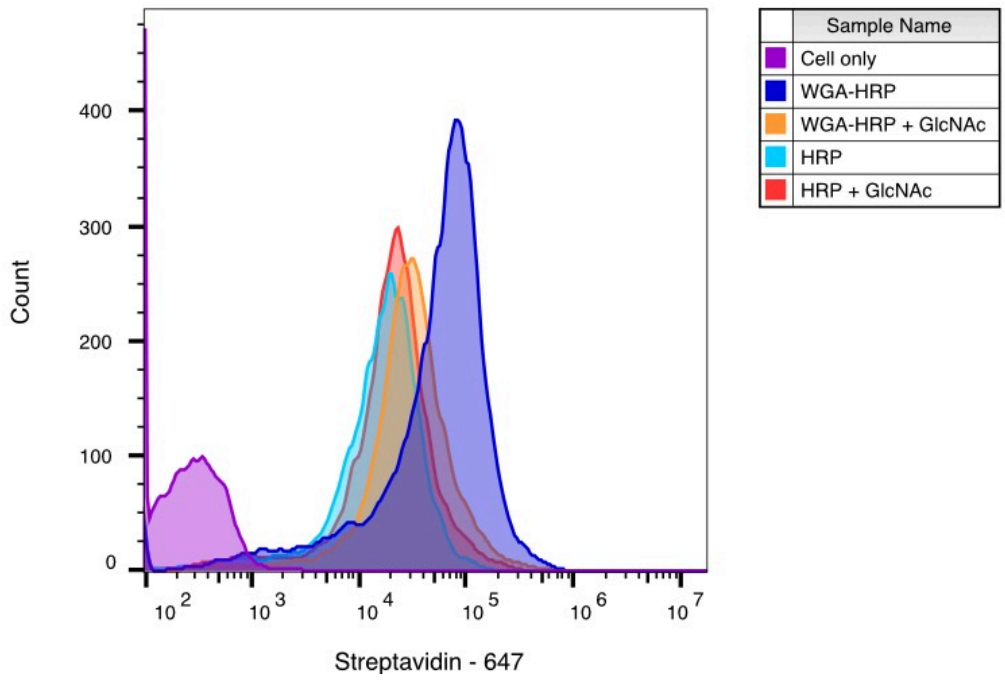

Figure 2.10: WGA-HRP labeling is N-acetyl-D-glucosamine (GlcNAc) dependent. Biotinylation of RWPE-1 Myc cells with WGA-HRP was determined with (orange) and without (dark blue) 100 mg/mL GlcNAc. There is a significant leftward shift in the degree of labeling in the absence of competing GlcNAc, demonstrating that the enhanced labeling by WGA-HRP is GlcNAc dependent. The degree of labeling is similar to soluble HRP, as shown in light blue. Importantly, presence of GlcNAc in solution did not generally affect HRP labeling as seen by the control in red. The data presented is from one biological replicate.

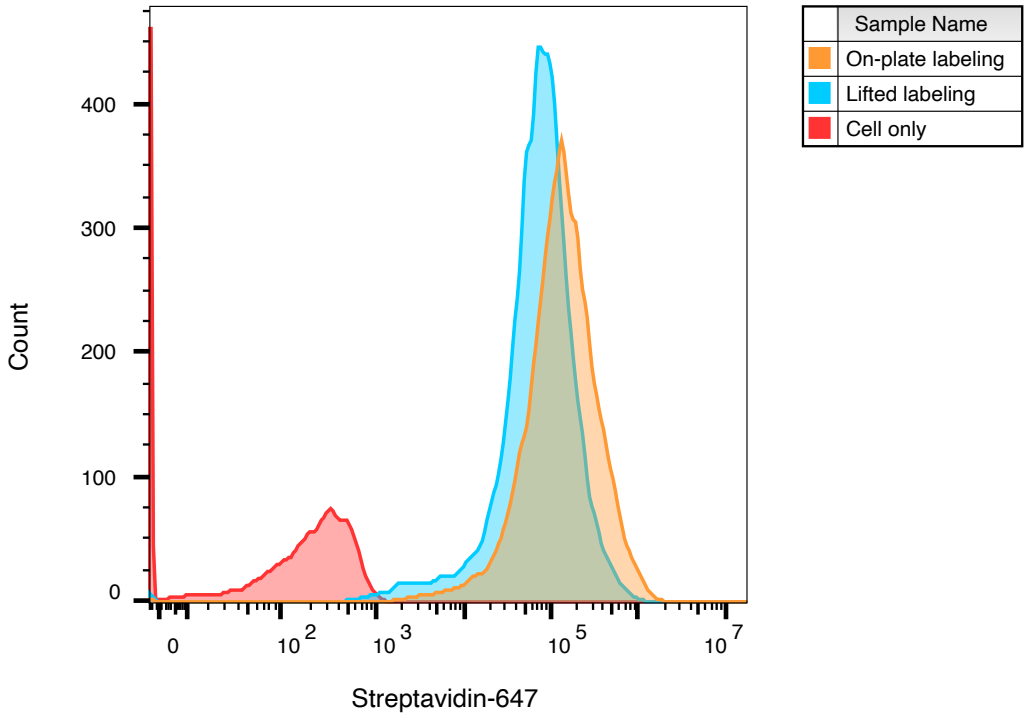

Figure 2.11: WGA-HRP can be used to label adherent cells on-plate. Cell surface labeling was compared between labeling adherent cells on a tissue culture plate vs. lifting cells and then performing labeling. Cell surface biotinylation was detected by streptavidin-Alexa Fluor 647. The data presented is from one biological replicate.

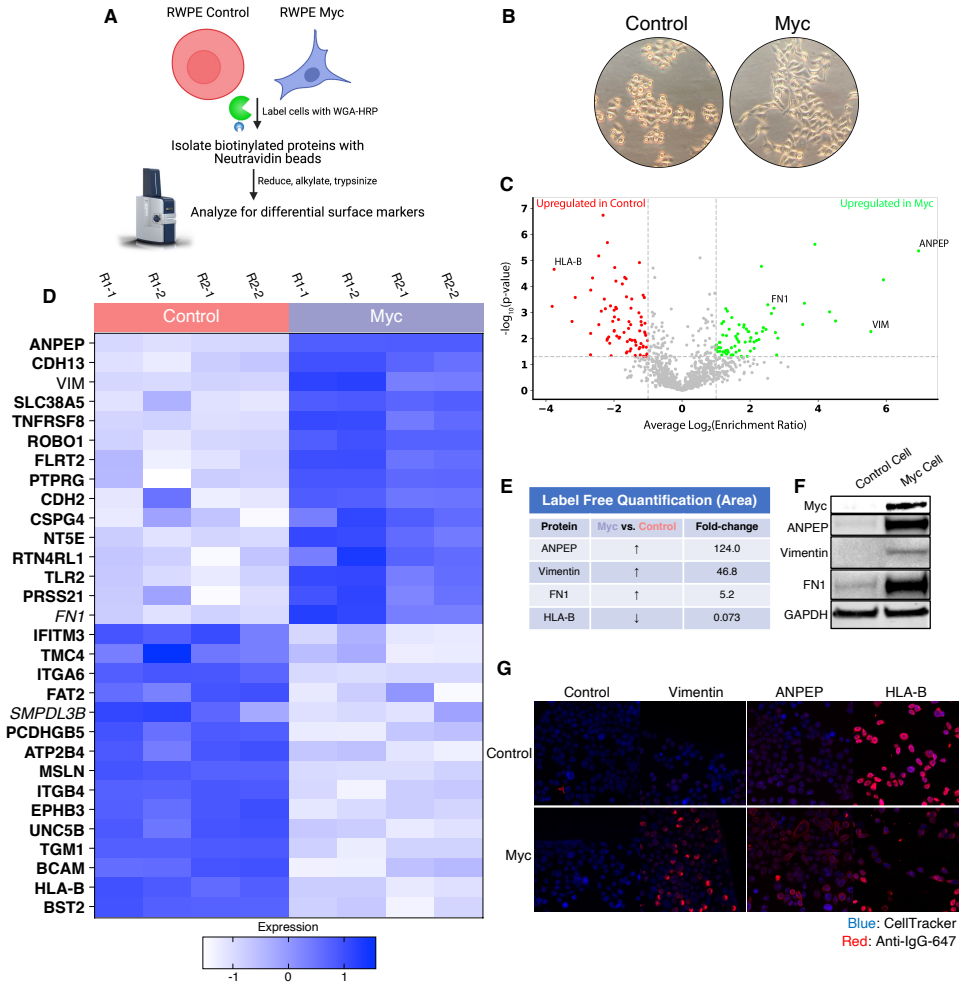

Figure 2.12: WGA-HRP identifies a number of enriched markers on Myc-driven prostate cancer cells. (A) Overall scheme for biotin labeling, and label-free quantification (LFQ) by LC-MS/MS for RWPE-1 Control and Myc over-expression cells. (B) Microscopy image depicting morphological differences between RWPE-1 Control and RWPE-1 Myc cells after 3 days in culture. (C) Volcano plot depicting the LFQ comparison of RWPE-1 Control and Myc labeled cells. Red labels indicate upregulated proteins in the RWPE-1 Control cells over Myc cells and green labels indicate upregulated proteins in the RWPE-1 Myc cells over Control cells. All colored proteins are at least 2-fold enriched in either dataset between four replicates (two technical, two biological, $p<0.05$). (D) Heatmap of the 30 most upregulated transmembrane (bold) or secreted (italics) proteins in either RWPE-1 Control or Myc cells. Scale indicates intensity, defined as (LFQ Area - Mean LFQ Area)/Standard Deviation. (E) Table indicating fold-change of most differentially regulated proteins by LC-MS/MS for RWPE-1 Control and Myc cells. (F) Upregulated proteins in RWPE-1 Myc cells (Myc, ANPEP, Vimentin, and FN1) are confirmed by western blot. (G) Upregulated surface proteins in RWPE-1 Myc cells (Vimentin, ANPEP, FN1) are detected by immunofluorescence microscopy. The downregulated protein HLA-B by Myc over-expression was also detected by immunofluorescence microscopy. All western blot images and microscopy images are representative of two biological replicates. Mass spectrometry data is based on two biological and two technical replicates (N = 4).

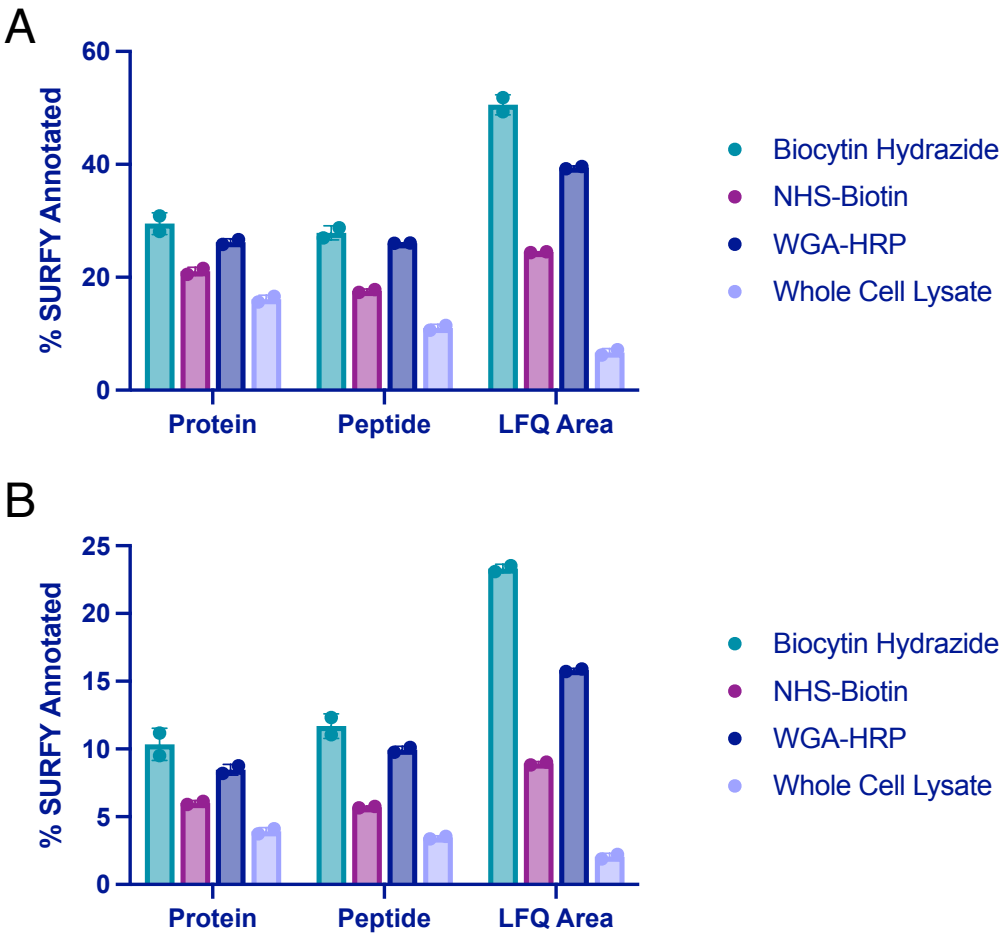

Figure 2.13: Comparison of surface enrichment between replicates for different mass spectrometry methods. (A)The top three methods (NHS-Biotin, Biocytin Hydrazide, and WGA-HRP) were compared for their ability to enrich cell surface proteins on 1.5 M RWPE-1 Control cells by LC-MS/MS after being searched with the Uniprot GOCC Plasma Membrane database. Shown are enrichment levels on the protein, peptide, and average MS1 intensity of top three peptides (LFQ area) levels. (B) The top three methods (NHS-Biotin, Biocytin Hydrazide, and WGA-HRP) were compared for their ability to enrich cell surface proteins on 1.5 M RWPE-1 Control cells by LC-MS/MS after being searched with the entire human Uniprot database. Shown are enrichment levels on the protein, peptide, and average MS1 intensity of top three peptides (LFQ area) levels. Proteins or peptides detected from cell surface annotated proteins (determined by the SURFY database) were divided by the total number of proteins or peptides detected. LFQ areas corresponding to cell surface annotated proteins (SURFY) were divided by the total area sum intensity for each sample. The corresponding percentages for two biological replicates were plotted.

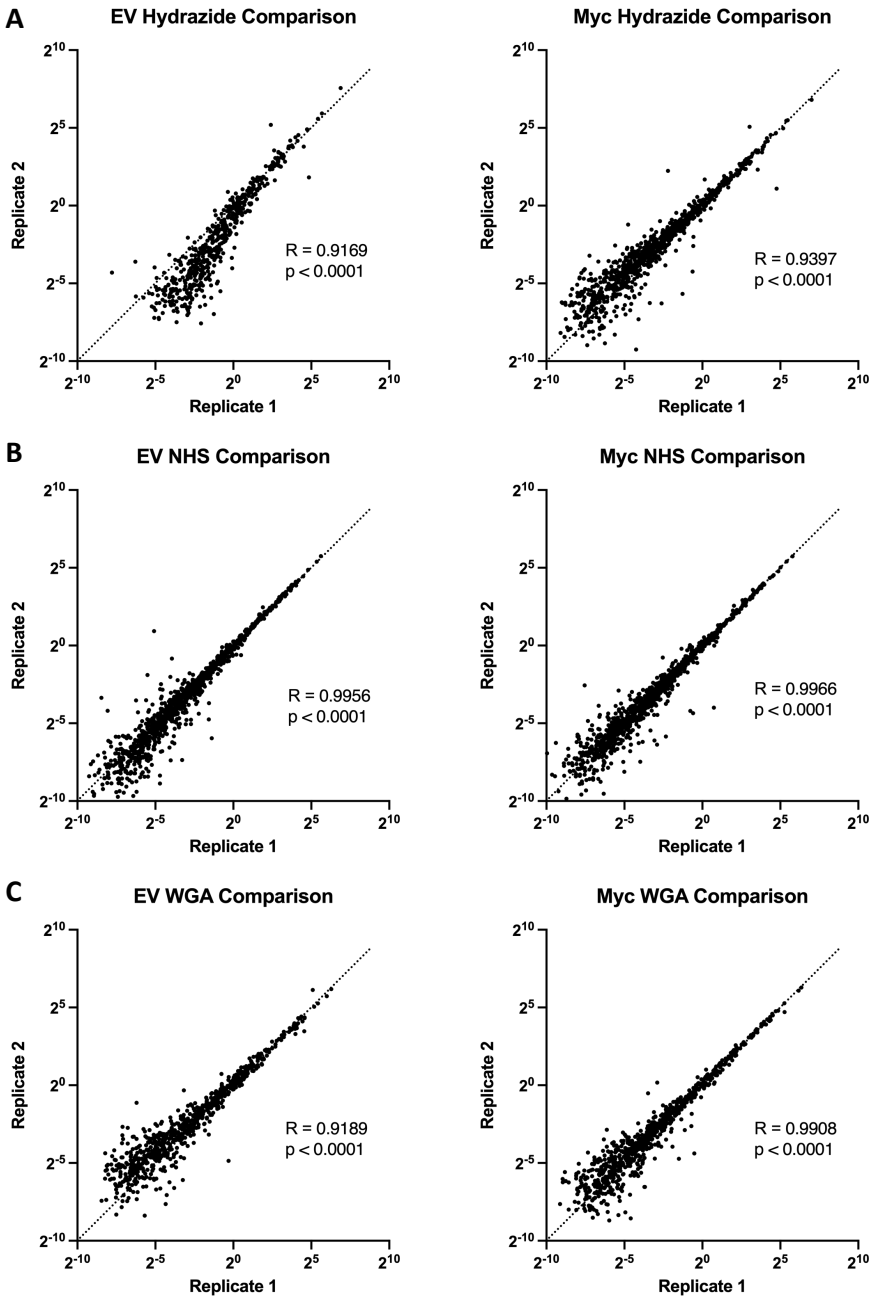

Figure 2.14: Comparison of replicates for different mass spectrometry methods show that WGA-HRP has comparable reproducibility to NHS-Biotin and Hydrazide labeling. (A) Spearman correlations of total area sum intensity normalized data from replicates of Hydrazide Control and Myc cells. (B) Spearman correlations of total area sum intensity normalized data from replicates of NHS Control and Myc cells. (C) Spearman correlations of total area sum intensity normalized data from replicates of WGA Control and Myc cells.

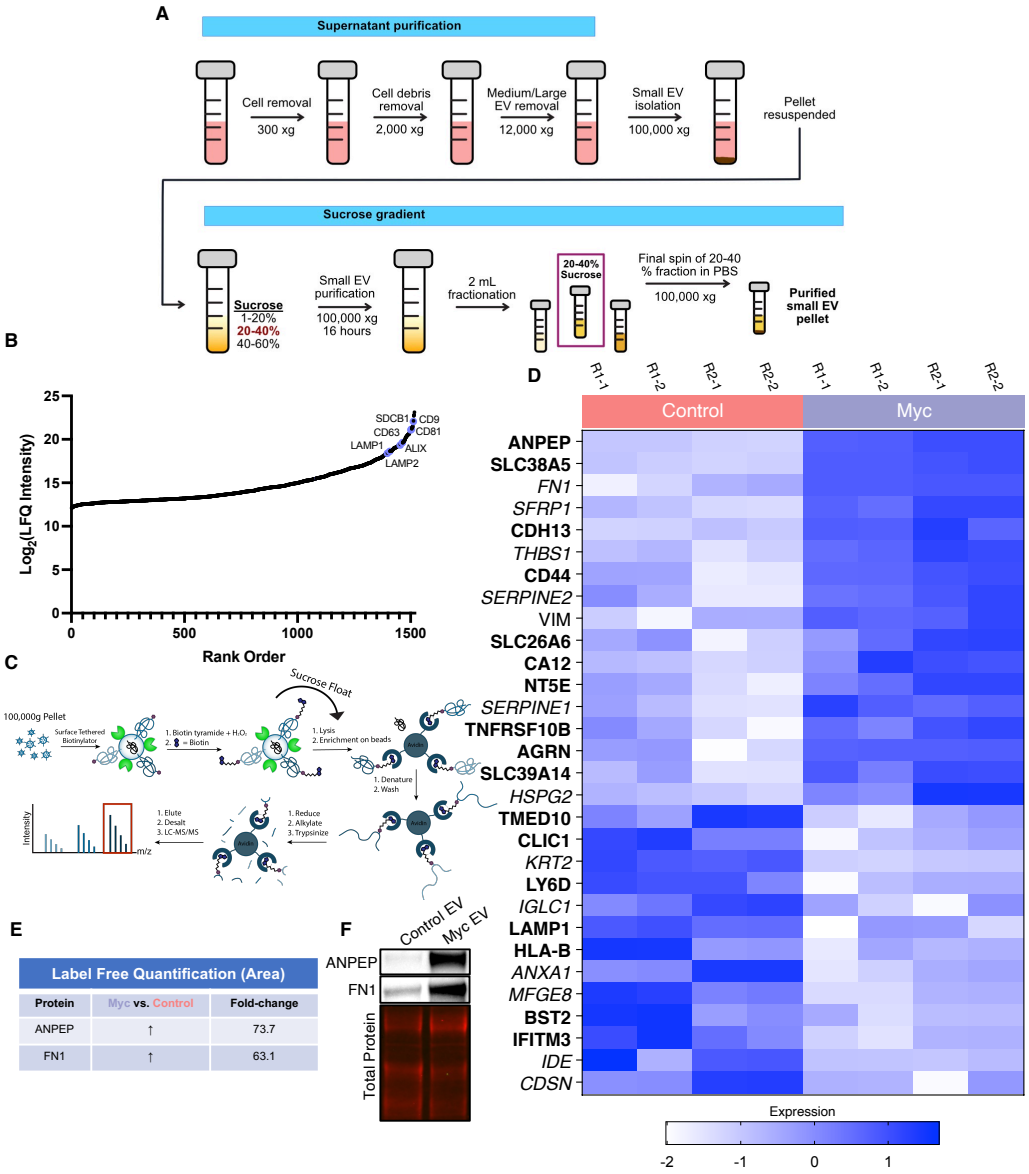

Figure 2.15: WGA-HRP identifies a number of enriched markers on Myc-driven prostate cancer EVs. (A) Workflow for small EV isolation from cultured cells. (B) Labeled proteins indicating canonical exosome markers (ExoCarta Top 100 List) detected after performing label-free quantification (LFQ) from whole EV lysate. The LFQ intensities were averaged for Control and Myc EVs, and the resulting protein list is graphed from least abundant to most abundant. (C) Workflow of EV labeling and preparation for mass spectrometry. (D) Heatmap of the 30 most upregulated proteins in either RWPE-1 Control or Myc EVs. Scale indicates intensity, defined as (LFQ Area - Mean LFQ Area)/Standard Deviation. (E) Table indicating fold-change of most differentially regulated proteins by LC-MS/MS for RWPE-1 Control and Myc cells. (F) Upregulated proteins in RWPE-1 Myc EVs (ANPEP and FN1) are confirmed by western blot. Mass spectrometry data is based on two biological and two technical replicates (N = 4). Due to limited sample yield, one replicate was performed for the EV western blot.

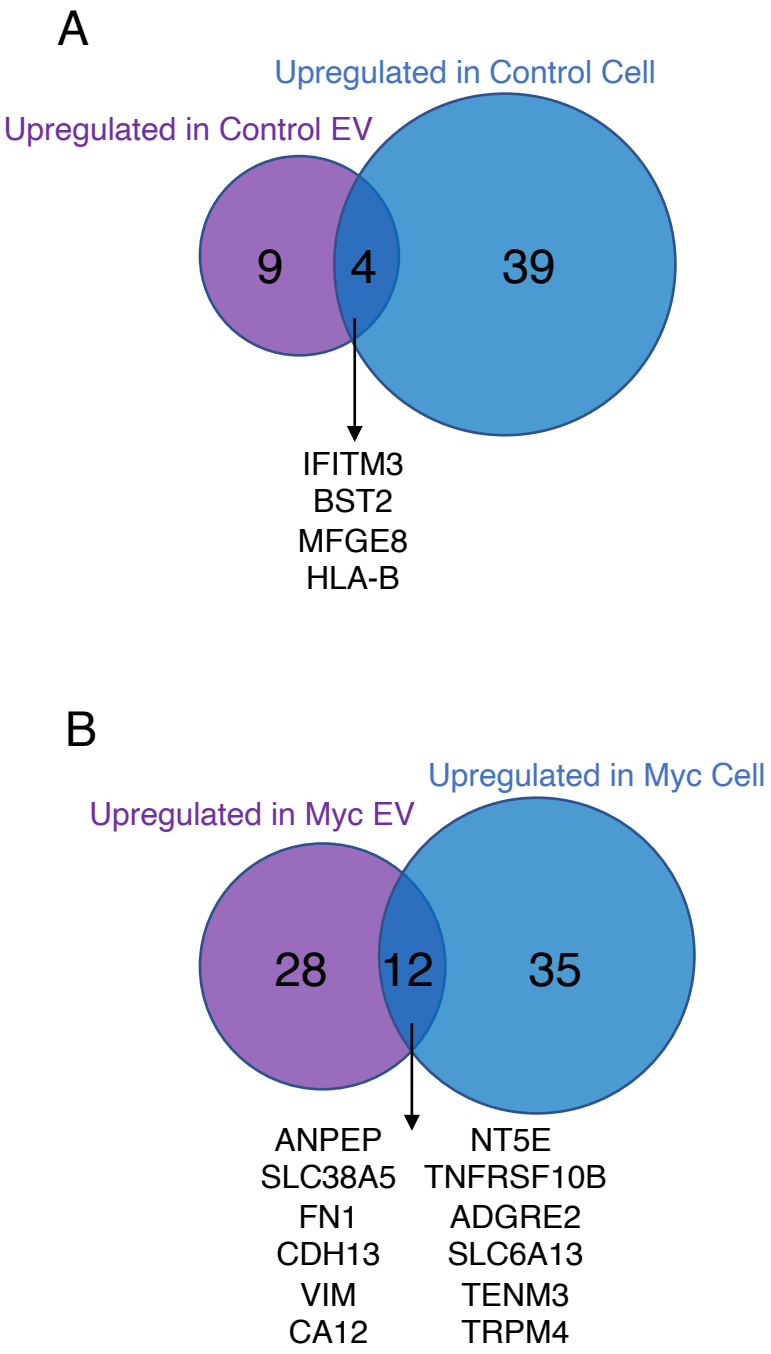

Figure 2.16: Venn diagram comparing enriched targets (>2-fold) in Cells and EVs. (A) Surface and secreted targets that were found enriched in the Control EVs (purple) and Control cells (blue) when each is separately compared to Myc EVs and Myc cells, respectively. The 4 overlapping enriched targets in common between Control cells and Control EVs are listed in the center. (B) Surface and secreted targets that were found enriched in the Myc EVs (purple) and Myc cells (blue) when each is separately compared to Control EVs and Control cells, respectively. The 12 overlapping enriched targets in common between Myc cells and Myc EVs are listed in the center.

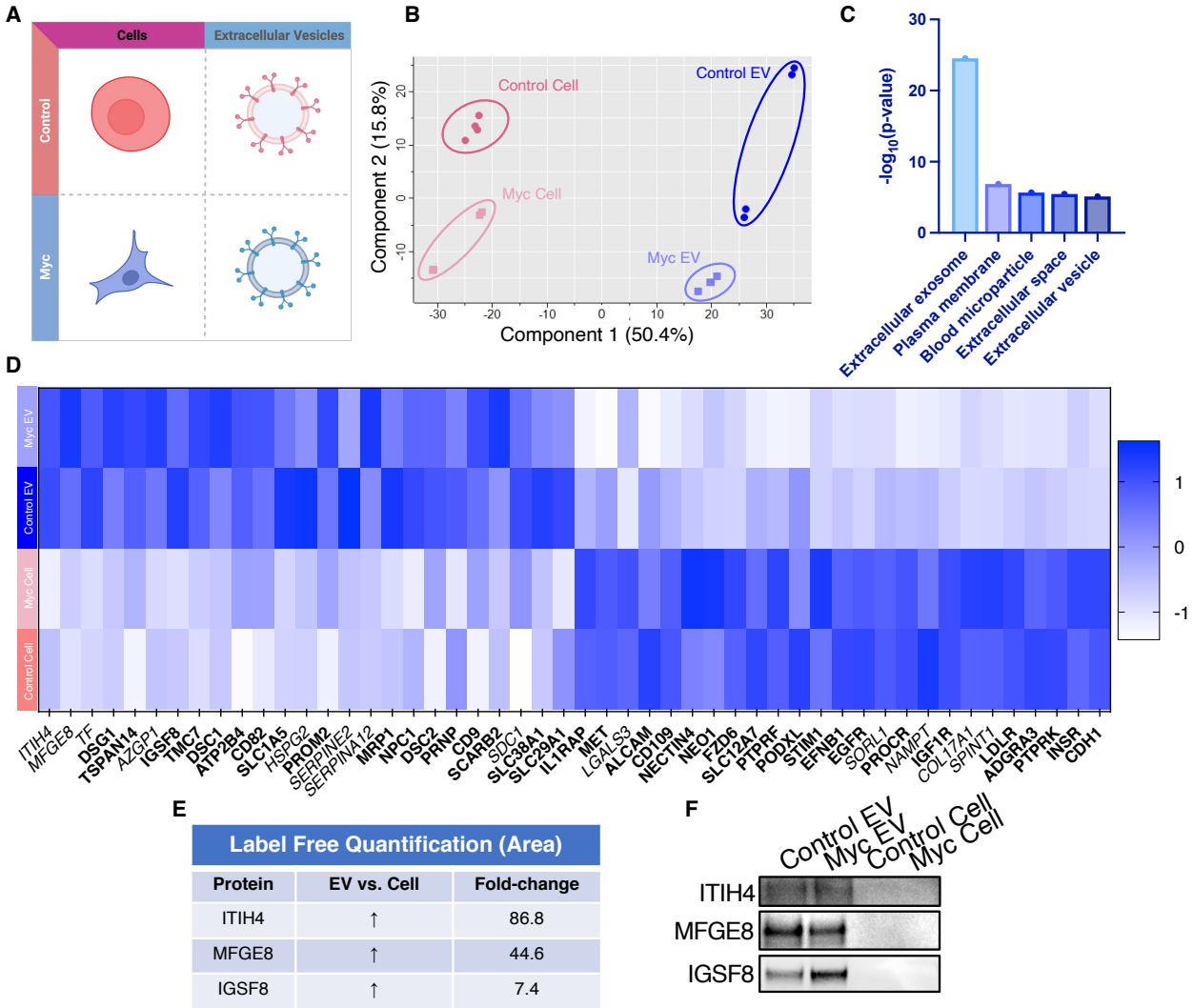

Label Free Quantification (Area)

Protein	EV vs. Cell	Fold-change
ITIH4	↑	86.8
MFGE8	↑	44.6
IGSF8	↑	7.4

Figure 2.17: WGA-HRP identifies a number of EV-specific markers that are present regardless of oncogene status. (A) Matrix depicting samples analyzed during LFQ comparison--Control and Myc cells, as well as Control and Myc EVs. (B) Principle component analysis (PCA) of all four groups analyzed by LFQ. Component 1 (50.4%) and component 2 (15.8%) are graphed. (C) Functional annotation was performed for each gene cluster using DAVID Bioinformatics Resource 6.8 and the highest ranking annotation features for the EV-specific gene cluster are shown. (D) Heatmap of the 50 most upregulated proteins in either RWPE-1 cells or EVs. Proteins are listed in decreasing order of expression with the most highly expressed proteins in EVs on the far left and the most highly expressed proteins in cells on the far right. Averages from all four replicates of each sample type are graphed. Scale indicates intensity, defined as (LFQ Area - Mean LFQ Area)/Standard Deviation. Extracellular proteins with annotated transmembrane domains are bolded and annotated secreted proteins are italicized. (E) Table indicating fold-change of most differentially regulated proteins by LC-MS/MS for RWPE-1 EVs compared to parent cells. (F) Western blot showing the EV specific marker ITIH4, IGSF8, and MFGE8.Mass spectrometry data is based on two biological and two technical replicates (N = 4). Due to limited sample yield, one replicate was performed for the EV western blot.

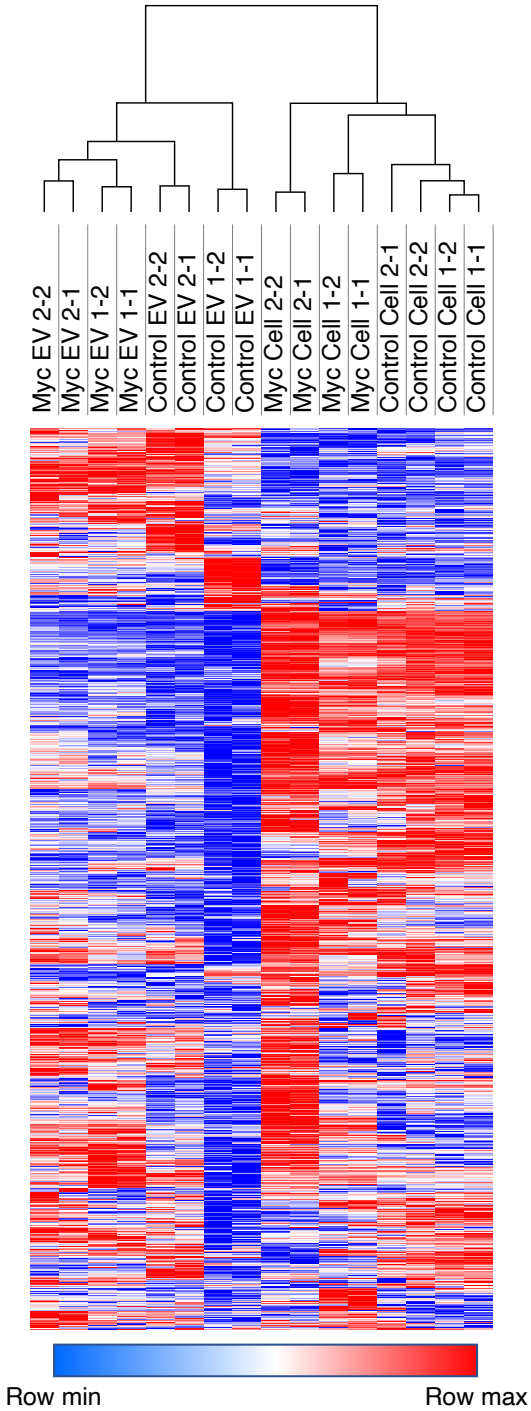

Figure 2.18: Heatmap comparison of biological and technical replicates of RWPE-1 Control/Myc cells and EVs. Biological and technical replicates cluster together based on both oncogene status and compartment for EV or cell surface. Proteins with no area values were assigned an imputed value using Perseus. Heatmap clustering is based off of the Pearson correlation between all replicates on both columns and rows. Heatmap was produced using Morpheus, https://software.broadinstitute.org/Morpheus. The first number following the sample name denotes the biological replicated and second number denotes the technical replicate

Chapter 3

Secreted HLA Fc-Fusion Profiles Immunopeptidome in Hypoxic PDAC and Cellular Senescence

Abstract

Human leukocyte antigens (HLA) present peptides from intracellular proteins on the surface of cells in MHC-peptide complexes. These complexes provide a biological window into the cell and peptides derived from disease-associated antigens can serve as biomarkers and therapeutic targets. Thus, proper identification of peptides and the corresponding presenting HLA allele in disease phenotypes is important for the design and execution of therapeutic strategies. Yet, current mass spectrometry methods for profiling the immunopeptidome limit progress as they typically require large sample input that are inherently complex, preventing study of several disease phenotypes and lowering confidence of peptide identification. Here, we describe a novel secreted HLA (sHLA) Fc-fusion construct that can capture HLA-associated peptides and allows for simple purification of peptides of a single HLA allele in different cell models. We used our sHLA immunopeptidomics method to profile the immunopeptidome of hypoxic pancreatic adenocarcinoma (PDAC) and senescent cells to identify MHC-peptide complexes that could serve as potential biomarkers for these diseases. Bispecific T cell engagers (BiTEs) targeting the identified IF44L peptide demonstrated enrichment in senescence, indicating our method can identify peptides presented on the surface of diseased cells. Overall, this method was used to profile the immunopeptidome of seven cell lines, across two different HLA alleles, and identified >30,000 unique HLA-associated peptides, ~9300 of which were previously unknown. This method enables the study of complex disease states in a temporally-controlled manner for the simple isolation and characterization of allele-restricted MHC-peptidomes using low cellular inputs. We believe this method will be useful in the study of the immunopeptidome as therapeutic interest in MHC-peptide complexes increases in cancer and beyond.

Introduction

Major histocompatibility complex (MHC) class I proteins are a vital mechanism for the removal of dysfunctional or diseased cells from the body by the adaptive immune system (Janeway, 2001).The role of MHC class I proteins is to bind peptide fragments derived from proteins inside the cell and display them to be surveilled by the surrounding adaptive immune system. This quality control mechanism plays a pivotal role in the removal of diseased cells from healthy surrounding tissues in the context of infection, senescence-induced aging, and cancer (Purcell et al., 2019a). This peptide pool, collectively known as the immunopeptidome, can reflect the proteome of a cell in a given phenotype and hence identifying such peptides are important for therapeutic targeting. Ongoing efforts focus on the elucidation and characterization of MHC peptide complexes for clinical use. Indeed, over the course of the past decade, antibodies targeting MHC-peptide complexes have expanded past neoantigens with successful targeting of disease-associated MHC-peptide complexes such as WT1 and PMEL (Dao et al., 2013, 2015; Douglass et al., 2021; Hsiue et al., 2021; Stopfer et al., 2022).

Given the therapeutic promise of MHC-peptides as biomarkers for disease, there is increasing interest in profiling the immunopeptidome of various disease phenotypes. To date, the most common and practical way to identify these peptides is through mass spectrometry analysis. However, the current methods are time and resource intensive, require large numbers of cells (upwards of 1e10 cells), are prone to contamination issues, and are not allele specific, which increases backend data processing and impairs target identification (Caron et al., 2015; Pollock et al., 2021; Purcell et al., 2019b). Additionally, current methods of sample preparation typically span 2-3 days in length, preventing high-throughput analysis. Moreover, many disease contexts, such

as cancer, exhibit decreased MHC presentation at the surface of cells, which preclude the use of traditional methods for MHC peptidome identification.

To circumvent these challenges, previous methods have introduced single HLA alleles into HLA-null engineered cell lines. Generation of membrane bound mono-allelic HLA cell lines, such as C1R and B721.221, have increased peptide identifications and informed predictive algorithms (Abelin et al., 2017; Purcell et al., 2019b; Sarkizova et al., 2020). While this method avoids deconvolution required in normal cells which can carry as many as 6 different HLA alleles, this method is restricted to cell lines that are engineered to be HLA-null, thereby restricting the breadth of biological contexts that can be surveyed. Additionally, these cell lines have been reported to have low, but residual, endogenous HLA expression thereby contaminating the samples (Purcell et al., 2019b). Others have developed soluble HLA constructs lacking the transmembrane domain, allowing the HLA to be loaded and subsequently secreted and immunoprecipitated from the surrounding milieu (Hawkins et al., 2008; Hilton et al., 2017). While this method retains allele specificity and can be expanded to different cell types, it remains unoptimized and typically relies on bioreactors for cell culture (Abelin et al., 2017). Additionally, these soluble HLA methods still require copious amounts of material (10-25 mg) as it demands several purification and fractionation steps (Hawkins et al., 2008; Hilton et al., 2017). Hence, current mono-allelic approaches are not amendable to study the immunopeptidome of cells under different phenotypes to identify disease-associated MHC-peptide complexes.

Here, we present a novel secreted HLA method for the simple isolation and characterization of allele-restricted MHC-peptidomes using low cellular inputs (< 20 M). This method provides temporal, mono-allelic analysis of the immunopeptidome in a matter of hours, not days, without requiring cell lysis and peptide fractionation. Using samples ranging from 12-

130 million cells, we identified >30,000 peptides, ranging from ~600 to 10,000 peptides per sample depending on cell line. We performed an antibody phage display campaign on a peptide confidently identified from senescent samples and used a BiTE to show enriched presentation on the surface of senescent cells. We believe this method will be useful in profiling the immunopeptidome of disease states and will be instrumental in target discovery of MHC-peptide complexes.

Results

sHLA Fc-fusion Captures HLA-associated Peptides in B721.221 cells

Fc-fusion proteins have served as structural scaffolds in the expression and solubilization of the extracellular domain of membrane proteins (Czajkowsky et al., 2012; Martinko et al., 2018b). As HLA proteins lacking the transmembrane domain have been shown to be properly folded and loaded with peptide cargo (Hawkins et al., 2008; Hilton et al., 2017), we hypothesized that a secreted HLA Fc-fusion (henceforth referred to as sHLA) could be loaded and secreted similarly **(Figure 3.1)**. With mono-allelic B721.221 cell lines providing a standard in the field by providing datasets for peptide processing and binding prediction, we sought to determine if our HLA Fc-fusion could capture HLA-associated peptides in this bona fide cell model. We engineered two B721.221 cells, each stably transduced to express a unique sHLA under doxycycline induction **(Figure 3.1)**. After 52 hours with or without doxycycline treatment, media was collected and sHLA proteins were immunoprecipitated using magnetic Protein A beads and analyzed by western blot **(Figures 3.2A & 3.2B)**. Cells treated with doxycycline demonstrated expression and secretion of each sHLA, indicating that this construct is processed as expected.

Using monoallelic sHLA B721.221 cells lines towards HLA-A*02:01 and HLA-B*35:01, we performed immunopeptidomics by immunoprecipitating sHLA proteins and purifying peptides

through acid elution and standard desalting procedures **(Figure 3.1)**. Data were analyzed using a stringent 1% FDR, and excluded low molecular weight singly charged species (data not shown). After a single unsupervised search, identified peptides aligned with expected peptide length **(Figures 3.2C & 3.2D)** and anchor residues **(Figures 3.2E &3.2F)** for HLA-A*02:01 and HLA-B*35:01 allele, respectively. The predicted affinity (NetMHC) of the 9-mers characterized in our dataset showed good overlap with a previous dataset using the full length, membrane bound MHC-peptide complexes in the same cell line. A random collection of 1e5 9-mers did not show appreciable predicted binding, indicating that our analysis yielded bona fide MHC-bound peptides **(Figures 3.2G & 3.2H)**(Abelin et al., 2017; Sarkizova et al., 2020). Additionally, our sHLA method identified similar numbers of peptides as those previously reported. Thus, our sHLA protein can capture HLA-associated peptides in a similar manner as membrane bound MHC-peptide complexes confirming our sHLA method binds and captures biologically relevant MHC peptides.

sHLA Fc-fusion Profiles Immunopeptidome in Hypoxic PDAC

Hypoxia, where oxygen levels become deficient, is a prominent feature in most solid tumors. The use of oxygen as a terminal electron acceptor is a critical component of mammalian cell biology (Babcock, 1999). As such, organisms have developed highly regulated cellular pathways and gene programs to deal with low-oxygen conditions. When available oxygen to cancer cells becomes unsustainable, hypoxic pathways are activated and promote all steps of the metastatic cascade, most importantly immune evasion, self-renewal, angiogenesis, and metastasis (Eales et al., 2016, 2016; Harris, 2002; Keith & Simon, 2007). As such, hypoxia and its downstream gene programs have largely been implicated in poor prognoses and low disease-free survival for patients with these hypoxic cancers. Hypoxia plays a major role across many solid tumor types, but more

recently, has been implicated particularly in the pathogenesis of pancreatic cancer (Akakura et al., 2001; Yuen & Díaz, 2014). Pancreatic tumors show the highest fold-change in oxygen tension across different cancers, decreasing by almost 20-fold upon solid tumor formation (McKiernan et al., 2016). Hence, identification and characterization of hypoxic-specific antigens is of great interest to the cancer field (Bourseau-Guilmain et al., 2016). Yet, the immunopeptidome of hypoxic cancers, specifically PDAC, has remained relatively understudied. Additionally, PDAC in particular has been shown to downregulate MHC-I expression at the cell surface, through either autophagic or transcriptional mechanisms, precluding the use of standard MHC-I isolation and characterization methods (Yamamoto et al., 2020). However, work has increasingly focused pharmacologic strategies for upregulating the surface expression and retention of these proteins to increase immune cell engagement (Gu et al., 2021). While increasing MHC-I retention at the cell surface is paramount for improving clinical efficacy of future therapeutics, we have focused our scope on providing robust and efficacious targets for next-generation therapeutic development.

We chose three different PDAC cell lines used in the study of hypoxia: MiaPaCa-2, KP4, and Capan-1. MiaPaCa-2 and KP4 cells were stably transduced with our sHLA-B*35:01construct and Capan-1 cells were stably transduced with the sHLA-A*02:01 construct. Cells were grown for either 96 hours under 20% O_2 (normoxia) or 1% O_2 (hypoxia), with Doxycycline-treatment beginning after 72 hours **(Figure 3.3A)**. Hypoxia was confirmed through western blotting of canonical hypoxia markers, Glut1 and HIF-1α **(Figure 3.5)**. Across normoxic and hypoxic samples, we identified 7,023 unique peptides in MiaPaCa-2 cells, 3,112 unique peptides in KP4 cells, and 14,257 unique peptides in Capan-1 cells **(Figure 3.3B)**. Impressively, normoxic Capan-1 peptide counts ranged from ~8,200-10,000 HLA-A*02:01-associated peptides from ~130 million cells, demonstrating the potential depth this method can profile the immunopeptidome of

a single allele. Moreover, the majority of peptides were identified across either three or four of the biological replicates, indicating that the method is robust in its peptide identification **(Figure 3.3C)**. Of the peptides identified exclusively in hypoxia within each cell line—99 in MiaPaCa-2, 61 in KP4, and 135 in Capan-1—were found with high confidence, appearing in at least 3 out of 4 hypoxic replicates and not present in the 4 normoxic replicates. Through further analysis of the HLA-A*02:01 peptides, we isolated a selection of peptides that were specific to hypoxia on the protein and peptide levels, which were not found in the healthy control populations deposited in the IEDB **(Figure 3.4A)**. Excitingly, from these high confidence peptides found within hypoxic samples, we identified peptides from several biomarkers of hypoxia, such as KAD4 (HLA-A*02:01: NLDFNPPHV)(Jan et al., 2019), CHRAC1 (HLA-A*02:01: VIMKSSPEV)(Hasan & Ahuja, 2019), and SPAG4 (HLA-A*02:01: SLGKFTFDV)(Knaup et al., 2014), which are all associated with poor disease prognosis in PDAC **(Figure 3.4B, C, D, & E)** (Goldman et al., 2020). Interestingly, there were peptides confidently found exclusively in hypoxic samples, such as HLA-B*35:01-associated LPQGPLGTSF derived from TXNIP, despite peptides from the same protein identified in normoxic samples. Interestingly, when analyzing the peptides found specifically in hypoxic samples—and not in normoxic controls, we find a marked association between these peptides and hypoxia-specific biological pathways, such as glycolytic flux and HIF-1 signaling pathways **(Figure 3.6A)**. This suggests that differential processing of peptides may be involved and exclusive to the hypoxic phenotype. More work will be required to dissect the underlying pathways that are over-represented in the immunopeptidome of hypoxia and could serve as therapeutic targets for treating solid tumors.

sHLA Fc-fusion Profiles Immunopeptidome in Cellular Senescence

Senescent cells, or those that have undergone permanent cell-cycle arrest due to compromised integrity or insult, have been shown to drive a host of age-related diseases. Recent senolytic strategies demonstrate a clear benefit of senescent cell removal, including increasing median healthy lifespan by upwards of 30% (Baker et al., 2016). Hence, identifying novel markers of senescence is of great interest to the anti-aging field. Yet, little is known regarding the immunopeptidome of senescent cells, likely due to the fragility of cells and difficulty culturing such a large volume of non-proliferative cells for classic methods. Using our sHLA immunopeptidomics method, we sought to identify HLA-associated peptides in senescence.

We chose three different cell lines commonly used in the study of cellular senescence: MCF7 (breast cancer), PC3 (prostate cancer), and A549 (lung cancer). MCF7 cells were transduced with our sHLA-B*35:01 construct while PC3 and A549 cells were transduced with the sHLA-A*02:01 construct. As chemotherapy drugs are frequently used to drive cancer cells into the non-proliferative state of senescence, we treated each cell line with 250 nM doxorubicin (a topoisomerase II inhibitor) for 24 hours and then cultured for 9 days post-treatment to allow for the senescent phenotype to develop. In parallel, each cell line was treated with DMSO for 24 hours to generate a growing sample (**Figure 3.7A**). Senescence was confirmed by beta-galactosidase activity staining and p21 expression (**Figures 3.7B & 3.8)**.

Across growing and senescent samples, we identified 5795 unique peptides in MCF7's, 11105 unique peptides in PC3's, and 3795 unique peptides in A549's (**Figure 3.7C**). Of the peptides identified exclusively in senescence within each cell line, 466 in MCF7's, 1021 in PC3's, 190 in A549's, were found with high confidence, appearing in at least 3 out of 4 samples. Excitingly, from these high confidence peptides exclusive to senescence, we identified peptides

from several biomarkers of senescence, such as GDF15 (HLA-A*02:01: ALPEGLPEA)(Acosta et al., 2013), PGH2 (HLA-A*02:01: SVPDPELIKTV)(Gonçalves et al., 2021), and CCPG1: (HLA-A*02:01: SLQEELNKL)(Catherman et al., 2013). Pathway analysis performed with peptides identified only in the context of senescence showed a strong signature of viral infection, which has been shown to be a major driver of senescence **(Figure 3.5B)** (Lee et al., 2021; Seoane et al., 2020). Remarkably, each MCF7 senescent sample averaged less than 17 million cells per sample with an average peptide ID count of ~3200. This highlights the potential of using this method with smaller cell samples without sacrificing peptide counts. Interestingly, we saw a universal shift across all cell lines where more peptides were identified in senescent samples than growing. As senescent cells have an active secretory phenotype, our sHLA construct may be advantageous and have improved trafficking in phenotypes and cells that already secrete proteins. While data analysis continues in order to understand how the profiled immunopeptidome reflects the biological context and pathways of the senescent phenotype, we demonstrate our sHLA method can capture and identify peptides in senescent cells.

Antibodies Targeting IF44L MHC-peptide Complex Show Increased Presentation in Senescent Cells

We sought to confirm that peptides identified using our sHLA construct have enriched presentation in our disease phenotypes and could serve as potential therapeutic targets. Our immunopeptidomics analysis revealed the HLA-A*02:01-associated peptide, FMLGNYINL, derived from the interferon-induced protein IF44L showed to be specific to senescent PC3 cells both on a peptide and protein level. As antibodies have proven to be useful tools in specifically recognizing and targeting naturally presented MHC-peptide complexes, we pursued a phage display campaign to select for antibodies against the IF44L MHC-peptide complex.

Using a Fab-phage library, we first performed a negative clearance using an immobilized MHC-peptide complex containing a peptide derived from the viral protein TAX1, thereby removing any Fab-phage that bound elsewhere on the complex other than the peptide epitope. Taking the remaining phage, we performed a positive selection against immobilized IF44L MHC-peptide complex and eluted any bound phage with TEV protease cleavage (**Figure 3.9A**).

After multiple rounds of selection, individual phage clones were screened via ELISA with one Fab (henceforth referred to as IFB2) demonstrating specific binding to the IF44L MHC peptide complex and not the TAX1 MHC-peptide complex (**Figure 3.9B).** Octet analysis revealed IFB2 bound to the IF44L MHC-peptide complex with an affinity of ~34 nM while exhibiting no binding to the TAX1 MHC-peptide complex (**Figures 3.9C & 3.9D**), highlighting IFB2 specificity. IFB2 bound to T2 lymphoblasts exogenously loaded with the IF44L peptide, demonstrating Fab ability to recognize the IF44L MHC-peptide complex on the surface of cells (**Figure 3.9E**). Therefore, we generated a high affinity, selective antibody that could be used to probe the surface of senescent cells for the IF44L MHC-peptide complex.

Historically, HLA-associated peptides have been suggested to be presented at extremely low copy numbers, with many quantitative analysis reporting well under 100 copies per cell – often times only reaching single digit levels(Holland et al., 2020; Høydahl et al., 2019). We converted our Fabs into bispecific T cell engagers (BiTEs) with the ability to activate T cells in the proximity to cells presenting IF44L MHC-peptide complexes (**Figure 3.9F**). T cell activation is highly sensitive and requires very few copies of antigen per cell to elicit a response, providing a suitable model to probe the surface of senescent cells. Using an NFAT-GFP Jurkats, in which GFP expression is a proxy for T cell activation, we were able to survey the surface of target cells for IF44L MHC-peptide presentation. When incubated with IFB2 BiTEs and T2 lymphoblasts

loaded with peptide, Jurkats showed significantly greater activation in the presence of cells displaying IF44L MHC-peptide complexes than those displaying TAX1 (**Figure 3.9G**). Hence, the IFB2 BiTE successfully recognizes and activates T cells as expected. When incubated with IFB2 BiTE and growing or senescent MCF7 cells, Jurkats showed >2 fold GFP signal with senescent cells over growing (**Figure 3.9H**). These data show the IF44L peptide identified using the sHLA construct is indeed enriched on the surface of senescent cells, highlighting the potential of this method to easily identify potential targets in the immunopeptidome of disease models and opens the door for potential therapeutics.

Discussion

MHC-peptide complexes are becoming increasingly attractive as therapeutic targets as they can provide extracellular access to disease-associated antigens. Hence, identifying HLA-associated peptides and for specific HLA-alleles is important for therapeutic development and design. Yet, common immunopeptidomics methods require lysis of large samples and use pan-HLA pulldowns to purify mixed peptides across multiple alleles. Mono-alleleic HLA samples have been engineered, but are limited by cell line restriction, culturing conditions, and large sample sizes. Here, we describe a fast, simple, method utilizing a secreted HLA Fc-fusion construct which can be used to purify allele-restricted HLA-associated peptides. Our method was able to profile the immunopeptidome of hypoxic PDAC and cellular senescence and identified several peptides to be disease-exclusive. Furthermore, Jurkats co-cultured with senescent cells and BiTEs targeting the IF44L peptide had increased activation over growing cells, indicating our sHLA method can identify MHC-peptide complexes enriched in disease phenotypes.

As immunopeptidomics becomes more mainstream and accessible, simpler and more rapid methods will be necessary. We believe this method, which takes mere hours as opposed to days to

complete, will be useful in the profiling of several disease models such as viral or bacterial transfection, chemical perturbation, or oncogenic transformation. Additionally, one could also co-culture different cells and only profile the immunopeptidome of a single allele in a single cell line, something that is currently unattainable with today's methods. Lastly, this method can be used to generate datasets that can inform peptide binding and generation prediction algorithms that will be important as more HLA alleles are uncovered and characterized.

While this method shows improvement over current techniques, there are a number of limitations. Given that this requires lentiviral transduction to generate stable cell lines, primary cell lines or those excised directly from patients may not be amenable. Additionally, due to variability in sHLA expression under different phenotypes, we do not believe this method could be used for absolute or relative quantification of HLA-associated peptides. Thus, this method is useful strictly for profiling and identification purposes. Interestingly, we also suspect that sHLA's of a particular allele will not express in cells that endogenously express that HLA allele. For example, HLA-A*02:01 sHLA constructs did not appear to express in IMR90 fibroblasts and Panc-1 cells (data not shown). While more work is necessary to outline the requirements for suitable cell lines, this may hinder the use of common alleles such as HLA-A*02:01 in the study of phenotypes with limited cell models.

In conclusion, this sHLA method can pull out HLA-associated peptides in an allele-restricted, disease-specific manner. As antibody-based therapeutics are developed and reactive TCR's are identified against specific MHC-peptide complexes, this powerful tool will be useful in target discovery and peptide triage. We believe this information of disease-associated peptides or neoantigens may drastically accelerate personalized medicine and reshape how we assess the potential of certain antigens.

Methods

Cloning

sHLA Fc-fusion was cloned into the lentiviral vector pLVX-TetOne-Puro. AviTag HLA-A*02:01 in the expression vector pMBio and β_2M in the expression vector pIN-III ompA2 were generous gifts from Dr. Ton Schumacher (Netherlands Cancer Institute). To generate our selection construct, we subcloned a TEV protease cleavage site in between HLA-A*02:01 and the AviTag. Fabs were subcloned from the phagemid into the expression vector pBL347. The light chain of the BiTE was cloned from the Fab plasmid into a pFUSE (InvivoGen) vector with the OKT3 anti-human CD3 scFv. The heavy chain of the BiTE was cloned from the Fab plasmid into the same vector but lacking the Fc domain. All constructs were sequence verified by Sanger sequencing.

Cell culture

B721.221 cells were a generous gift from Dr. Lewis Lanier (UCSF). Capan-1 pancreatic cancer cells were from Wells lab frozen stocks. KP4 and MiaPaCa-2 pancreatic cells were generous gifts from Dr. Rushika Perera (UCSF). A549 lung cancer cells were a gift from Dr. Oren Rosenberg (UCSF). PC3 prostate cancer cells and MCF7 breast cancer cells were purchased from the UCSF Cell Culture Facility. B721.221, A549, PC3, and MCF7 cells were all grown in RPMI+10% Tetracycline-negative FBS+1% Pen/Strep. Capan-1, KP4, and MiaPaCa-2 cells were all grown in IMDM+10% Tetracycline-negative FBS+1% Pen/Strep. Cell lines transduced with the sHLA Fc-fusion were cultured in media with 2 μg/mL puromycin. sHLA Fc-fusion cell lines were cultured in respective media without FBS and with Doxycycline for sample collection. The NFAT-GFP reporter Jurkat cells used were a generous gift from Dr. Arthur Weiss (UCSF). Jurkats were cultured in RPMI+10% FBS+1% Pen/Strep+2 mg/mL G418. All cells were grown at 37°C, 5% O_2 unless otherwise stated.

To generate normoxic Capan-1, KP4, and MiaPaCa-2 cells, cells were grown for 3 days in IMDM+10% Tetracycline-negative FBS+1% Pen/Strep at 37°C, 5% O_2 before beginning Doxycycline treatment. Hypoxic cells were grown in a hypoxic chamber in IMDM+10% Tetracycline-negative FBS+1% Pen/Strep at 37°C, 1% O_2 prior to Doxycycline treatment. Hypoxic cells were only removed from the chamber to replaced media for the appropriate condition and exchange was conducted as quickly as possible to avoid the onset of the normoxic phenotype.

A549, MCF7, and PC3 cells were seeded one day prior to treatment. Cells were incubated in media containing either 250 nM Doxorubicin (Sigma-Aldrich) or the equivalent volume of DMSO for 24 hours. Growing samples were treated with Doxycycline immediately after DMSO treatment. For the senescent samples, media was replaced and then subsequently replaced every other day for 8 days post-doxorubicin treatment before Doxycycline treatment. Cells were seeded separately for western blot analysis and β-galactosidase activity staining. β-galactosidase activity staining was performed using a Senescence β-Galactosidase Staining Kit (Cell Signaling) following the manufacturer's protocol.

Lentivirus and cell line generation

HEK293T cells were cultured in DMEM+10% FBS+1% Pen/Strep. Cells were seeded $5x10^5$ per well of a 6-well plate a day prior to transfection. Plasmids at the designated concentrations (1.35 μg pCMV delta8.91, 0.165 μg pMD2-G, 1.5 μg sHLA plasmid) were added to OptiMEM media with 9 μL FuGENE HD Transfection Reagent (Promega) at a 3:1 FuGENE:DNA ratio, incubated for 30 minutes, and subsequently transfected into HEK293T cells. The supernatant was harvested and cleared by passing through a 0.45-μm filter 72 hours post transfection. Cleared supernatant was added to target cells (~1 million cells) with 8 μg/mL polybrene and centrifuged at 1000 x g at

33°C for 3 hours. 24 hours post-transduction, media was replaced with appropriate fresh media. After an additional 24 hours, drug selection for stable cell lines was initiated by the addition of 2 µg/mL puromycin and expanded.

To expand successfully transduced B721.221 cells, live cells were isolated using SepMate™-50 (IVD) tubes and Lymphoprep™ (Stemcell Technologies). For isolation, cell cultures were centrifuged at 300 x g for 5 minutes and resuspended in 5 mL of cell culture media. 15mL Lymphoprep™ was added to each SepMate™-50 (IVD) tube, and the 5 mL cell suspension was subsequently added. Tubes were centrifuged at 400 x g for 10 minutes, and then supernatant was quickly decanted into 30 mL cell media and the SepMate™-50 (IVD) tube was discarded. The cell culture was spun at 300 x g for 5 minutes and supernatant was removed. Pellets were resuspended in cell media containing appropriate drug and expanded. A total of 2 isolations occurred for each cell line.

Mass Spectrometry Sample Preparation

Cell phenotypes were induced as described. Cells were cultured in media with 2 µg/mL Doxycycline for 24 hours, and then subsequently cultured in serum-free media with 2 µg/mL Doxycycline for 28 hours prior to media collection. For each 50 mL of media sample, 100 µL of Pierce™ Protein A Magnetic beads (Thermo Scientific) were washed twice with PBS prior to use. Beads were added to media was filtered with 0.45-µm filters and rotated for 1 hour at 4°C. Samples were spun at 500 x g for 5 minutes and media removed. Beads were washed strenuously with 10 mM Tris pH 8.0 made with Optima™ LC/MS water (Thermo Scientific). After washing, protein/peptides were eluted by incubating beads with 10% acetic acid for 10 minutes at room temperature. Beads were washed twice with 10% acetic acid, and washes and elution were pooled together. Samples were dried in a Genevac prior to desalting.

Dried down samples were resuspended in 75 µL of 1% TFA and vortexed vigorously. Samples were centrifuged at 21,000 x g for 5 minutes at RT to remove any remaining precipitate. Sample was placed in a magnetic rack, after which the supernatant was removed gently from the tube and placed in a prepared Pierce C18 column as per manufacturer's instruction. Shortly, each column was washed with 200 µL of 70% acetonitrile in water and spun down at 1500xg until dry. The columns were further washed with 200 µL of 50% acetonitrile in water and spun still dryness. Following the pre-wash steps, each column was further washed twice with 200 µL of 5% acetonitrile/0.5% TFA in water and spun till dryness. The sample was then loaded onto the column and spun till dryness. Each sample was reloaded onto the column to maximize peptide yield. Samples were then washed with 2x 200 µL of 5% acetonitrile/0.5% TFA in water, 200 µL of 5% acetonitrile/1% FA in water, and eluted in 2x 50 µL of 70% acetonitrile in water. Samples were dried to completion.

Mass Spectrometry

Liquid chromatography and mass spectrometry was performed as previously described(Meier et al., 2020). Briefly, each sample was brought up in 6.5 µL of 2% acetonitrile/0.1% formic acid in water, vortexed vigorously, and spun down at maximum speed to remove any precipitate. The sample was transferred and 6 µL of the peptide supernatant was separated using a nanoElute UHPLC system (Bruker) with a pre-packed 25 cm x 75 µm Aurora Series UHPLC column + CaptiveSpray insert (CSI) column (120 A pore size, IonOpticks, AUR2-25075C18A-CSI) and analyzed on a timsTOF Pro (Bruker) mass spectrometer. Peptides were separated using a linear gradient of 7-30% (Solvent A: 2% acetonitrile, 0.1% formic acid, solvent B: acetonitrile, 0.1% formic acid) over 60min at 400 nL/min. Data-dependent acquisition was performed with parallel accumulation-serial fragmentation (PASEF) and trapped ion mobility spectrometry (TIMS)

enabled with 10 PASEF scans per top N acquisition cycles. The TIMS analyzer was operated at a fixed duty cycles close to 100%using equal accumulation and ramp times of 100 ms each. Singly charged precursors below 800m/z were excluded by their position in the m/z-ion mobility plane, and precursors that reached a target value of 20,000 arbitrary units were dynamically excluded for 0.4 min. The quadrupole isolation width was set to 2 m/z for m/z < 700 and 3 m/z for m/z > 700 and a mass scan range of 100-1800 m/z. TIMS elution voltages were calibrated linearly to obtain the reduced ion mobility coefficients (1/K0) using three Agilent ESI-L Tuning Mix ions (m/z 622, 922, and 1,222).

Data Analysis

Briefly, for general database searching, peptides for each individual dataset were searched using PEAKS Online X version 1.5 against the entire Swiss-prot Human Proteome (Swiss-prot). Enzyme specificity was set to Unspecific. Peptide length was specified between 8-12 amino acids. No fixed modifications were set, while acetylation (N-term) and methionine oxidation were set as variable modifications. The precursor mass error tolerance was set to 20 PPM and the fragment mass error tolerance was set to 0.03Da. Data was filtered at 1% for both protein and peptide FDR. All mass spectrometry database searching was based off of four biological replicates. Biological replicates underwent preparation, washing, and downstream LC-MS/MS preparation separately.

Western Blot

sHLA Fc-fusion samples from B721.221 cells were generated and purified as described. Beads were washed three times with PBS and protein was eluted with 0.1 M acetic acid. For growing and senescent samples, cells were washed twice on plate with PBS prior to lysis. Lysis buffer contained 1x RIPA (EMD Millipore), 1% protease inhibitor cocktail (Sigma-Aldrich), and 1 mM EDTA.

Cells were lysed for 20 minutes on ice prior to sonication (1 minute, 20% amp, 1 second on/off pulse). Cells were spun at 16000 x g at 4°C for 5 minutes, and lysate protein concentration was determined using a Pierce™ BCA Protein Assay (Thermo Scientific).

Samples were run on a Bolt 4-12% Bis-Tris gel (Invitrogen), and transferred to a PVDF membrane (Thermo Scientific) using an Iblot™ (Thermo Scientific). Membranes were blocked in Odyssey® Blocking Buffer (TBS) (LiCOR) prior to staining. Membranes were stained with primary anti-FLAG (Cell Signaling, 14793S), anti-human HLA-A (Thermo Scientific, PA5-29911), anti-human HLA-B (Proteintech, 17260), anti-human p21 (Abcam, ab109520), and anti-human α-tubulin (Sigma-Aldrich, T6199) antibodies in blocking buffer for 1 hour at room temperature or overnight at 4°C. Secondary staining was performed using goat anti-rabbit IRDye® 800CW and goat anti-rabbit IRDye® 680RD antibodies (LiCOR Biosciences) in blocking buffer for 1 hour at room temperature. Membranes were washed with three 5 minute washes of TBST between each staining step. Membranes were imaged using an Odyssey® CLx (LiCOR Biosciences).

Protein Expression and Purification

MHC-peptide complexes were expressed and refolded as previously described(Rodenko et al., 2006). Peptides were purchased from ELIM Biopharmaceuticals, Inc. All peptides were >98% purity. MHC-peptide complexes were refolded at 10°C for 3 days and SEC-purified on a HiLoad 16/600 Superdex 75 pg column equilibrated in 10 mM Tris pH 8. After purification, MHC-peptide complexes were biotinylated using a BirA reaction kit (Avidity) per manufacturer's instructions in the presence of excess peptide and β_2M at 25°C for 4 hours. After biotinylation, MHC-peptide complexes were purified again via SEC to remove excess biotin. Proper folding was assessed by

SDS-PAGE. Biotinylation was assessed by pre-incubating MHC-peptide complexes with NeutrAvidin and subsequently assessed by SDS-PAGE.

Fabs were expressed in E. coli C43 (DE3) Pro+ as previously described using an optimized autoinduction medium and purified by protein A affinity chromatography(Hornsby et al., 2015). Fabs were subsequently buffer exchanged into PBS pH 7.4 and stored in 10% glycerol at -80°C and assessed by SDS-PAGE.

BiTEs were expressed and purified from Expi293F-BirA cells using transient transfection (Expifectamine, Thermo Scientific). Enhancers were added 20 hrs after transfection. Cells were incubated for 5 days at 37ºC and 8% CO_2. Media was then harvested by centrifugation at 4,000xg for 20 min. BiTEs were purified by protein A affinity chromatography and buffer exchanged into PBS pH 7.4, then stored in 10% glycerol at -80°C and assessed by SDS-PAGE.

Fab-phage selection

Phage selections were run as previously described(Hornsby et al., 2015). Selections were performed on a KingFischer^{TM} System (Thermo Scientific). Biotinylated antigens were immobilized using streptavidin-coated magnetic beads (Promega). In each round, phage was first cleared by incubation with beads loaded with MHC-peptide complexes loaded with TAX1 peptide. Unbound phage was next incubated with beads loaded with IF44L MHC-peptide complex. Beads were washed and bound phage was eluted with 50 μg/mL of TEV protease. Four rounds of selection were performed with decreasing amounts of IF44L MHC-peptide complex. Selections were performed in PBS+0.02% Tween-20+0.2% bovine serum albumin (PBSTB). Individual phage clones from the fourth round of selections were analyzed by ELISA.

Phage ELISA

For each phage clone, four different conditions were tested – Direct: IF44L MHC-peptide complex, Competition: IF44L MHC-peptide complex with an equal concentration of IF44L MHC-peptide complex in solution, Negative selection: TAX1 MHC-peptide complex, and Control: PBSTB. 384-well Nunc Maxisorp flat-bottom clear plates (Thermo Fisher Scientific) were coated with 0.5 μg/mL of NeutrAvidin in PBS overnight at 4°C and subsequently blocked with PBSTB. Plates were washed 3x with PBS containing 0.05% Tween-20 (PBST) and were washed similarly between each of the steps. 20 nM biotinylated IF44L MHC-peptide complex or TAX1 MHC-peptide complex was diluted in PBSTB and immobilized on the NeutrAvidin-coated wells for 30 minutes at room temperature, then blocked with PBSTB +10 μM biotin for 10 minutes. For the competition samples, phage supernatant was diluted 1:5 into PBSTB with 20 nM IF44L MHC-peptide complex 30 minutes prior to addition to the plate. For the direct samples, phage supernatant was diluted 1:5 in PBSTB. Competition and direct samples were added to the plate for 30 minutes at room temperature. Bound phage was detected by incubation with anti-M13-horseradish peroxidase conjugate (Sino Biologics, 1:5000) for 30 minutes, followed by the addition of TMB substrate (VWR International). The reaction was quenched with the addition of 1 M phosphoric acid and the absorbance at 450 nm was measured using a Tecan M200 Pro spectrophotometer. Clones with high binding to IF44L MHC-peptide complex and low binding to PBSTB/TAX1 MHC-peptide complex were carried forward. Clones were further filtered using the competition ELISA where appropriate.

Bio-layer Interferometry

BLI measurements were made using an Octet RED384 (ForteBio) instrument. MHC-peptide complex was immobilized on a streptavidin biosensor and loaded for 200 seconds. After blocking

with 10 μM biotin, purified binders in solution were used as the analyte. PBSTB was used for all buffers. Data were analyzed using the ForteBio Octet analysis software and kinetic parameters were determined using a 1:1 monovalent binding model.

Flow Cytometry of T2 Lymphoblasts

The day prior to Fab staining, T2 lymphoblasts were cultured in RPMI serum-free media containing 50 μg/mL peptide of interest at a concentration of 1 million cells/mL. Cells were spun down at 125 x g for 7 minutes and washed 1x in PBS pH 7.4+3% BSA. Each sample was resuspended in 10 μg/mL Fab for 30 minutes, and then washed 3x in PBS pH 7.4+3% BSA. Each sample was then stained with Protein A, Alexa Fluor® 647 conjugate (Life Technologies) for 30 minutes, and then washed 3x in PBS pH 7.4+3% BSA. Samples were resuspended in sterile PBS pH 7.4 and analyzed on a CytoFLEX (Beckman Coulter). Data were processed using FlowJo.

BiTE Assays

T2 lymphoblasts and NFAT-GFP Jurkats were seeded at 1:1 ratio ($5x10^4$:$5x10^4$) in a 96-well round bottom plate containing 50 μg/mL peptide of interest and 100 pM BiTE for 24 hours with n=3 technical replicates per condition. Cells where the percentage of GFP+ cells is gated so ~97% of Jurkat cells with no BiTE are classified as GFP negative. SKMEL5 cells were analyzed on the LSRII, T2 on the CytoFLEX. Growing and senescent MCF7 cells were prepared as described. Cells were lifted using 0.05% Trypsin-EDTA, and seeded with Jurkat NFAT-GFP cells in a 5:1 (MCF7:Jurkat, $2.5x10^5$:$5x10^4$) for 24 hours. All samples were analyzed on the CytoFlex and analyzed on FlowJo.

Figures and Tables

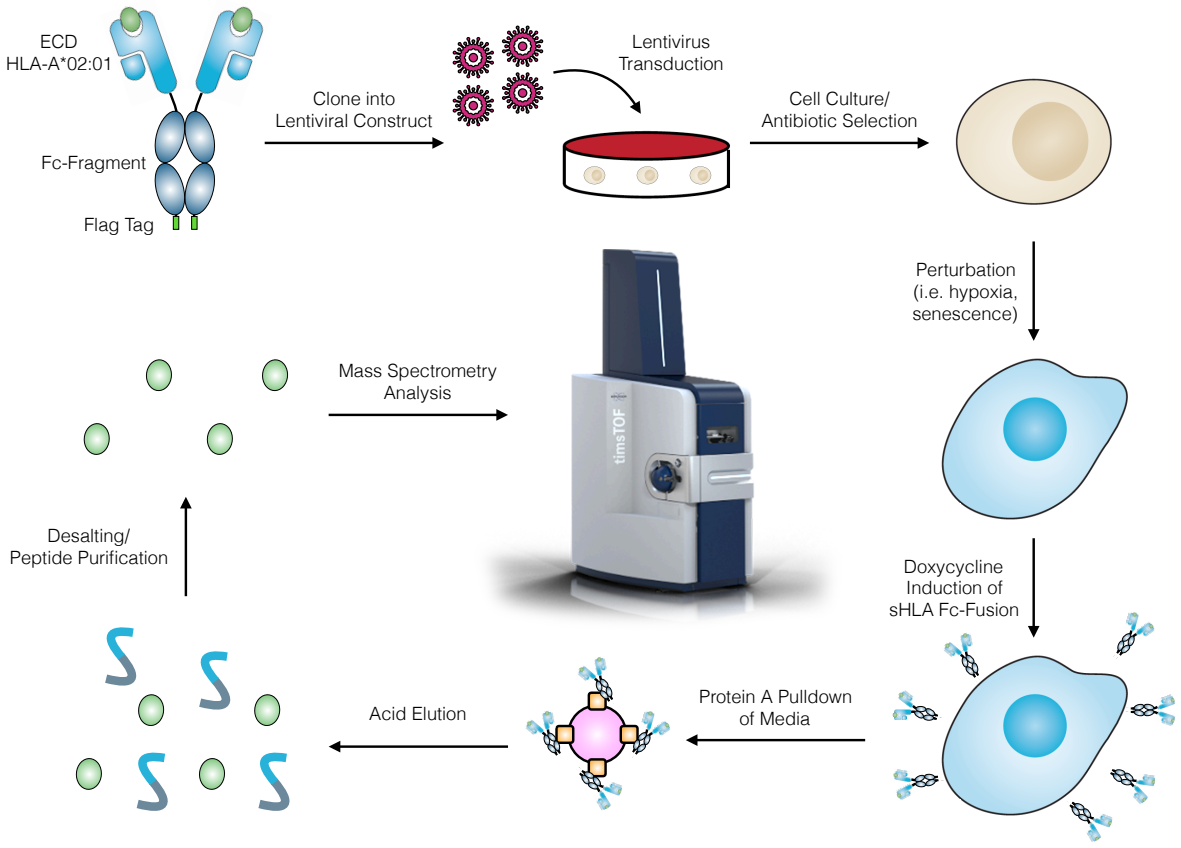

Figure 3.1: Workflow for sHLA cell line generation and subsequent immunopeptidomics. Secreted HLA (sHLA) Fc-fusion is virally transduced into cells of interest. Cells are grown under disease contexts and the expression of the sHLA is induced using doxycycline. The media from cells is isolated and sHLA are immunoprecipitated, washed, and the peptides are eluted for analysis by LC-MS/MS.

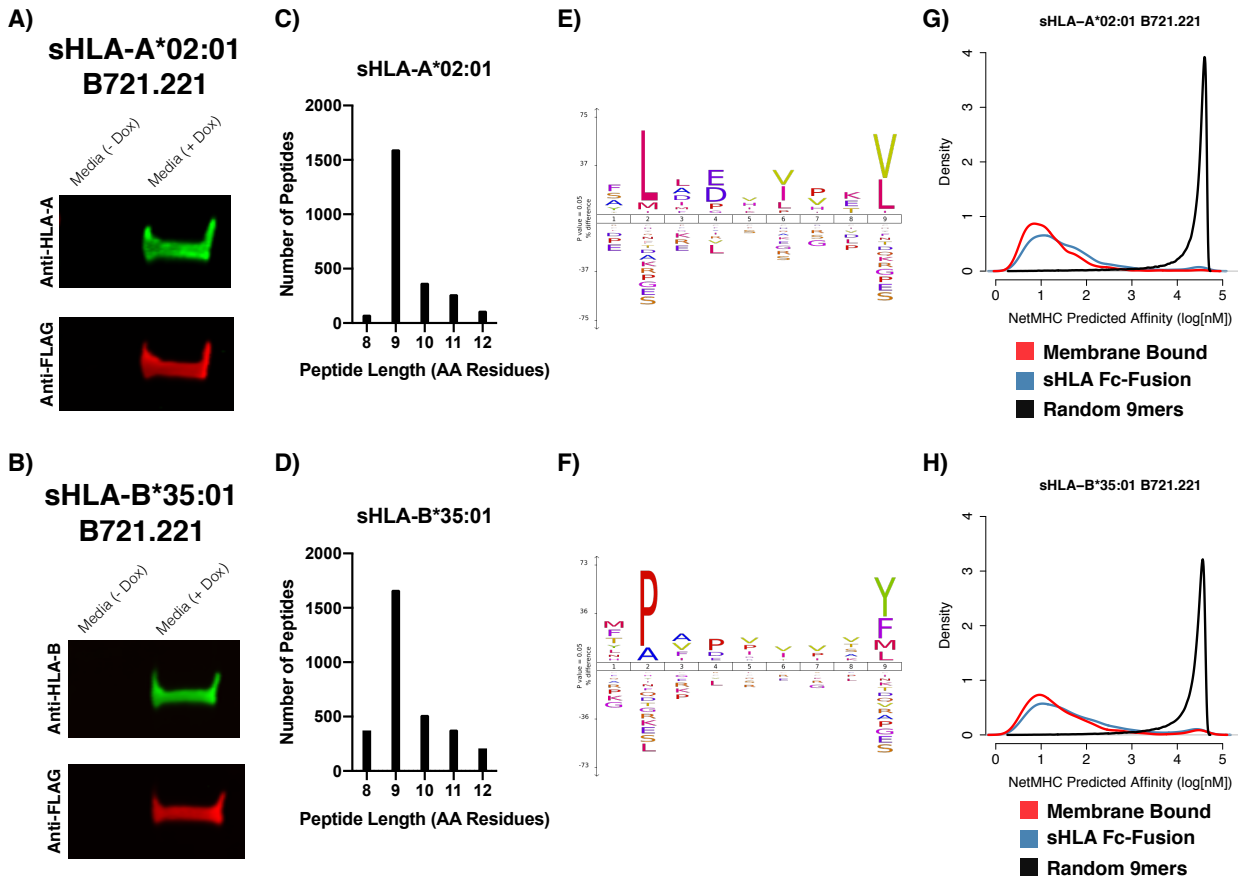

Figure 3.2: Secreted HLA Fc-fusions capture HLA-associated peptides in B721.221 cells. A & B) Western blot of eluted sHLA Fc-fusion protein captured from Doxycycline-treated or –free media of sHLA monoallelic B721.221 cell lines. C &D) Quantification of peptide length from each sHLA B721.221 immunopeptidomics dataset. E & F) ICE logos of 9mer peptides from each sHLA B721.221 immunopeptidomics dataset. G &H) NetMHC predicted affinities of our 9mer peptides from sHLA B721.221 immunopeptidomics dataset compared to published 9mers identified from membrane bound monoallelic B721.221 cells and a published list of 100,000 9mer peptides.

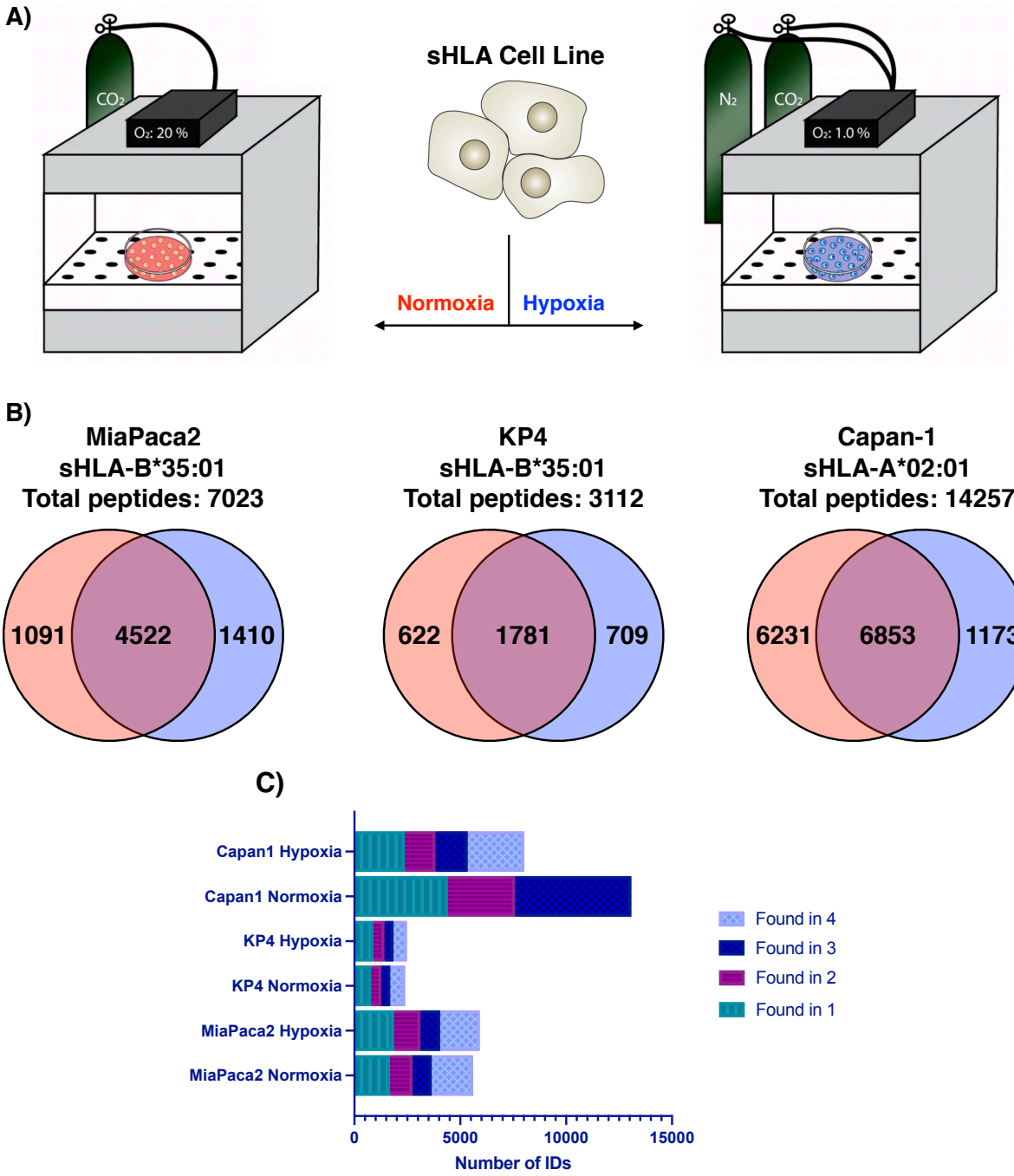

Figure 3.3: Immunopeptidomics of hypoxic PDAC cells using sHLA Fc-fusions. A) Strategy for generating normoxic and hypoxic cells for immunopeptidomics. B) Number of peptides identified in normoxic and hypoxic samples for each cell line. (C) Number of peptides identified across four biological replicates.

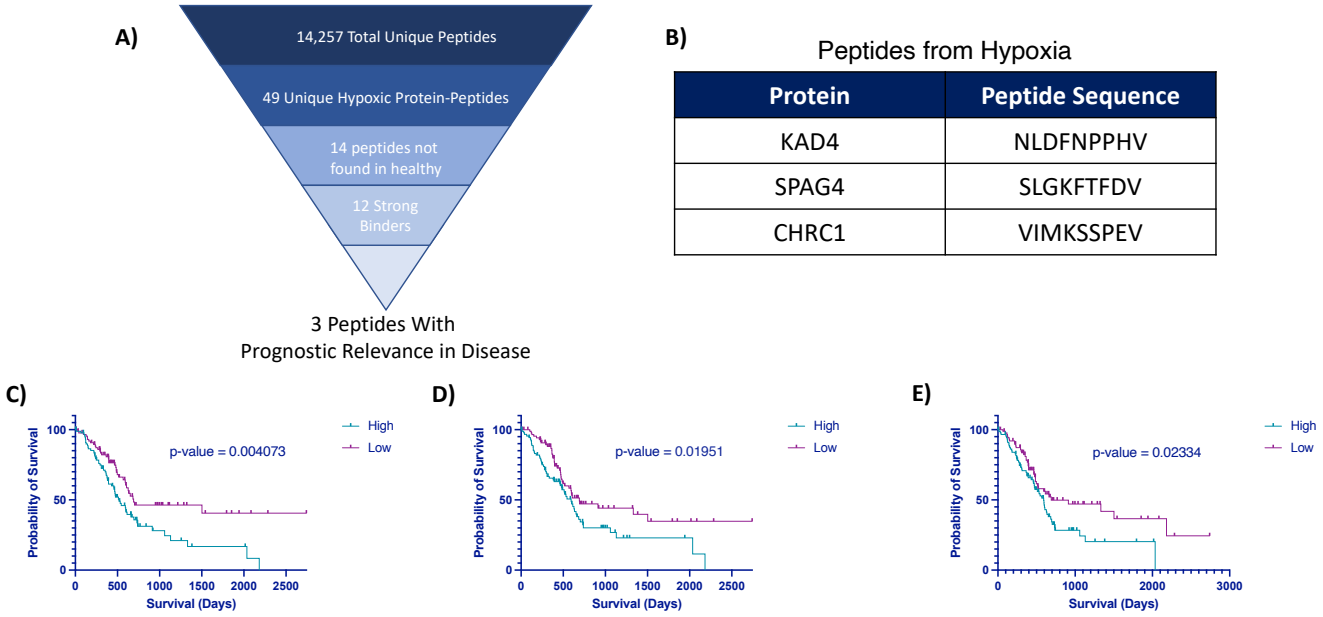

Figure 3.4: Survival analysis for PDAC patients with high and low expression of KAD4, CHRAC1, and SPAG4. A) Target triage for all unique peptides identified in the Capan-1 HLA-A*02:01 dataset. B) The identity of the three prognostically relevant peptides in hypoxic PDAC. C) Survival statistics for PDAC patients with high and low expression of KAD4. D) Survival statistics for PDAC patients with high and low expression of CHRAC1. E) Survival statistics for PDAC patients with high and low expression of SPAG4.

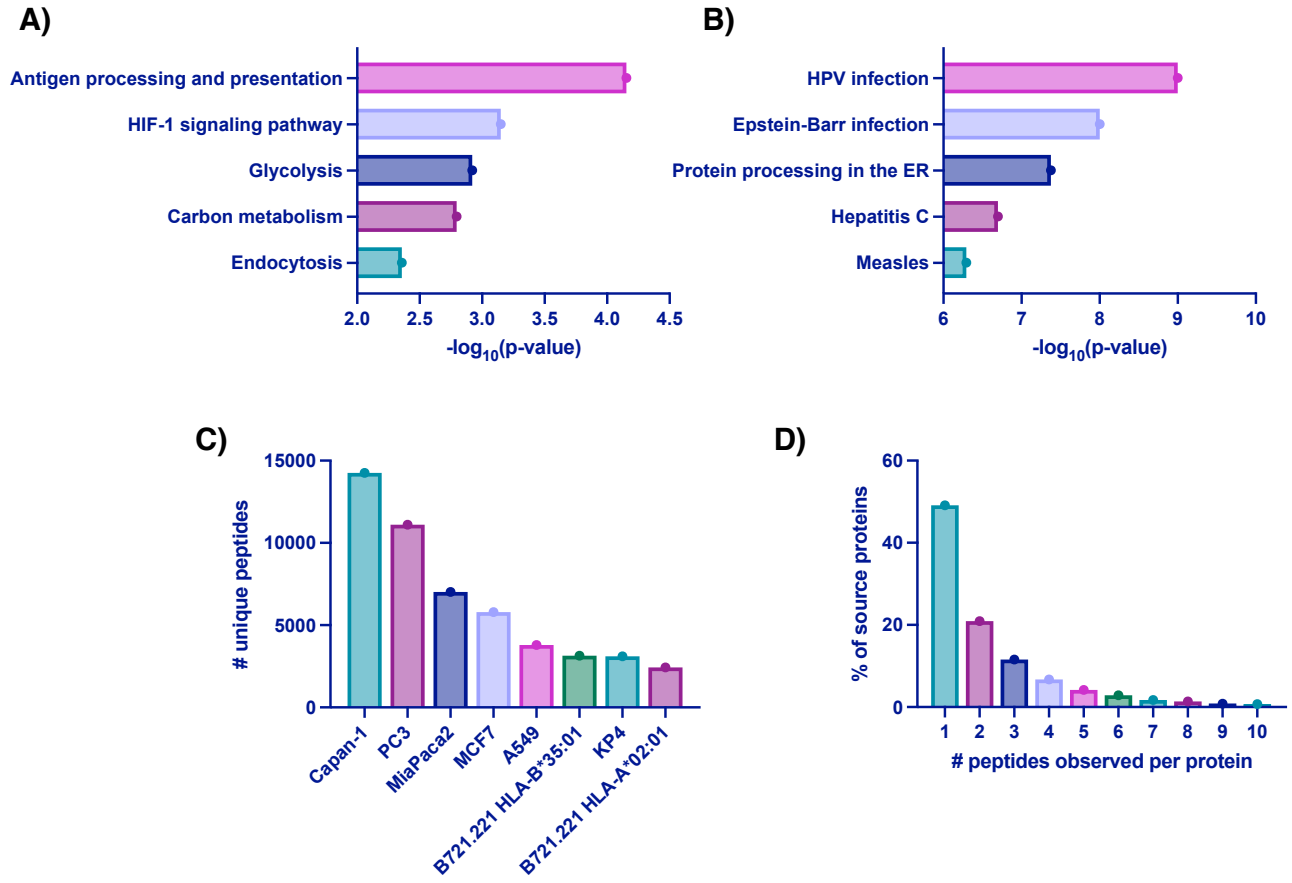

Figure 3.5: Analysis of peptides across hypoxic and senescent datasets. (A) Pathway analysis of hypoxia-specific peptide identifications. (B) Pathway analysis of senescence-specific peptide identifications. (C) Number of unique peptides identified across all datasets. (D) Statistical overview of the number of peptides identified per protein across all datasets.

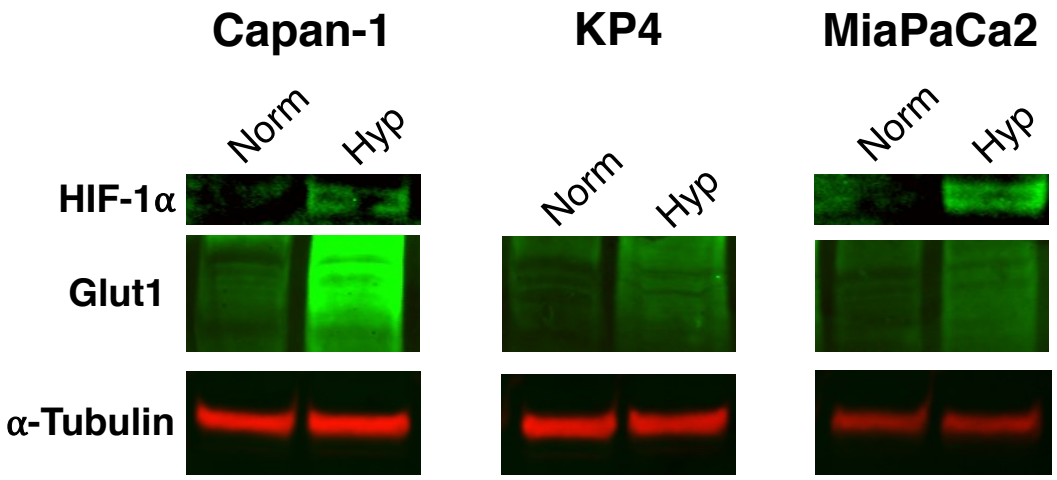

Figure 3.6: Western blot observing HIF1alpha and Glut1 levels in normoxic and hypoxic PDAC cells Capan-1, KP4, and MiaPaca2. Whole cell lysate samples from hypoxic and normoxic treated Capan-1, KP4, and MiaPaCa2 cells were blotted against HIF-1α and Glut1 markers. α-tubulin was used as a loading control. KP4 did not have detectable HIF1α.

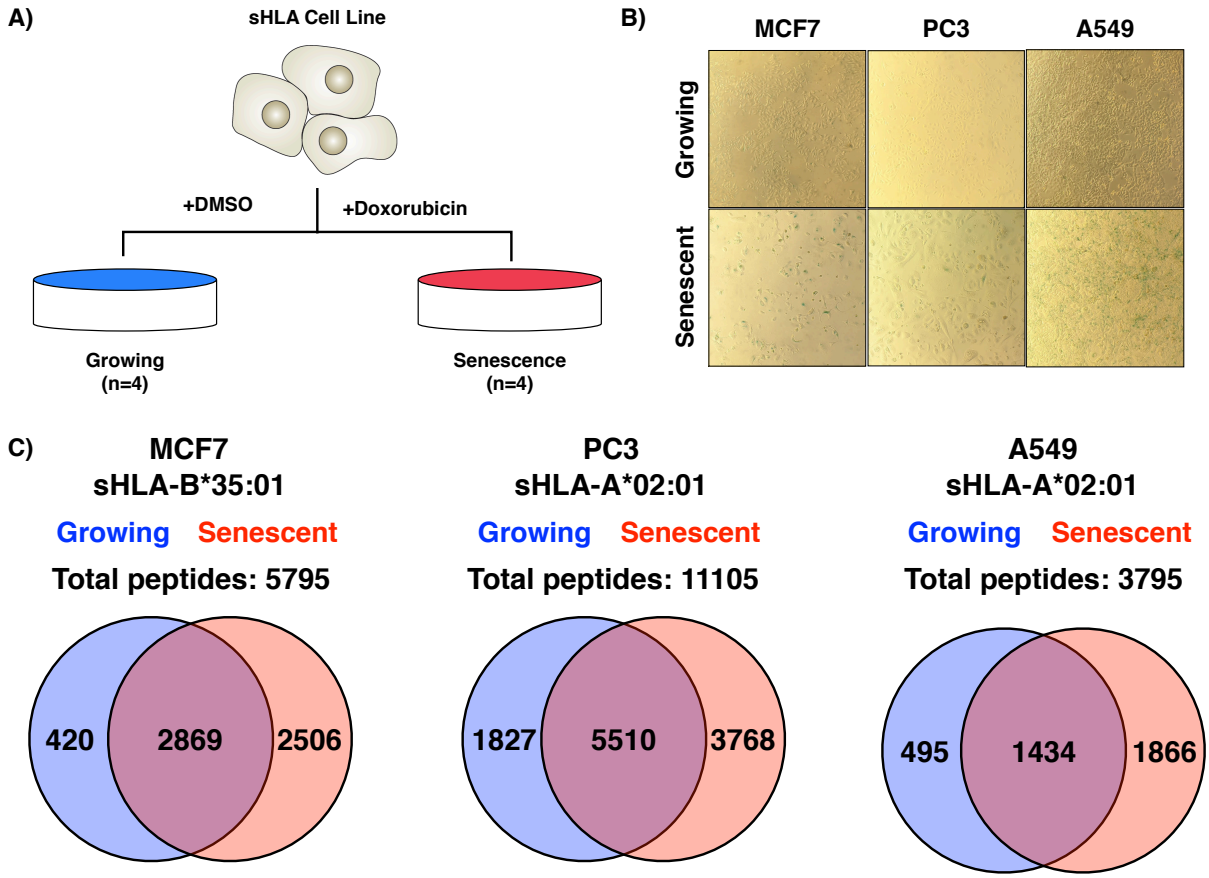

Figure 3.7: Immunopeptidomics of senescent cells using sHLA Fc-fusions. A) Strategy for generating growing and senescent cells for immunopeptidomics. Each cell line was treated for 24 hours with respective reagent. Growing cells were Doxycycline-treated immediately after DMSO removal while senescent cells were cultured for 9 days prior to doxycycline-treatment. B) β-galactosidase activity staining of growing and senescent cell lines. C) Number of peptides identified in growing and senescent samples for each cell line.

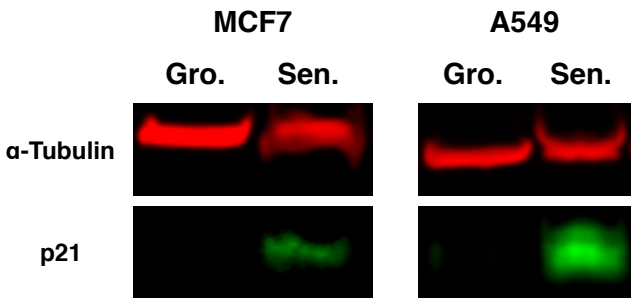

Figure 3.8: Western blot of growing and senescent cell lines for the expression of the senescence-associated marker p21. Whole cell lysate samples from growing and senescent MCF7 and A549 cells were blotted against p21. α-tubulin was used as a loading control. PC3 cells did not have detectable levels of p21.

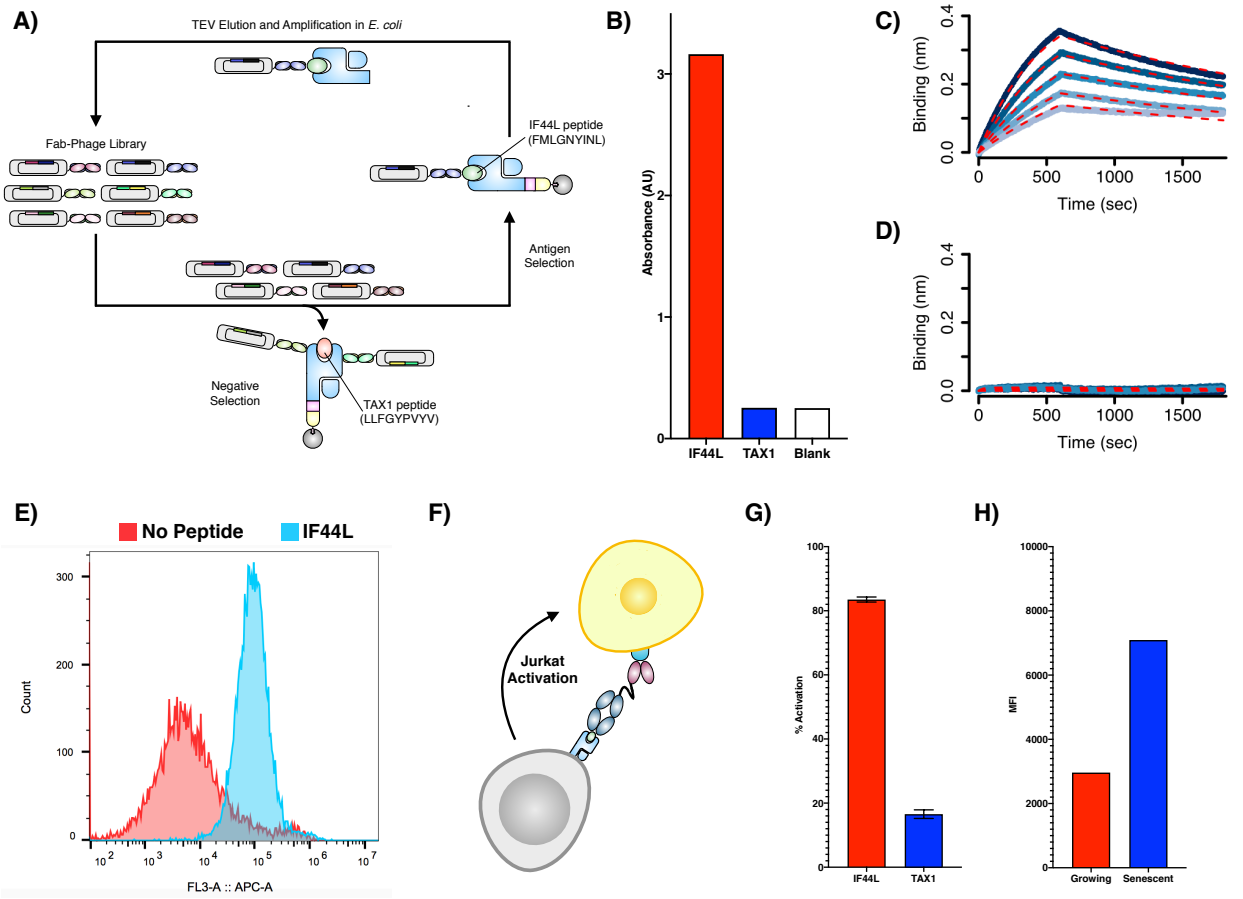

Figure 3.9: Antibodies targeting IF44L MHC-peptide complex show increased presentation in senescent cells. A) Differential phage display selection strategy to select for IF44L MHC-peptide complexes. B) ELISA results of the Fab-phage clone IFB2. C) Octet analysis of IFB2 Fab against the IF44L MHC-peptide complex. Concentrations in descending order are 200 nM, 150 nM, 100 nM, 75 nM, and 50 nM. D) Octet analysis of IFB2 Fab against the TAX1 MHC-peptide complex. Concentrations in descending order are 200 nM, 150 nM, and 100 nM. E) Flow cytometry analysis of IFB2 Fab using T2 lymphoblasts loaded with no peptide or the IF44L peptide. F) Schematic of IFB2 BiTE assays, where one arm binds to the IF44L MHC-peptide complex on target cells and the other binds CD3 on NFAT-GFP Jurkats, thereby inducing Jurkat activation. G) Percent activation of NFAT-GFP Jurkats incubated with 100 pM IFB2 BiTE and T2 lymphoblasts loaded with either IF44L or TAX1 peptide. H) Median FITC-A of NFAT-GFP Jurkats incubated with 100 pM IFB2 BiTE and either growing or senescent MCF7 breast cancer cells.

References

Abelin, J. G., Keskin, D. B., Sarkizova, S., Hartigan, C. R., Zhang, W., Sidney, J., Stevens, J., Lane, W., Zhang, G. L., Eisenhaure, T. M., Clauser, K. R., Hacohen, N., Rooney, M. S., Carr, S. A., & Wu, C. J. (2017). Mass Spectrometry Profiling of HLA-Associated Peptidomes in Mono-allelic Cells Enables More Accurate Epitope Prediction. *Immunity*, *46*(2), 315–326. https://doi.org/10.1016/j.immuni.2017.02.007

Acosta, J. C., Banito, A., Wuestefeld, T., Georgilis, A., Janich, P., Morton, J. P., Athineos, D., Kang, T.-W., Lasitschka, F., Andrulis, M., Pascual, G., Morris, K. J., Khan, S., Jin, H., Dharmalingam, G., Snijders, A. P., Carroll, T., Capper, D., Pritchard, C., … Gil, J. (2013). A complex secretory program orchestrated by the inflammasome controls paracrine senescence. *Nature Cell Biology*, *15*(8), 978–990. https://doi.org/10.1038/ncb2784

Adams, C. R., Htwe, H. H., Marsh, T., Wang, A. L., Montoya, M. L., Subbaraj, L., Tward, A. D., Bardeesy, N., & Perera, R. M. (2019). Transcriptional control of subtype switching ensures adaptation and growth of pancreatic cancer. *ELife*, *8*, e45313. https://doi.org/10.7554/eLife.45313

Akakura, N., Kobayashi, M., Horiuchi, I., Suzuki, A., Wang, J., Chen, J., Niizeki, H., Kawamura, K., Hosokawa, M., & Asaka, M. (2001). Constitutive Expression of Hypoxia-inducible Factor-1α Renders Pancreatic Cancer Cells Resistant to Apoptosis Induced by Hypoxia and Nutrient Deprivation. *Cancer Research*, *61*(17), 6548.

Akoto, T., & Saini, S. (2021). Role of Exosomes in Prostate Cancer Metastasis. *International Journal of Molecular Sciences*, *22*(7), 3528. https://doi.org/10.3390/ijms22073528

Al-Nedawi, K., Meehan, B., Micallef, J., Lhotak, V., May, L., Guha, A., & Rak, J. (2008). Intercellular transfer of the oncogenic receptor EGFRvIII by microvesicles derived from tumour cells. *Nature Cell Biology*, *10*(5), 619–624. https://doi.org/10.1038/ncb1725

Apweiler, R. (1999). On the frequency of protein glycosylation, as deduced from analysis of the SWISS-PROT database. *Biochimica et Biophysica Acta (BBA) - General Subjects*, *1473*(1), 4–8. https://doi.org/10.1016/S0304-4165(99)00165-8

Australian Pancreatic Cancer Genome Initiative, Bailey, P., Chang, D. K., Nones, K., Johns, A. L., Patch, A.-M., Gingras, M.-C., Miller, D. K., Christ, A. N., Bruxner, T. J. C., Quinn, M. C., Nourse, C., Murtaugh, L. C., Harliwong, I., Idrisoglu, S., Manning, S., Nourbakhsh, E., Wani, S., Fink, L., … Grimmond, S. M. (2016). Genomic analyses identify molecular subtypes of pancreatic cancer. *Nature*, *531*(7592), 47–52. https://doi.org/10.1038/nature16965

Babcock, G. T. (1999). How oxygen is activated and reduced in respiration. *Proceedings of the National Academy of Sciences*, *96*(23), 12971–12973. https://doi.org/10.1073/pnas.96.23.12971

Baker, D. J., Childs, B. G., Durik, M., Wijers, M. E., Sieben, C. J., Zhong, J., Saltness, R. A., Jeganathan, K. B., Verzosa, G. C., Pezeshki, A., Khazaie, K., Miller, J. D., & van Deursen, J. M. (2016). Naturally occurring p16(Ink4a)-positive cells shorten healthy lifespan. *Nature*, *530*(7589), 184–189. https://doi.org/10.1038/nature16932

Bandu, R., Oh, J. W., & Kim, K. P. (2019). Mass spectrometry-based proteome profiling of extracellular vesicles and their roles in cancer biology. *Experimental & Molecular Medicine*, *51*(3), 30. https://doi.org/10.1038/s12276-019-0218-2

Bausch-Fluck, D., Goldmann, U., Müller, S., van Oostrum, M., Müller, M., Schubert, O. T., & Wollscheid, B. (2018). The in silico human surfaceome. *Proceedings of the National Academy of Sciences*, *115*(46), E10988–E10997. https://doi.org/10.1073/pnas.1808790115

Bausch-Fluck, D., Hofmann, A., & Wollscheid, B. (2012). Cell Surface Capturing Technologies for the Surfaceome Discovery of Hepatocytes. In D. Josic & D. C. Hixson (Eds.), *Liver Proteomics* (pp. 1–16). Humana Press. https://doi.org/10.1007/978-1-61779-959-4_1

Bhutia, Y. D., & Ganapathy, V. (2016). Glutamine transporters in mammalian cells and their functions in physiology and cancer. *Biochimica et Biophysica Acta (BBA) - Molecular Cell Research*, *1863*(10), 2531–2539. https://doi.org/10.1016/j.bbamcr.2015.12.017

Bilen, M. A., Pan, T., Lee, Y.-C., Lin, S.-C., Yu, G., Pan, J., Hawke, D., Pan, B.-F., Vykoukal, J., Gray, K., Satcher, R. L., Gallick, G. E., Yu-Lee, L.-Y., & Lin, S.-H. (2017). Proteomics Profiling of Exosomes from Primary Mouse Osteoblasts under Proliferation versus Mineralization Conditions and Characterization of Their Uptake into Prostate Cancer Cells. *Journal of Proteome Research*, *16*(8), 2709–2728. https://doi.org/10.1021/acs.jproteome.6b00981

Blades, R. A., Keating, P. J., McWilliam, L. J., George, N. J. R., & Stern, P. L. (1995). Loss of HLA class I expression in prostate cancer: Implications for immunotherapy. *Urology*, *46*(5), 681–687. https://doi.org/10.1016/S0090-4295(99)80301-X

Bourseau-Guilmain, E., Menard, J. A., Lindqvist, E., Indira Chandran, V., Christianson, H. C., Cerezo Magaña, M., Lidfeldt, J., Marko-Varga, G., Welinder, C., & Belting, M. (2016). Hypoxia regulates global membrane protein endocytosis through caveolin-1 in cancer cells. *Nature Communications*, *7*, 11371. PMC. https://doi.org/10.1038/ncomms11371

Brunner, M., Wu, Z., Krautz, C., Pilarsky, C., Grützmann, R., & Weber, G. F. (2019). Current Clinical Strategies of Pancreatic Cancer Treatment and Open Molecular Questions. *International Journal of Molecular Sciences*, *20*(18), 4543. https://doi.org/10.3390/ijms20184543

Caron, E., Kowalewski, D., Koh, C. C., Sturm, T., Schuster, H., & Aebersold, R. (2015). Analysis of Major Histocompatibility Complex (MHC) Immunopeptidomes Using Mass Spectrometry*. *Molecular & Cellular Proteomics*, *14*(12), 3105–3117. https://doi.org/10.1074/mcp.O115.052431

Catherman, A. D., Durbin, K. R., Ahlf, D. R., Early, B. P., Fellers, R. T., Tran, J. C., Thomas, P. M., & Kelleher, N. L. (2013). Large-scale Top-down Proteomics of the Human Proteome: Membrane Proteins, Mitochondria, and Senescence. *Molecular & Cellular Proteomics*, *12*(12), 3465–3473. https://doi.org/10.1074/mcp.M113.030114

Cen, J., Feng, L., Ke, H., Bao, L., Li, L. Z., Tanaka, Y., Weng, J., & Su, L. (2019). Exosomal Thrombospondin-1 Disrupts the Integrity of Endothelial Intercellular Junctions to Facilitate Breast Cancer Cell Metastasis. *Cancers*, *11*(12). https://doi.org/10.3390/cancers11121946

Chandler, K. B., & Costello, C. E. (2016). Glycomics and glycoproteomics of membrane proteins and cell-surface receptors: Present trends and future opportunities. *Electrophoresis*, *37*(11), 1407–1419. https://doi.org/10.1002/elps.201500552

Cheek, J., Mandelman, D., Poulos, T. L., & Dawson, J. H. (1999). A study of the K+-site mutant of ascorbate peroxidase: Mutations of protein residues on the proximal side of the heme cause changes in iron ligation on the distal side. *JBIC Journal of Biological Inorganic Chemistry*, *4*(1), 64–72. https://doi.org/10.1007/s007750050290

Chen, C., Zhao, S., Karnad, A., & Freeman, J. W. (2018). The biology and role of CD44 in cancer progression: Therapeutic implications. *Journal of Hematology & Oncology*, *11*(1), 64. https://doi.org/10.1186/s13045-018-0605-5

Chouaib, S., Noman, M. Z., Kosmatopoulos, K., & Curran, M. A. (2017). Hypoxic stress: Obstacles and opportunities for innovative immunotherapy of cancer. *Oncogene*, *36*(4), 439–445.

Collisson, E. A., Sadanandam, A., Olson, P., Gibb, W. J., Truitt, M., Gu, S., Cooc, J., Weinkle, J., Kim, G. E., Jakkula, L., Feiler, H. S., Ko, A. H., Olshen, A. B., Danenberg, K. L., Tempero, M. A., Spellman, P. T., Hanahan, D., & Gray, J. W. (2011). Subtypes of pancreatic ductal adenocarcinoma and their differing responses to therapy. *Nature Medicine*, *17*(4), 500–503. https://doi.org/10.1038/nm.2344

Colombo, M., Raposo, G., & Théry, C. (2014). Biogenesis, Secretion, and Intercellular Interactions of Exosomes and Other Extracellular Vesicles. *Annual Review of Cell and Developmental Biology*, *30*(1), 255–289. https://doi.org/10.1146/annurev-cellbio-101512-122326

Cornel, A. M., Mimpen, I. L., & Nierkens, S. (2020). MHC Class I Downregulation in Cancer: Underlying Mechanisms and Potential Targets for Cancer Immunotherapy. *Cancers*, *12*(7), E1760. https://doi.org/10.3390/cancers12071760

Costa-Silva, B., Aiello, N. M., Ocean, A. J., Singh, S., Zhang, H., Thakur, B. K., Becker, A., Hoshino, A., Mark, M. T., Molina, H., Xiang, J., Zhang, T., Theilen, T.-M., García-Santos, G., Williams, C., Ararso, Y., Huang, Y., Rodrigues, G., Shen, T.-L., … Lyden, D. (2015). Pancreatic cancer exosomes initiate pre-metastatic niche formation in the liver. *Nature Cell Biology*, *17*(6), 816–826. https://doi.org/10.1038/ncb3169

Czajkowsky, D. M., Hu, J., Shao, Z., & Pleass, R. J. (2012). Fc-fusion proteins: New developments and future perspectives. *EMBO Molecular Medicine*, *4*(10), 1015–1028. https://doi.org/10.1002/emmm.201201379

Dao, T., Pankov, D., Scott, A., Korontsvit, T., Zakhaleva, V., Xu, Y., Xiang, J., Yan, S., de Morais Guerreiro, M. D., Veomett, N., Dubrovsky, L., Curcio, M., Doubrovina, E., Ponomarev, V., Liu, C., O'Reilly, R. J., & Scheinberg, D. A. (2015). Therapeutic bispecific T-cell engager antibody targeting the intracellular oncoprotein WT1. *Nature Biotechnology*, *33*(10), 1079–1086. https://doi.org/10.1038/nbt.3349

Dao, T., Yan, S., Veomett, N., Pankov, D., Zhou, L., Korontsvit, T., Scott, A., Whitten, J., Maslak, P., Casey, E., Tan, T., Liu, H., Zakhaleva, V., Curcio, M., Doubrovina, E., O'Reilly, R. J., Liu, C., & Scheinberg, D. A. (2013). Targeting the intracellular WT1 oncogene product with a therapeutic human antibody. *Science Translational Medicine*, *5*(176), 176ra33. https://doi.org/10.1126/scitranslmed.3005661

Daubon, T., Léon, C., Clarke, K., Andrique, L., Salabert, L., Darbo, E., Pineau, R., Guérit, S., Maitre, M., Dedieu, S., Jeanne, A., Bailly, S., Feige, J.-J., Miletic, H., Rossi, M., Bello, L., Falciani, F., Bjerkvig, R., & Bikfalvi, A. (2019). Deciphering the complex role of thrombospondin-1 in glioblastoma development. *Nature Communications*, *10*(1), 1146. https://doi.org/10.1038/s41467-019-08480-y

Deer, E. L., Gonzalez-Hernandez, J., Coursen, J. D., Shea, J. E., Ngatia, J., Scaife, C. L., Firpo, M. A., & Mulvihill, S. J. (2010). Phenotype and Genotype of Pancreatic Cancer Cell Lines. *Pancreas*, *39*(4), 425–435. PMC. https://doi.org/10.1097/MPA.0b013e3181c15963

Demory Beckler, M., Higginbotham, J. N., Franklin, J. L., Ham, A.-J., Halvey, P. J., Imasuen, I. E., Whitwell, C., Li, M., Liebler, D. C., & Coffey, R. J. (2013). Proteomic Analysis of

Exosomes from Mutant KRAS Colon Cancer Cells Identifies Intercellular Transfer of Mutant KRAS. *Molecular & Cellular Proteomics*, *12*(2), 343–355. https://doi.org/10.1074/mcp.M112.022806

Dewhirst, M. W., Cao, Y., & Moeller, B. (2008). Cycling hypoxia and free radicals regulate angiogenesis and radiotherapy response. *Nat Rev Cancer*, *8*(6), 425–437. https://doi.org/10.1038/nrc2397

Dhatchinamoorthy, K., Colbert, J. D., & Rock, K. L. (2021). Cancer Immune Evasion Through Loss of MHC Class I Antigen Presentation. *Frontiers in Immunology*, *12*, 636568. https://doi.org/10.3389/fimmu.2021.636568

Douglass, J., Hsiue, E. H.-C., Mog, B. J., Hwang, M. S., DiNapoli, S. R., Pearlman, A. H., Miller, M. S., Wright, K. M., Azurmendi, P. A., Wang, Q., Paul, S., Schaefer, A., Skora, A. D., Molin, M. D., Konig, M. F., Liu, Q., Watson, E., Li, Y., Murphy, M. B., … Zhou, S. (2021). Bispecific antibodies targeting mutant RAS neoantigens. *Science Immunology*, *6*(57), eabd5515. https://doi.org/10.1126/sciimmunol.abd5515

Doyle, L. M., & Wang, M. Z. (2019). Overview of Extracellular Vesicles, Their Origin, Composition, Purpose, and Methods for Exosome Isolation and Analysis. *Cells*, *8*(7). https://doi.org/10.3390/cells8070727

Duijvesz, D., Burnum-Johnson, K. E., Gritsenko, M. A., Hoogland, A. M., Vredenbregt-van den Berg, M. S., Willemsen, R., Luider, T., Paša-Tolić, L., & Jenster, G. (2013). Proteomic Profiling of Exosomes Leads to the Identification of Novel Biomarkers for Prostate Cancer. *PLoS ONE*, *8*(12), e82589. https://doi.org/10.1371/journal.pone.0082589

Dyer, K. F. (1971). The Quiet Revolution: A New Synthesis of Biological Knowledge. *Journal of Biological Education*, *5*(1), 15–24. https://doi.org/10.1080/00219266.1971.9653663

Eales, K. L., Hollinshead, K. E. R., & Tennant, D. A. (2016). Hypoxia and metabolic adaptation of cancer cells. *Oncogenesis*, *5*, e190.

Edgar, J. R. (2016). Q&A: What are exosomes, exactly? *BMC Biology*, *14*(1), 46. https://doi.org/10.1186/s12915-016-0268-z

Efthymiou, G., Saint, A., Ruff, M., Rekad, Z., Ciais, D., & Van Obberghen-Schilling, E. (2020). Shaping Up the Tumor Microenvironment With Cellular Fibronectin. *Frontiers in Oncology*, *10*, 641. https://doi.org/10.3389/fonc.2020.00641

Elschenbroich, S., Kim, Y., Medin, J. A., & Kislinger, T. (2010). Isolation of cell surface proteins for mass spectrometry-based proteomics. *Expert Review of Proteomics*, *7*(1), 141–154. https://doi.org/10.1586/epr.09.97

Goldman, M. J., Craft, B., Hastie, M., Repečka, K., McDade, F., Kamath, A., Banerjee, A., Luo, Y., Rogers, D., Brooks, A. N., Zhu, J., & Haussler, D. (2020). Visualizing and interpreting cancer genomics data via the Xena platform. *Nature Biotechnology*, *38*(6), 675–678. https://doi.org/10.1038/s41587-020-0546-8

Gonçalves, S., Yin, K., Ito, Y., Chan, A., Olan, I., Gough, S., Cassidy, L., Serrao, E., Smith, S., Young, A., Narita, M., & Hoare, M. (2021). COX2 regulates senescence secretome composition and senescence surveillance through PGE2. *Cell Reports*, *34*(11), 108860. https://doi.org/10.1016/j.celrep.2021.108860

Griffin, N. M., & Schnitzer, J. E. (2011). Overcoming Key Technological Challenges in Using Mass Spectrometry for Mapping Cell Surfaces in Tissues. *Molecular & Cellular Proteomics*, *10*(2), S1–S14. https://doi.org/10.1074/mcp.R110.000935

Gu, S. S., Zhang, W., Wang, X., Jiang, P., Traugh, N., Li, Z., Meyer, C., Stewig, B., Xie, Y., Bu, X., Manos, M. P., Font-Tello, A., Gjini, E., Lako, A., Lim, K., Conway, J., Tewari, A. K.,

Zeng, Z., Sahu, A. D., … Liu, X. S. (2021). Therapeutically Increasing MHC-I Expression Potentiates Immune Checkpoint Blockade. *Cancer Discovery*, *11*(6), 1524–1541. https://doi.org/10.1158/2159-8290.CD-20-0812

Gupte, T. M., Ritt, M., Dysthe, M., Malik, R. U., & Sivaramakrishnan, S. (2019). Minute-scale persistence of a GPCR conformation state triggered by non-cognate G protein interactions primes signaling. *Nature Communications*, *10*(1), 4836. https://doi.org/10.1038/s41467-019-12755-9

Guzman-Rojas, L., Rangel, R., Salameh, A., Edwards, J. K., Dondossola, E., Kim, Y.-G., Saghatelian, A., Giordano, R. J., Kolonin, M. G., Staquicini, F. I., Koivunen, E., Sidman, R. L., Arap, W., & Pasqualini, R. (2012). Cooperative effects of aminopeptidase N (CD13) expressed by nonmalignant and cancer cells within the tumor microenvironment. *Proceedings of the National Academy of Sciences*, *109*(5), 1637–1642. https://doi.org/10.1073/pnas.1120790109

Hacker, S. M., Backus, K. M., Lazear, M. R., Forli, S., Correia, B. E., & Cravatt, B. F. (2017). Global profiling of lysine reactivity and ligandability in the human proteome. *Nature Chemistry*, *9*(12), 1181–1190. https://doi.org/10.1038/nchem.2826

Harris, A. L. (2002). Hypoxia—A key regulatory factor in tumour growth. *Nat Rev Cancer*, *2*. https://doi.org/10.1038/nrc704

Hasan, N., & Ahuja, N. (2019). The Emerging Roles of ATP-Dependent Chromatin Remodeling Complexes in Pancreatic Cancer. *Cancers*, *11*(12), 1859. https://doi.org/10.3390/cancers11121859

Hawkins, O. E., Vangundy, R. S., Eckerd, A. M., Bardet, W., Buchli, R., Weidanz, J. A., & Hildebrand, W. H. (2008). Identification of breast cancer peptide epitopes presented by

HLA-A*0201. *Journal of Proteome Research*, *7*(4), 1445–1457. https://doi.org/10.1021/pr700761w

Hilton, H. G., McMurtrey, C. P., Han, A. S., Djaoud, Z., Guethlein, L. A., Blokhuis, J. H., Pugh, J. L., Goyos, A., Horowitz, A., Buchli, R., Jackson, K. W., Bardet, W., Bushnell, D. A., Robinson, P. J., Mendoza, J. L., Birnbaum, M. E., Nielsen, M., Garcia, K. C., Hildebrand, W. H., & Parham, P. (2017). The Intergenic Recombinant HLA-B∗46:01 Has a Distinctive Peptidome that Includes KIR2DL3 Ligands. *Cell Reports*, *19*(7), 1394–1405. https://doi.org/10.1016/j.celrep.2017.04.059

Holland, C. J., Crean, R. M., Pentier, J. M., de Wet, B., Lloyd, A., Srikannathasan, V., Lissin, N., Lloyd, K. A., Blicher, T. H., Conroy, P. J., Hock, M., Pengelly, R. J., Spinner, T. E., Cameron, B., Potter, E. A., Jeyanthan, A., Molloy, P. E., Sami, M., Aleksic, M., … Cole, D. K. (2020). Specificity of bispecific T cell receptors and antibodies targeting peptide-HLA. *The Journal of Clinical Investigation*, *130*(5), 2673–2688. https://doi.org/10.1172/JCI130562

Hornsby, M., Paduch, M., Miersch, S., Sääf, A., Matsuguchi, T., Lee, B., Wypisniak, K., Doak, A., King, D., Usatyuk, S., Perry, K., Lu, V., Thomas, W., Luke, J., Goodman, J., Hoey, R. J., Lai, D., Griffin, C., Li, Z., … Wells, J. (2015). A High Through-put Platform for Recombinant Antibodies to Folded Proteins. *Molecular & Cellular Proteomics: MCP*, *14*(10), 2833–2847. https://doi.org/10.1074/mcp.O115.052209

Hoshino, A., Costa-Silva, B., Shen, T.-L., Rodrigues, G., Hashimoto, A., Tesic Mark, M., Molina, H., Kohsaka, S., Di Giannatale, A., Ceder, S., Singh, S., Williams, C., Soplop, N., Uryu, K., Pharmer, L., King, T., Bojmar, L., Davies, A. E., Ararso, Y., … Lyden, D. (2015). Tumour exosome integrins determine organotropic metastasis. *Nature*, *527*(7578), 329–335. https://doi.org/10.1038/nature15756

Hosseini-Beheshti, E., Pham, S., Adomat, H., Li, N., & Tomlinson Guns, E. S. (2012). Exosomes as Biomarker Enriched Microvesicles: Characterization of Exosomal Proteins Derived from a Panel of Prostate Cell Lines with Distinct AR Phenotypes. *Molecular & Cellular Proteomics*, *11*(10), 863–885. https://doi.org/10.1074/mcp.M111.014845

Howarth, M., & Ting, A. Y. (2008). Imaging proteins in live mammalian cells with biotin ligase and monovalent streptavidin. *Nature Protocols*, *3*(3), 534–545. https://doi.org/10.1038/nprot.2008.20

Høydahl, L. S., Frick, R., Sandlie, I., & Løset, G. Å. (2019). Targeting the MHC Ligandome by Use of TCR-Like Antibodies. *Antibodies (Basel, Switzerland)*, *8*(2), E32. https://doi.org/10.3390/antib8020032

Hsiue, E. H.-C., Wright, K. M., Douglass, J., Hwang, M. S., Mog, B. J., Pearlman, A. H., Paul, S., DiNapoli, S. R., Konig, M. F., Wang, Q., Schaefer, A., Miller, M. S., Skora, A. D., Azurmendi, P. A., Murphy, M. B., Liu, Q., Watson, E., Li, Y., Pardoll, D. M., … Zhou, S. (2021). Targeting a neoantigen derived from a common TP53 mutation. *Science (New York, N.Y.)*, *371*(6533), eabc8697. https://doi.org/10.1126/science.abc8697

Huang, G. N. (2012). Biotinylation of Cell Surface Proteins. *Bio-Protocol*, *2*(9). https://doi.org/10.21769/BioProtoc.170

Hung, V., Udeshi, N. D., Lam, S. S., Loh, K. H., Cox, K. J., Pedram, K., Carr, S. A., & Ting, A. Y. (2016). Spatially resolved proteomic mapping in living cells with the engineered peroxidase APEX2. *Nature Protocols*, *11*(3), 456–475. https://doi.org/10.1038/nprot.2016.018

Ilic, M., & Ilic, I. (2016). Epidemiology of pancreatic cancer. *World Journal of Gastroenterology*, *22*(44), 9694–9705. PMC. https://doi.org/10.3748/wjg.v22.i44.9694

Jan, Y.-H., Lai, T.-C., Yang, C.-J., Lin, Y.-F., Huang, M.-S., & Hsiao, M. (2019). Adenylate kinase 4 modulates oxidative stress and stabilizes HIF-1α to drive lung adenocarcinoma metastasis. *Journal of Hematology & Oncology*, *12*(1), 12. https://doi.org/10.1186/s13045-019-0698-5

Janeway, C. (Ed.). (2001). *Immunobiology: The immune system in health and disease ; [animated CD-ROM inside]* (5. ed). Garland Publ. [u.a.].

Kalluri, R., & LeBleu, V. S. (2020). The biology **,** function **,** and biomedical applications of exosomes. *Science*, *367*(6478), eaau6977. https://doi.org/10.1126/science.aau6977

Kalxdorf, M., Gade, S., Eberl, H. C., & Bantscheff, M. (2017). Monitoring Cell-surface N-Glycoproteome Dynamics by Quantitative Proteomics Reveals Mechanistic Insights into Macrophage Differentiation. *Molecular & Cellular Proteomics*, *16*(5), 770–785. https://doi.org/10.1074/mcp.M116.063859

Keith, B., & Simon, M. C. (2007). Hypoxia Inducible Factors, stem cells and cancer. *Cell*, *129*(3), 465–472. PMC. https://doi.org/10.1016/j.cell.2007.04.019

Kilinc, S., Paisner, R., Camarda, R., Gupta, S., Momcilovic, O., Kohnz, R. A., Avsaroglu, B., L'Etoile, N. D., Perera, R. M., Nomura, D. K., & Goga, A. (2021). Oncogene-regulated release of extracellular vesicles. *Developmental Cell*, *56*(13), 1989-2006.e6. https://doi.org/10.1016/j.devcel.2021.05.014

Knaup, K. X., Monti, J., Hackenbeck, T., Jobst-Schwan, T., Klanke, B., Schietke, R. E., Wacker, I., Behrens, J., Amann, K., Eckardt, K.-U., Warnecke, C., & Wiesener, M. S. (2014). Hypoxia regulates the sperm associated antigen 4 (SPAG4) via HIF, which is expressed in renal clear cell carcinoma and promotes migration and invasion in vitro. *Molecular Carcinogenesis*, *53*(12), 970–978. https://doi.org/10.1002/mc.22065

Koh, C. M., Bieberich, C. J., Dang, C. V., Nelson, W. G., Yegnasubramanian, S., & De Marzo, A. M. (2010). MYC and Prostate Cancer. *Genes & Cancer*, *1*(6), 617–628. https://doi.org/10.1177/1947601910379132

Kuhlmann, L., Cummins, E., Samudio, I., & Kislinger, T. (2018). Cell-surface proteomics for the identification of novel therapeutic targets in cancer. *Expert Review of Proteomics*, *15*(3), 259–275. https://doi.org/10.1080/14789450.2018.1429924

Lam, S. S., Martell, J. D., Kamer, K. J., Deerinck, T. J., Ellisman, M. H., Mootha, V. K., & Ting, A. Y. (2015). Directed evolution of APEX2 for electron microscopy and proximity labeling. *Nature Methods*, *12*(1), 51–54. https://doi.org/10.1038/nmeth.3179

Lee, S., Yu, Y., Trimpert, J., Benthani, F., Mairhofer, M., Richter-Pechanska, P., Wyler, E., Belenki, D., Kaltenbrunner, S., Pammer, M., Kausche, L., Firsching, T. C., Dietert, K., Schotsaert, M., Martínez-Romero, C., Singh, G., Kunz, S., Niemeyer, D., Ghanem, R., … Schmitt, C. A. (2021). Virus-induced senescence is a driver and therapeutic target in COVID-19. *Nature*, *599*(7884), 283–289. https://doi.org/10.1038/s41586-021-03995-1

Leth-Larsen, R., Lund, R. R., & Ditzel, H. J. (2010). Plasma Membrane Proteomics and Its Application in Clinical Cancer Biomarker Discovery. *Molecular & Cellular Proteomics*, *9*(7), 1369–1382. https://doi.org/10.1074/mcp.R900006-MCP200

Leung, K. K., Wilson, G. M., Kirkemo, L. L., Riley, N. M., Coon, J. J., & Wells, J. A. (2020). Broad and thematic remodeling of the surfaceome and glycoproteome on isogenic cells transformed with driving proliferative oncogenes. *Proceedings of the National Academy of Sciences*, *117*(14), 7764–7775. https://doi.org/10.1073/pnas.1917947117

Li, J., Han, S., Li, H., Udeshi, N. D., Svinkina, T., Mani, D. R., Xu, C., Guajardo, R., Xie, Q., Li, T., Luginbuhl, D. J., Wu, B., McLaughlin, C. N., Xie, A., Kaewsapsak, P., Quake, S. R.,

Carr, S. A., Ting, A. Y., & Luo, L. (2020). Cell-Surface Proteomic Profiling in the Fly Brain Uncovers Wiring Regulators. *Cell*, *180*(2), 373-386.e15. https://doi.org/10.1016/j.cell.2019.12.029

Li, Y., Wang, Y., Yao, Y., Lyu, J., Qiao, Q., Mao, J., Xu, Z., & Ye, M. (2021). Rapid Enzyme-Mediated Biotinylation for Cell Surface Proteome Profiling. *Analytical Chemistry*, *93*(10), 4542–4551. https://doi.org/10.1021/acs.analchem.0c04970

Liang, X., Potter, J., Kumar, S., Zou, Y., Quintanilla, R., Sridharan, M., Carte, J., Chen, W., Roark, N., Ranganathan, S., Ravinder, N., & Chesnut, J. D. (2015). Rapid and highly efficient mammalian cell engineering via Cas9 protein transfection. *Journal of Biotechnology*, *208*, 44–53. https://doi.org/10.1016/j.jbiotec.2015.04.024

Linkert, M., Rueden, C. T., Allan, C., Burel, J.-M., Moore, W., Patterson, A., Loranger, B., Moore, J., Neves, C., MacDonald, D., Tarkowska, A., Sticco, C., Hill, E., Rossner, M., Eliceiri, K. W., & Swedlow, J. R. (2010). Metadata matters: Access to image data in the real world. *Journal of Cell Biology*, *189*(5), 777–782. https://doi.org/10.1083/jcb.201004104

Litwin, M. S., & Tan, H.-J. (2017). The Diagnosis and Treatment of Prostate Cancer: A Review. *JAMA*, *317*(24), 2532. https://doi.org/10.1001/jama.2017.7248

Liu, C.-Y., Lin, H.-H., Tang, M.-J., & Wang, Y.-K. (2015). Vimentin contributes to epithelial-mesenchymal transition cancer cell mechanics by mediating cytoskeletal organization and focal adhesion maturation. *Oncotarget*, *6*(18), 15966–15983. https://doi.org/10.18632/oncotarget.3862

Lorenc, T., Klimczyk, K., Michalczewska, I., Słomka, M., Kubiak-Tomaszewska, G., & Olejarz, W. (2020). Exosomes in Prostate Cancer Diagnosis, Prognosis and Therapy. *International Journal of Molecular Sciences*, *21*(6). https://doi.org/10.3390/ijms21062118

Malapeira, J., Esselens, C., Bech-Serra, J. J., Canals, F., & Arribas, J. (2011). ADAM17 (TACE) regulates TGFβ signaling through the cleavage of vasorin. *Oncogene*, *30*(16), 1912–1922. https://doi.org/10.1038/onc.2010.565

Man, J., Yu, X., Huang, H., Zhou, W., Xiang, C., Huang, H., Miele, L., Liu, Z., Bebek, G., Bao, S., & Yu, J. S. (2018). Hypoxic Induction of Vasorin Regulates Notch1 Turnover to Maintain Glioma Stem-like Cells. *Cell Stem Cell*, *22*(1), 104-118.e6. https://doi.org/10.1016/j.stem.2017.10.005

Martell, J. D., Yamagata, M., Deerinck, T. J., Phan, S., Kwa, C. G., Ellisman, M. H., Sanes, J. R., & Ting, A. Y. (2016). A split horseradish peroxidase for the detection of intercellular protein–protein interactions and sensitive visualization of synapses. *Nature Biotechnology*, *34*(7), 774–780. https://doi.org/10.1038/nbt.3563

Martinko, A. J., Truillet, C., Julien, O., Diaz, J. E., Horlbeck, M. A., Whiteley, G., Blonder, J., Weissman, J. S., Bandyopadhyay, S., Evans, M. J., & Wells, J. A. (2018a). Targeting RAS-driven human cancer cells with antibodies to upregulated and essential cell-surface proteins. *ELife*, *7*, e31098. https://doi.org/10.7554/eLife.31098

Martinko, A. J., Truillet, C., Julien, O., Diaz, J. E., Horlbeck, M. A., Whiteley, G., Blonder, J., Weissman, J. S., Bandyopadhyay, S., Evans, M. J., & Wells, J. A. (2018b). Targeting RAS-driven human cancer cells with antibodies to upregulated and essential cell-surface proteins. *ELife*, *7*, e31098. https://doi.org/10.7554/eLife.31098

Mathiasen, M. L., Dillingham, C. M., Kinnavane, L., Powell, A. L., & Aggleton, J. P. (2017). Asymmetric cross-hemispheric connections link the rat anterior thalamic nuclei with the cortex and hippocampal formation. *Neuroscience*, *349*, 128–143. https://doi.org/10.1016/j.neuroscience.2017.02.026

Mathieu, M., Névo, N., Jouve, M., Valenzuela, J. I., Maurin, M., Verweij, F. J., Palmulli, R., Lankar, D., Dingli, F., Loew, D., Rubinstein, E., Boncompain, G., Perez, F., & Théry, C. (2021). Specificities of exosome versus small ectosome secretion revealed by live intracellular tracking of CD63 and CD9. *Nature Communications*, *12*(1), 4389. https://doi.org/10.1038/s41467-021-24384-2

McGinnis, C. S., Patterson, D. M., Winkler, J., Conrad, D. N., Hein, M. Y., Srivastava, V., Hu, J. L., Murrow, L. M., Weissman, J. S., Werb, Z., Chow, E. D., & Gartner, Z. J. (2019). MULTI-seq: Sample multiplexing for single-cell RNA sequencing using lipid-tagged indices. *Nature Methods*, *16*(7), 619–626. https://doi.org/10.1038/s41592-019-0433-8

McKiernan, J., Donovan, M. J., O'Neill, V., Bentink, S., Noerholm, M., Belzer, S., Skog, J., Kattan, M. W., Partin, A., Andriole, G., Brown, G., Wei, J. T., Thompson, I. M., & Carroll, P. (2016). A Novel Urine Exosome Gene Expression Assay to Predict High-grade Prostate Cancer at Initial Biopsy. *JAMA Oncology*, *2*(7), 882. https://doi.org/10.1001/jamaoncol.2016.0097

Meier, F., Brunner, A.-D., Frank, M., Ha, A., Bludau, I., Voytik, E., Kaspar-Schoenefeld, S., Lubeck, M., Raether, O., Bache, N., Aebersold, R., Collins, B. C., Röst, H. L., & Mann, M. (2020). diaPASEF: Parallel accumulation–serial fragmentation combined with data-independent acquisition. *Nature Methods*, *17*(12), 1229–1236. https://doi.org/10.1038/s41592-020-00998-0

Mitra, A., Satelli, A., Xia, X., Cutrera, J., Mishra, L., & Li, S. (2015). Cell-surface Vimentin: A mislocalized protein for isolating csVimentin(+) CD133(-) novel stem-like hepatocellular carcinoma cells expressing EMT markers. *International Journal of Cancer*, *137*(2), 491–496. https://doi.org/10.1002/ijc.29382

Moffitt, R. A., Marayati, R., Flate, E. L., Volmar, K. E., Loeza, S. G. H., Hoadley, K. A., Rashid, N. U., Williams, L. A., Eaton, S. C., Chung, A. H., Smyla, J. K., Anderson, J. M., Kim, H. J., Bentrem, D. J., Talamonti, M. S., Iacobuzio-Donahue, C. A., Hollingsworth, M. A., & Yeh, J. J. (2015). Virtual microdissection identifies distinct tumor- and stroma-specific subtypes of pancreatic ductal adenocarcinoma. *Nature Genetics*, *47*(10), 1168–1178. https://doi.org/10.1038/ng.3398

Mohan, M. J., Seaton, T., Mitchell, J., Howe, A., Blackburn, K., Burkhart, W., Moyer, M., Patel, I., Waitt, G. M., Becherer, J. D., Moss, M. L., & Milla, M. E. (2002). The Tumor Necrosis Factor-α Converting Enzyme (TACE): A Unique Metalloproteinase with Highly Defined Substrate Selectivity. *Biochemistry*, *41*(30), 9462–9469. https://doi.org/10.1021/bi0260132

Molls, M. (Ed.). (2009). *The impact of tumor biology on cancer treatment and multidisciplinary strategies*. Springer.

Nakajima, S., Doi, R., Toyoda, E., Tsuji, S., Wada, M., Koizumi, M., Tulachan, S. S., Ito, D., Kami, K., Mori, T., Kawaguchi, Y., Fujimoto, K., Hosotani, R., & Imamura, M. (2004). N-Cadherin Expression and Epithelial-Mesenchymal Transition in Pancreatic Carcinoma. *Clinical Cancer Research*, *10*(12), 4125–4133. https://doi.org/10.1158/1078-0432.CCR-0578-03

Noh, H., Yan, J., Hong, S., Kong, L.-Y., Gabrusiewicz, K., Xia, X., Heimberger, A. B., & Li, S. (2016). Discovery of cell surface vimentin targeting mAb for direct disruption of GBM tumor initiating cells. *Oncotarget*, *7*(44), 72021–72032. https://doi.org/10.18632/oncotarget.12458

Peinado, H., Alečković, M., Lavotshkin, S., Matei, I., Costa-Silva, B., Moreno-Bueno, G., Hergueta-Redondo, M., Williams, C., García-Santos, G., Ghajar, C. M., Nitadori-Hoshino,

A., Hoffman, C., Badal, K., Garcia, B. A., Callahan, M. K., Yuan, J., Martins, V. R., Skog, J., Kaplan, R. N., … Lyden, D. (2012). Melanoma exosomes educate bone marrow progenitor cells toward a pro-metastatic phenotype through MET. *Nature Medicine*, *18*(6), 883–891. https://doi.org/10.1038/nm.2753

Philley, J. V., Kannan, A., Griffith, D. E., Devine, M. S., Benwill, J. L., Wallace, R. J., Brown-Elliott, B. A., Thakkar, F., Taskar, V., Fox, J. G., Alqaid, A., Bains, H., Gupta, S., & Dasgupta, S. (2017). Exosome secretome and mediated signaling in breast cancer patients with nontuberculous mycobacterial disease. *Oncotarget*, *8*(11), 18070–18081. https://doi.org/10.18632/oncotarget.14964

Poggio, M., Hu, T., Pai, C.-C., Chu, B., Belair, C. D., Chang, A., Montabana, E., Lang, U. E., Fu, Q., Fong, L., & Blelloch, R. (2019). Suppression of Exosomal PD-L1 Induces Systemic Anti-tumor Immunity and Memory. *Cell*, *177*(2), 414-427.e13. https://doi.org/10.1016/j.cell.2019.02.016

Pollock, S. B., Rose, C. M., Darwish, M., Bouziat, R., Delamarre, L., Blanchette, C., & Lill, J. R. (2021). Sensitive and Quantitative Detection of MHC-I Displayed Neoepitopes Using a Semiautomated Workflow and TOMAHAQ Mass Spectrometry. *Molecular & Cellular Proteomics*, *20*. https://doi.org/10.1016/j.mcpro.2021.100108

Purcell, A. W., Ramarathinam, S. H., & Ternette, N. (2019a). Mass spectrometry–based identification of MHC-bound peptides for immunopeptidomics. *Nature Protocols*, *14*(6), 1687–1707. https://doi.org/10.1038/s41596-019-0133-y

Purcell, A. W., Ramarathinam, S. H., & Ternette, N. (2019b). Mass spectrometry–based identification of MHC-bound peptides for immunopeptidomics. *Nature Protocols*, *14*(6), 1687–1707. https://doi.org/10.1038/s41596-019-0133-y

Rawla, P. (2019). Epidemiology of Prostate Cancer. *World Journal of Oncology*, *10*(2), 63–89. https://doi.org/10.14740/wjon1191

Rebello, R., Pearson, R., Hannan, R., & Furic, L. (2017). Therapeutic Approaches Targeting MYC-Driven Prostate Cancer. *Genes*, *8*(2), 71. https://doi.org/10.3390/genes8020071

Rees, J. S., Li, X., Perrett, S., Lilley, K. S., & Jackson, A. P. (2015). Selective Proteomic Proximity Labeling Assay Using Tyramide (SPPLAT): A Quantitative Method for the Proteomic Analysis of Localized Membrane-Bound Protein Clusters. *Current Protocols in Protein Science*, *80*(1). https://doi.org/10.1002/0471140864.ps1927s80

Reily, C., Stewart, T. J., Renfrow, M. B., & Novak, J. (2019). Glycosylation in health and disease. *Nature Reviews. Nephrology*, *15*(6), 346–366. https://doi.org/10.1038/s41581-019-0129-4

Rodenko, B., Toebes, M., Hadrup, S. R., van Esch, W. J. E., Molenaar, A. M., Schumacher, T. N. M., & Ovaa, H. (2006). Generation of peptide-MHC class I complexes through UV-mediated ligand exchange. *Nature Protocols*, *1*(3), 1120–1132. https://doi.org/10.1038/nprot.2006.121

Saber, S. H., Ali, H. E. A., Gaballa, R., Gaballah, M., Ali, H. I., Zerfaoui, M., & Abd Elmageed, Z. Y. (2020). Exosomes are the Driving Force in Preparing the Soil for the Metastatic Seeds: Lessons from the Prostate Cancer. *Cells*, *9*(3), E564. https://doi.org/10.3390/cells9030564

Santucci, L., Bruschi, M., Del Zotto, G., Antonini, F., Ghiggeri, G. M., Panfoli, I., & Candiano, G. (2019). Biological surface properties in extracellular vesicles and their effect on cargo proteins. *Scientific Reports*, *9*(1), 13048. https://doi.org/10.1038/s41598-019-47598-3

Sarkizova, S., Klaeger, S., Le, P. M., Li, L. W., Oliveira, G., Keshishian, H., Hartigan, C. R., Zhang, W., Braun, D. A., Ligon, K. L., Bachireddy, P., Zervantonakis, I. K., Rosenbluth, J.

M., Ouspenskaia, T., Law, T., Justesen, S., Stevens, J., Lane, W. J., Eisenhaure, T., … Keskin, D. B. (2020). A large peptidome dataset improves HLA class I epitope prediction across most of the human population. *Nature Biotechnology*, *38*(2), 199–209. https://doi.org/10.1038/s41587-019-0322-9

Schäffer, C., & Messner, P. (2017). Emerging facets of prokaryotic glycosylation. *FEMS Microbiology Reviews*, *41*(1), 49–91. https://doi.org/10.1093/femsre/fuw036

Schindelin, J., Arganda-Carreras, I., Frise, E., Kaynig, V., Longair, M., Pietzsch, T., Preibisch, S., Rueden, C., Saalfeld, S., Schmid, B., Tinevez, J.-Y., White, D. J., Hartenstein, V., Eliceiri, K., Tomancak, P., & Cardona, A. (2012). Fiji: An open-source platform for biological-image analysis. *Nature Methods*, *9*(7), 676–682. https://doi.org/10.1038/nmeth.2019

Sears, R. M., May, D. G., & Roux, K. J. (2019). BioID as a Tool for Protein-Proximity Labeling in Living Cells. In T. Nuijens & M. Schmidt (Eds.), *Enzyme-Mediated Ligation Methods* (Vol. 2012, pp. 299–313). Springer New York. https://doi.org/10.1007/978-1-4939-9546-2_15

Seoane, R., Vidal, S., Bouzaher, Y. H., El Motiam, A., & Rivas, C. (2020). The Interaction of Viruses with the Cellular Senescence Response. *Biology*, *9*(12), 455. https://doi.org/10.3390/biology9120455

Shen, X., Wang, C., Zhu, H., Wang, Y., Wang, X., Cheng, X., Ge, W., & Lu, W. (2021). Exosome-mediated transfer of CD44 from high-metastatic ovarian cancer cells promotes migration and invasion of low-metastatic ovarian cancer cells. *Journal of Ovarian Research*, *14*(1), 38. https://doi.org/10.1186/s13048-021-00776-2

Shimagaki, T., Yoshio, S., Kawai, H., Sakamoto, Y., Doi, H., Matsuda, M., Mori, T., Osawa, Y., Fukai, M., Yoshida, T., Ma, Y., Akita, T., Tanaka, J., Taketomi, A., Hanayama, R., Yoshizumi, T., Mori, M., & Kanto, T. (2019). Serum milk fat globule-EGF factor 8 (MFG-E8) as a diagnostic and prognostic biomarker in patients with hepatocellular carcinoma. *Scientific Reports*, *9*(1), 15788. https://doi.org/10.1038/s41598-019-52356-6

Shurtleff, M. J., Temoche-Diaz, M. M., & Schekman, R. (2018). Extracellular Vesicles and Cancer: Caveat Lector. *Annual Review of Cancer Biology*, *2*(1), 395–411. https://doi.org/10.1146/annurev-cancerbio-030617-050519

Skog, J., Würdinger, T., van Rijn, S., Meijer, D. H., Gainche, L., Curry, W. T., Carter, B. S., Krichevsky, A. M., & Breakefield, X. O. (2008). Glioblastoma microvesicles transport RNA and proteins that promote tumour growth and provide diagnostic biomarkers. *Nature Cell Biology*, *10*(12), 1470–1476. https://doi.org/10.1038/ncb1800

Sørensen, K. D., Abildgaard, M. O., Haldrup, C., Ulhøi, B. P., Kristensen, H., Strand, S., Parker, C., Høyer, S., Borre, M., & Ørntoft, T. F. (2013). Prognostic significance of aberrantly silenced ANPEP expression in prostate cancer. *British Journal of Cancer*, *108*(2), 420–428. https://doi.org/10.1038/bjc.2012.549

Soung, Y., Ford, S., Zhang, V., & Chung, J. (2017). Exosomes in Cancer Diagnostics. *Cancers*, *9*(12), 8. https://doi.org/10.3390/cancers9010008

Stopfer, L. E., Rettko, N. J., Leddy, O., Mesfin, J. M., Brown, E., Winski, S., Bryson, B., Wells, J. A., & White, F. M. (2022). *MEK inhibition enhances presentation of targetable MHC-I tumor antigens in mutant melanomas* (p. 2022.01.10.475285). https://doi.org/10.1101/2022.01.10.475285

Tutanov, O., Orlova, E., Proskura, K., Grigor'eva, A., Yunusova, N., Tsentalovich, Y., Alexandrova, A., & Tamkovich, S. (2020). Proteomic Analysis of Blood Exosomes from Healthy Females and Breast Cancer Patients Reveals an Association between Different Exosomal Bioactivity on Non-tumorigenic Epithelial Cell and Breast Cancer Cell Migration in Vitro. *Biomolecules*, *10*(4), 495. https://doi.org/10.3390/biom10040495

Valitutti, S., Coombs, D., & Dupré, L. (2010). The space and time frames of T cell activation at the immunological synapse. *FEBS Letters*, *584*(24), 4851–4857. https://doi.org/10.1016/j.febslet.2010.10.010

Vaupel, P., & Mayer, A. (2007). Hypoxia in cancer: Significance and impact on clinical outcome. *Cancer Metastasis Rev*, *26*. https://doi.org/10.1007/s10555-007-9055-1

Wang, J. P., & Hielscher, A. (2017). Fibronectin: How Its Aberrant Expression in Tumors May Improve Therapeutic Targeting. *Journal of Cancer*, *8*(4), 674–682. https://doi.org/10.7150/jca.16901

Wang, T., & Miller, K. E. (2016). Characterization of glutamatergic neurons in the rat atrial intrinsic cardiac ganglia that project to the cardiac ventricular wall. *Neuroscience*, *329*, 134–150. https://doi.org/10.1016/j.neuroscience.2016.05.002

Weber, R. J., Liang, S. I., Selden, N. S., Desai, T. A., & Gartner, Z. J. (2014). Efficient Targeting of Fatty-Acid Modified Oligonucleotides to Live Cell Membranes through Stepwise Assembly. *Biomacromolecules*, *15*(12), 4621–4626. https://doi.org/10.1021/bm501467h

Weekes, M. P., Antrobus, R., Lill, J. R., Duncan, L. M., Hör, S., & Lehner, P. J. (2010). Comparative analysis of techniques to purify plasma membrane proteins. *Journal of Biomolecular Techniques: JBT*, *21*(3), 108–115.

Weeks, A. M., Byrnes, J. R., Lui, I., & Wells, J. A. (2021). Mapping proteolytic neo-N termini at the surface of living cells. *Proceedings of the National Academy of Sciences*, *118*(8), e2018809118. https://doi.org/10.1073/pnas.2018809118

Wei, J., Leung, K., Truillet, C., Ruggero, D., Wells, J. A., & Evans, M. J. (2020). Profiling the Surfaceome Identifies Therapeutic Targets for Cells with Hyperactive mTORC1 Signaling. *Molecular & Cellular Proteomics*, *19*(2), 294–307. https://doi.org/10.1074/mcp.RA119.001785

Wickström, M., Larsson, R., Nygren, P., & Gullbo, J. (2011). Aminopeptidase N (CD13) as a target for cancer chemotherapy. *Cancer Science*, *102*(3), 501–508. https://doi.org/10.1111/j.1349-7006.2010.01826.x

Wise, D. R., DeBerardinis, R. J., Mancuso, A., Sayed, N., Zhang, X.-Y., Pfeiffer, H. K., Nissim, I., Daikhin, E., Yudkoff, M., McMahon, S. B., & Thompson, C. B. (2008). Myc regulates a transcriptional program that stimulates mitochondrial glutaminolysis and leads to glutamine addiction. *Proceedings of the National Academy of Sciences*, *105*(48), 18782–18787. https://doi.org/10.1073/pnas.0810199105

Wollscheid, B., Bausch-Fluck, D., Henderson, C., O'Brien, R., Bibel, M., Schiess, R., Aebersold, R., & Watts, J. D. (2009). Mass-spectrometric identification and relative quantification of N-linked cell surface glycoproteins. *Nat Biotech*, *27*(4), 378–386. https://doi.org/10.1038/nbt.1532

Yamamoto, K., Venida, A., Yano, J., Biancur, D. E., Kakiuchi, M., Gupta, S., Sohn, A. S. W., Mukhopadhyay, S., Lin, E. Y., Parker, S. J., Banh, R. S., Paulo, J. A., Wen, K. W., Debnath, J., Kim, G. E., Mancias, J. D., Fearon, D. T., Perera, R. M., & Kimmelman, A. C. (2020).

Autophagy promotes immune evasion of pancreatic cancer by degrading MHC-I. *Nature*, *581*(7806), 100–105. https://doi.org/10.1038/s41586-020-2229-5

Yuen, A., & Díaz, B. (2014). The impact of hypoxia in pancreatic cancer invasion and metastasis. *Hypoxia*, *2*, 91–106. PMC. https://doi.org/10.2147/HP.S52636

Zhou, B., Xu, K., Zheng, X., Chen, T., Wang, J., Song, Y., Shao, Y., & Zheng, S. (2020). Application of exosomes as liquid biopsy in clinical diagnosis. *Signal Transduction and Targeted Therapy*, *5*(1), 144. https://doi.org/10.1038/s41392-020-00258-9

Zhu, L., Li, Q., Wang, X., Liao, J., Zhang, W., Gao, L., Liu, Y., Zhang, C., Zhang, X., Rao, J., & Kong, P. (2020). THBS1 Is a Novel Serum Prognostic Factors of Acute Myeloid Leukemia. *Frontiers in Oncology*, *9*, 1567. https://doi.org/10.3389/fonc.2019.01567

Publishing Agreement

It is the policy of the University to encourage open access and broad distribution of all theses, dissertations, and manuscripts. The Graduate Division will facilitate the distribution of UCSF theses, dissertations, and manuscripts to the UCSF Library for open access and distribution. UCSF will make such theses, dissertations, and manuscripts accessible to the public and will take reasonable steps to preserve these works in perpetuity.

I hereby grant the non-exclusive, perpetual right to The Regents of the University of California to reproduce, publicly display, distribute, preserve, and publish copies of my thesis, dissertation, or manuscript in any form or media, now existing or later derived, including access online for teaching, research, and public service purposes.

DocuSigned by:
LisaKirkemo
ECEA29F1A2F0462...
Author Signature

2/23/2022
Date